Doctoral Thesis

Coordinated Frequency Control of Hybrid Onshore Power System by PMSG-based Offshore Wind Farm

(PMSGに基づく洋上ウィンドファームによるハイブリッド陸上電力システムの協調周波数制御)

Effat Jahan

September 2019

Kitami Institute of Technology (KIT), Japan

Abstract

This thesis deals with the coordinated frequency control method of hybrid onshore power system by using variable speed wind turbines with permanent magnet synchronous generators (VSWT-PMSGs) based offshore wind farm (OWF), which is connected to the main onshore grid through voltage source converter (VSC) based high voltage DC (HVDC) transmission system. Penetration of large-scale WF into the power grid has increased significantly and it inevitably leads to the retirements of conventional synchronous generators (SGs). Thus, the frequency fluctuations of the power system due to the high penetration of WF is a major concern. Therefore, to maintain the frequency stability of the power system WF is required to operate like conventional unit. They need not only supply power to the grid, but also need to damp frequency fluctuations. Therefore, the interaction of large-scale WF along with the existing power system is an important issue to be analyzed in order to minimize the frequency fluctuations.

Normally, VSWT-PMSG is preferable for OWF due to its gear-less feature, brushless operation, and lower losses compared to doubly fed induction generator (DFIG). Additionally, to integrate large-scale OWF into the onshore grid, VSC-HVDC transmission system is attractive and more preferable than high voltage AC (HVAC) transmission system from an economic and technical point of view. Normally, detailed model of VSC-HVDC is used in the simulation analysis, which requires, however, large computational time due to the switching phenomena of the power converters. Therefore, detailed model of the VSC-HVDC should be simplified in the analysis in order to diminish complexity and long simulation time. In this thesis, a simplified model of VSC-HVDC transmission system is developed for fast dynamic simulation analysis. Comparative analysis between the proposed simplified and detailed models of VSC-HVDC is also performed and presented. The simulation results show that the proposed simplified model of VSC-HVDC has sufficient accuracy for analyzing dynamic characteristics.

Usually, the characteristics of VSWT-PMSG based OWFs are different from that of the conventional power plants. To contribute to the primary frequency regulation in a similar way to conventional SGs, the VSWT-PMSG based OWF requires additional active power control loop and primary reserve. In this case, power reserve is possible by operating the VSWT-PMSGs at a reduced power level instead of maximum power point tracking (MPPT) mode which is called

deloaded operation. Therefore, this thesis proposes firstly a primary frequency regulation method of hybrid power system by fixed deloaded operation of PMSG-based OWF. A new centralized droop control technique is also embedded for VSWT-PMSGs based OWF connected through VSC-HVDC transmission system to damp frequency oscillation of the main power grid in which a large-scale of WF composed of fixed speed wind turbines with squirrel cage induction generators (FSWT-SCIGs) and photovoltaic (PV) power station are installed. The centralized droop control technique is implemented with the dead band to limit the frequency variation within the permissible limit. Thus, better frequency regulation performance can be achieved.

The active power injected to the grid system from OWF is reduced by a fixed ratio at all times in the fixed deloaded operation, and hence, the energy loss become large. Therefore, this thesis also proposes secondly a centralized frequency control scheme with a novel variable deloaded operation for VSWT-PMSGs based OWF connected to the onshore grid through VSC-HVDC transmission system. This is one of the salient features of this thesis. A centralized droop controller with dead band is designed for VSWT-PMSGs to utilize this reserve power to suppress the frequency fluctuations of the onshore grid due to the installations of large-scale FSWT-SCIGs based WF and PV power station. The combination of variable deloaded operation and centralized droop controller can give better frequency regulation and decrease energy loss. To verify the effectiveness of the proposed control system, simulation analyses are performed on a multi-machine hybrid power system model. The simulation results reveal that the variable deloaded operation can decrease the energy loss compared to the fixed deloaded operation as well as suppress the frequency fluctuations in the same level as the fixed deloaded operation.

Simulations are carried out by PSCAD/EMTDC software. Real wind speed data and solar irradiance data measured in Hokkaido Island, Japan, are used in the simulation analyses to obtain the realistic responses. The standard IEEE nine-bus model is used to evaluate the performance of the proposed control strategies.

Considering all the features, it is concluded that the frequency oscillation can be minimized effectively by the proposed control strategies of PMSG.

Contents

Pages 12, 38, 84 and 88 are intentionally left blank.

Chapter 1

Introduction

1.1 Renewable Energy

Conventional fossil fuel based energy sources like coal, oil and natural gas has been proven to be highly effective drivers of economic growth. Due to the rapid depletion of conventional energy sources and increasing energy demand, primary energy consumption has grown by 1.8% worldwide [1, 2]. In spite of that, the conventional power plants generate air pollutants (e.g. Sulphur dioxide, nitrogen oxide and carbon dioxide), which are initiating serious environmental problems [3]. Consequently, global warming and acid rain are observed as main reasons of the environmental pollution [4-6]. Thus, conservation of the environment has become the main inspiration to integrate more renewable energy sources (RESs) in power systems.

RESs are energy sources that are repeatedly refilled by nature and generated directly from the sun (i.e. thermal, photo-chemical, and photo-electric), indirectly from the sun (i.e. wind, hydropower, and photosynthetic energy stored in biomass), or from other natural movements and mechanisms of the environment (i.e. geothermal and tidal energy) [7-10]. RES does not include energy resources resulting from fossil fuels, and does not waste products from fossil sources. Fig. 1.1 shows an overview of renewable energy sources [11, 12].

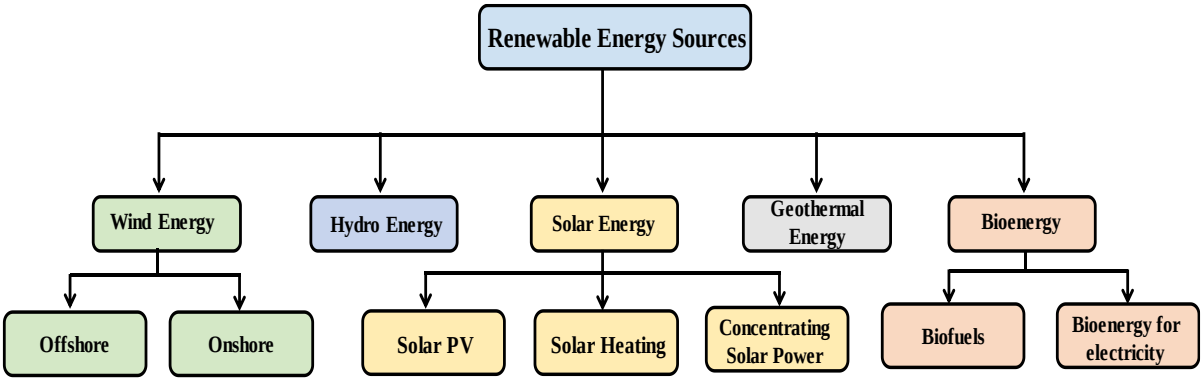

Fig. 1.1. Classification of RESs.

Renewable power generating capacity saw its largest annual increase ever in 2017, raising total capacity by almost 9% over 2016 [13]. Overall, renewables accounted for an estimated 70%

of net additions to global power capacity in 2017, due in large part to continued improvements in the cost-competitiveness of solar photovoltaic (PV) and wind power [13]. Solar PV led the way, accounting for nearly 55% of newly installed renewable power capacity in 2017 [13]. Wind (29%) and hydropower (11%) accounted for most of the remaining capacity additions [13]. Several countries are successfully integrating increasingly larger shares of variable renewable power into electricity systems. Renewable-based stand-alone and off-grid single home or mini-grid systems represented about 6% of new electricity connections worldwide between 2012 and 2016 [13]. Table 1.1 illustrates the total installed capacity of RESs in worldwide [13].

Table 1.1. Total installed capacity of RESs in 2016-2017.

	2016	**2017**
Renewable power capacity (including hydro)	2,017 GW	2,195 GW
Renewable power capacity (not including hydro)	922 GW	1,081 GW
Hydropower capacity	1,095 GW	1,114 GW
Bio-power capacity	114 GW	122 GW
Bio-power generation (annual)	501 TWh	555 TWh
Geothermal power capacity	12.1 GW	12.8 GW
Solar PV capacity	303 GW	402 GW
Concentrating solar thermal power (CSP) capacity	4.8 GW	4.9 GW
Wind power capacity	487 GW	539 GW
Ocean energy capacity	0.5 GW	0.5 GW

1.2 Context of Wind Power Penetration Worldwide

Since 2001 wind energy has become ongoing trend of renewable energy resource in market and industry highlights. Figs. 1.2 and 1.3 show the total annual and global installed capacity of wind power in 2001-2017 reported by global wind energy council (GWEC) [14].

More than 52,000 MW of clean, emissions-free wind power was added in 2017 [14], bringing total installations to 539,123 MW globally which will reach over 840,000 MW by the end of 2022 [14].

According to GWEC, the ten leading countries represent together a total share of 85% of the cumulative global wind capacity as shown in Fig. 1.4. The PR China represents by far the largest wind markets. By the end of 2017, China has had an overall installed capacity of around 188,232

MW. In second place, the US had total installed capacity of around 89,077 MW at the end of 2017. Also, Germany is in the third position with 56,132 MW cumulative installed capacity at the end of 2017.

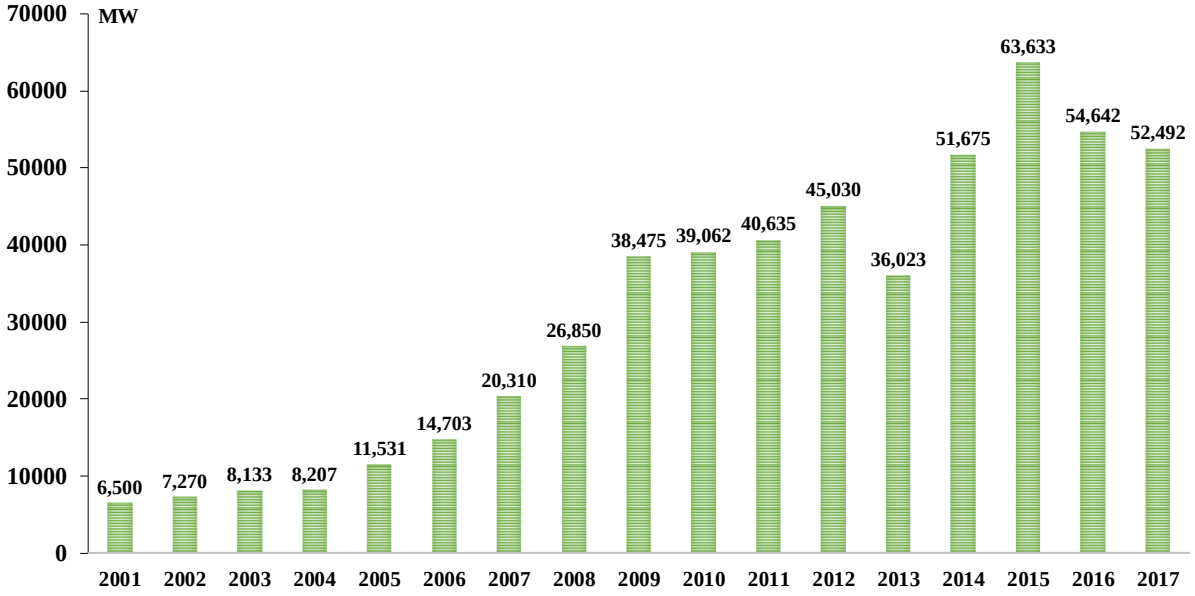

Fig. 1.2. Global annual installed capacity of wind power in 2001-2017.

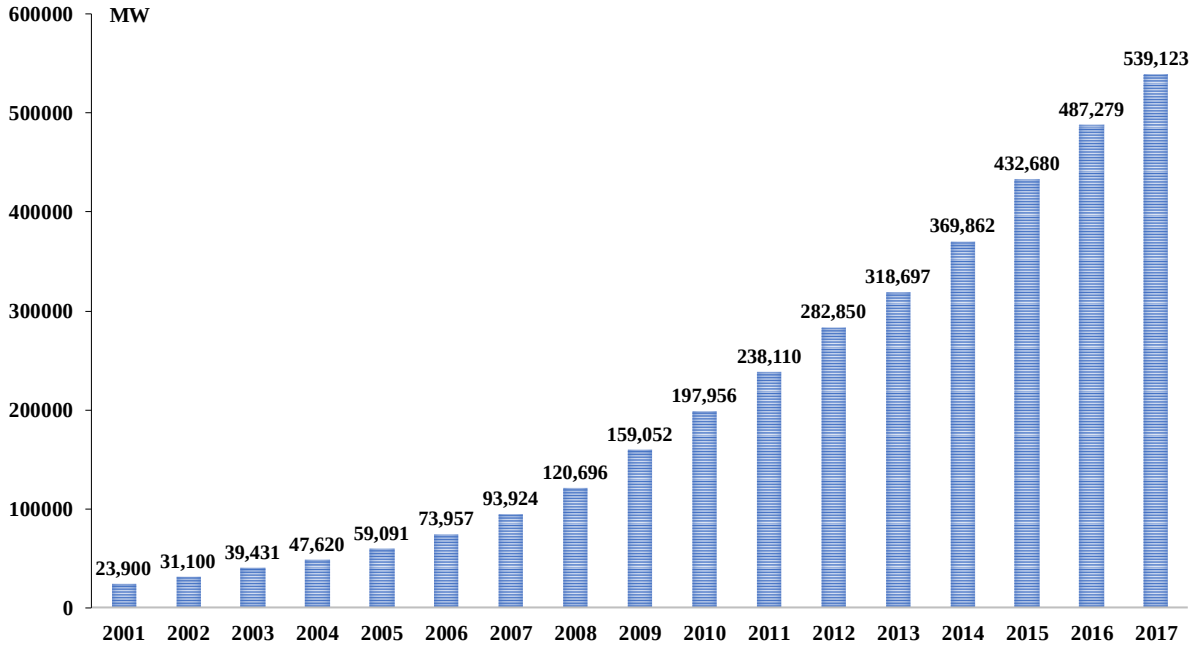

Fig. 1.3. Global cumulative installed capacity of wind power in 2001-2017.

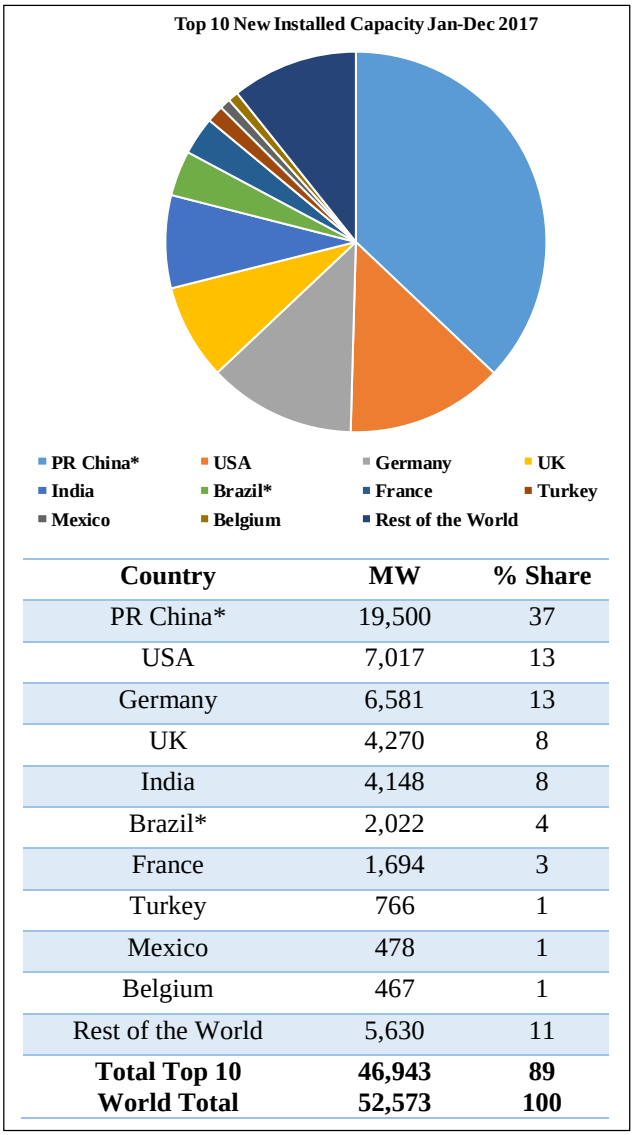

Country	MW	% Share
PR China*	19,500	37
USA	7,017	13
Germany	6,581	13
UK	4,270	8
India	4,148	8
Brazil*	2,022	4
France	1,694	3
Turkey	766	1
Mexico	478	1
Belgium	467	1
Rest of the World	5,630	11
Total Top 10	**46,943**	**89**
World Total	**52,573**	**100**

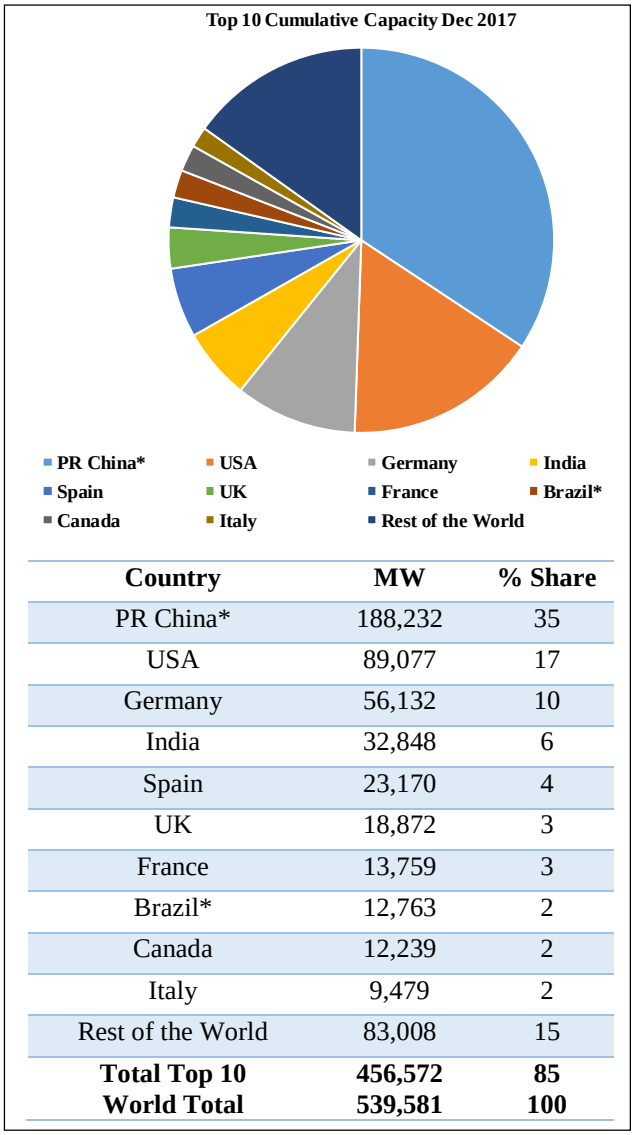

Country	MW	% Share
PR China*	188,232	35
USA	89,077	17
Germany	56,132	10
India	32,848	6
Spain	23,170	4
UK	18,872	3
France	13,759	3
Brazil*	12,763	2
Canada	12,239	2
Italy	9,479	2
Rest of the World	83,008	15
Total Top 10	**456,572**	**85**
World Total	**539,581**	**100**

Fig. 1.4. New and cumulative installed capacity of wind power of top 10 countries in 2017 [14].

1.3 Scenarios of Offshore Wind Farm Worldwide

Offshore wind power (OWP) or offshore wind energy is the use of wind farms (WFs) constructed in bodies of water, usually in the ocean on the continental shelf, to harvest wind energy to generate electricity. Higher wind speeds are available at offshore compared to on land, so OWP can achieve higher electricity generation per amount of capacity installed than onshore wind power [15].

At the end of 2017, the total worldwide OWP capacity was 18.8 GW [16]. Fig. 1.5 shows the cumulative offshore wind capacity in 2011-2017 reported by GWEC [16]. Fig 1.6 illustrates the global cumulative offshore wind capacity for 2017 reported by GWEC [16]. According to GWEC, the offshore segment had a record year with 4,334 MW of installations, an 87% increase on the 2016 market, bringing total global installations to 18,814 MW, and representing a 30% increase in cumulative capacity. Offshore is still only about 8% of the global annual market, and represents about 3.5% of cumulative installed capacity, but it is growing quickly [16].

Projections for 2020 estimate an offshore WF (OWF) capacity of 40 GW in European waters, which would provide 4% of the European Union's demand of electricity [17]. The European Wind Energy Association has set a target of 40 GW installed by 2020 and 150 GW by 2030 [18]. OWP capacity is expected to reach a total of 75 GW worldwide by 2020, with significant contributions from China and the United States [19]. The organization for Economic co-operation and development (OECD) predicted in 2016 that OWP will grow to 8% of ocean economy by 2030 [20]. Fig. 1.7 illustrate the global forecast projects for offshore wind development [16].

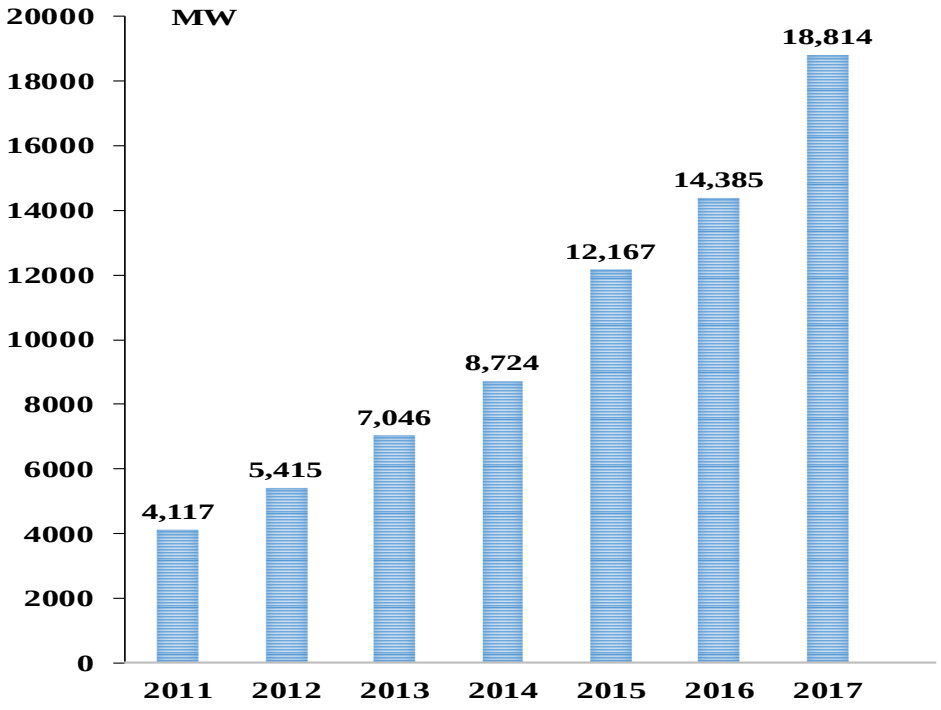

Fig. 1.5. Global cumulative installed capacity of OWP in 2011-2017.

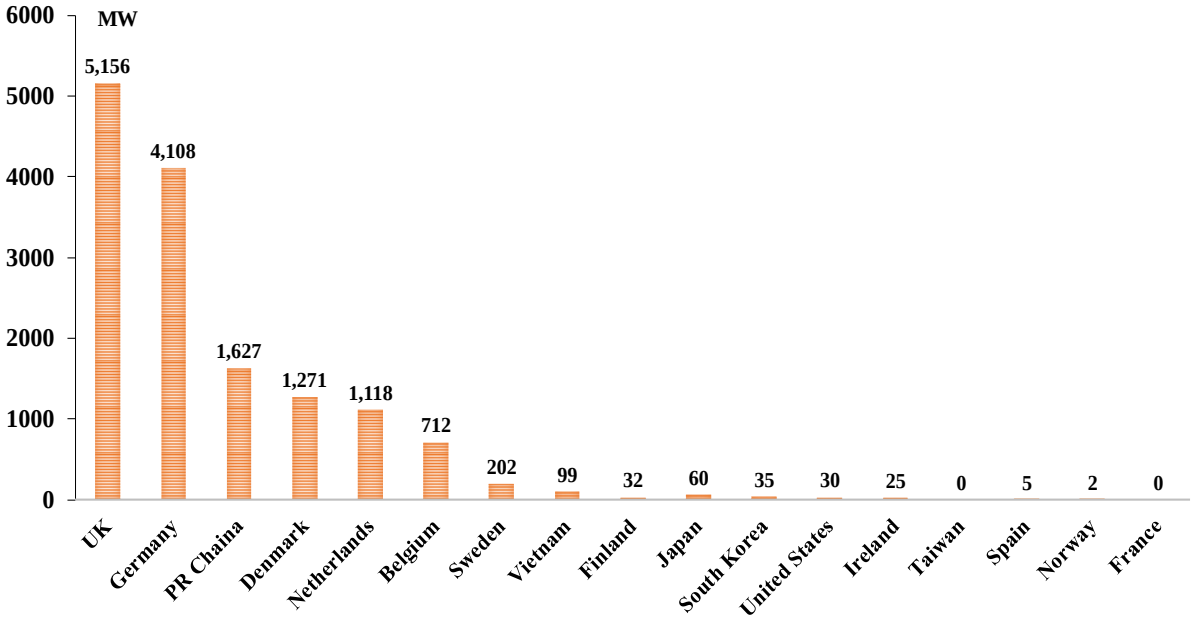

Fig. 1.6. Global cumulative installed capacity of OWP for 2017.

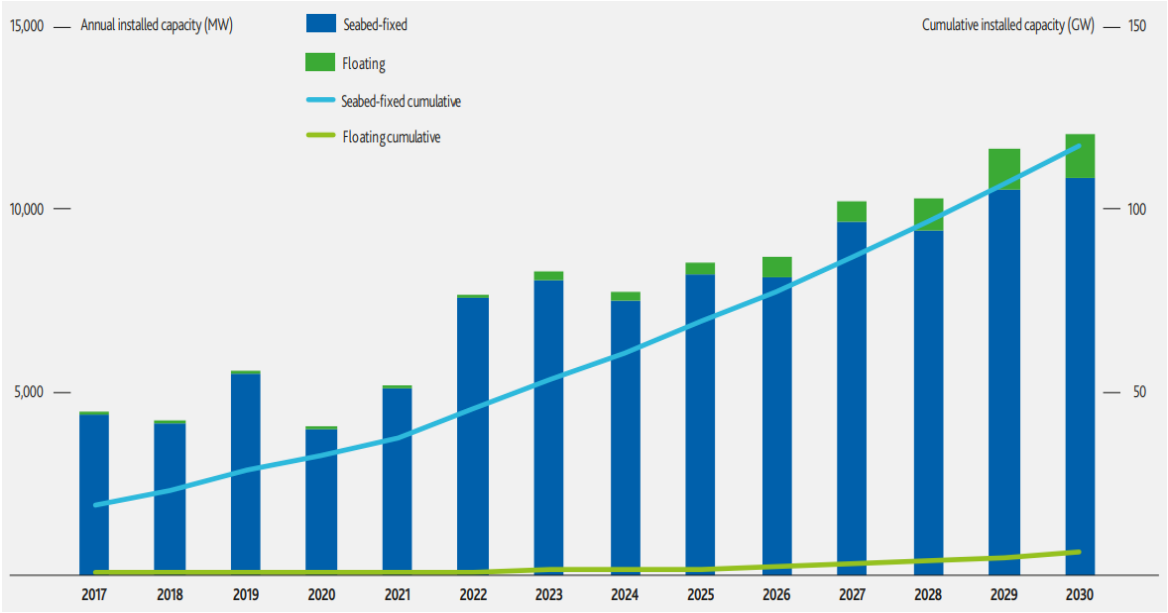

Fig. 1.7. Offshore wind development globally out to 2030 [16].

1.4 Background of the Thesis

Due to the drawback of the conventional power plants based on fossil fuels and their negative impacts on the environment, recently the attention on RESs has been increasing all over the world. Solar PV is a popular type of RES which will occupy an important place and supply nearly 28% of all the overall energy demand [21-25], until 2040. Also, penetration of gird-connected OWF has

been increasing since the last decade because of the stronger and steadier wind resources in offshore areas compared to onshore sites [16, 26-28].

However, grid integration issues of OWFs could seriously impact the operation and stability of their interconnected onshore power system. OWFs are located, in general, several 10s km or more far from the onshore grid connection point. It is a great challenge for both WF developer and transmission system operator (TSO) to transmit hundreds of MW OWP over such a long distance. Most commonly, high voltage AC (HVAC) transmission systems are used for the integration of OWFs to the onshore power grid. However, there can be a case in which HVAC is not suitable from an economical and technical points of view.

To integrate large-scale OWF into the onshore grid, voltage source converter based high voltage DC (VSC-HVDC) transmission system is attractive and more preferable than HVAC transmission system from an economic and technical point of view [29], especially in the case of very long transmission system. VSC-HVDC system has some advantages, i.e. lower cable losses, independent and fast control of active and reactive power, and stabilization potential of connected AC networks [30-35].

The use of VSC-HVDC for connecting OWF to onshore grid has been reported already in some literature [36-39]. In [36, 37], the WF considered is composed of fixed speed induction generators. In [38], synchronous generators (SGs) are used in the OWF. Doubly fed induction generator (DFIG) is chosen as wind generator for OWF in [39].

However, permanent magnets synchronous generator (PMSG) is becoming very popular nowadays as variable speed wind generator. In PMSG, the excitation is provided by permanent magnets instead of field winding. Permanent magnet machines are characterized as having large air gaps, which reduce flux linkage even in machines with multi magnetic poles [40]. As a result, low rotational speed generators can be manufactured with relatively small sizes with respect to its power rating. Moreover, gearbox can be omitted due to low rotational speed in PMSG wind generation system, resulting in low cost. Also the amplitude and frequency of the generator voltage can be fully controlled by the converter [41-52]. Therefore, variable speed wind turbine (VSWT) with PMSG (VSWT-PMSG) is preferable for OWF compared to DFIG.

Simulation analysis in PSCAD/EMTDC software of detailed model of VSC-HVDC connecting OWF to the onshore multi-machine power system requires large computational time due to the

switching phenomena of the power converters. Therefore, detailed model of the VSC-HVDC should be simplified in the analysis to diminish complexity and long simulation time.

As mentioned earlier, large number of wind turbine generators (WTGs) have been already connected to the existing power grid and in the near future the penetration ratio will increase more [53-57]. This large penetration of RESs into the existing grid has introduced some vulnerabilities to the power grid [58-61]. Due to increasing penetration of OWF and PV stations into the grid system certainly leads to the retirements of conventional synchronous generators (SGs) [62]. Thus, the frequency fluctuations due to varying output of WFs and PV stations have become a major concern [62].

Normally, the frequency fluctuation is damped by the conventional units, which are equipped with automatic generation control (AGC) or load frequency control (LFC) system [63]. Therefore, to maintain the frequency stability of the power system with large penetration ratio of RESs, RESs are required to operate like conventional units. They need to not only supply power to the grid, but also need to damp frequency fluctuations [62, 64]. One possible solution is a frequency control by OWF.

For the frequency regulation of the onshore grid system, the VSWT-PMSG-based OWF connected to the onshore grid through VSC-HVDC transmission system should have sufficient power reserve. In this case, power reserve is possible by operating the VSWT-PMSGs at a reduced power level instead of MPPT mode which is called deloaded operation [65]. Many researchers have focused on the primary reserve implementation by the fixed level of deloaded operation of VSWT with some auxiliary control loop [66-101]. For example, the deloaded operation is performed by the modified pitch angle control of VSWT-PMSG in [66-67,79, 85, 94]; the rotor speed controller is used for the deloaded operation in [68, 78, 87, 89]; and the over-speeding and pitching techniques are used for the deloaded operation of wind turbines in [69-75, 101]. However, in the above mentioned schemes for the deloaded operation, output power injected to the grid system from OWF is reduced by a fixed ratio at all times, and hence, the energy loss becomes large. Therefore, a variable deloaded operation is needed in order to decrease the energy loss as well damping the frequency fluctuations, in which deloading level is variable.

1.5 Scope and Contributions

The main purpose of this thesis is the design of centralized frequency control scheme with a novel variable deloaded operation for VSWT-PMSGs based OWF connected to the onshore grid through VSC-HVDC transmission system to damp frequency fluctuations of the onshore grid, in which a large-scale WF composed of fixed speed wind turbines with squirrel cage induction generators (FSWT-SCIGs) and solar PV station are installed. In order to improve the frequency stability of hybrid power system, the control system modeling of variable speed wind generators and system design are important issues in this thesis. The results of this study are expected to provide valuable contributions in the following aspects:

(1) This thesis presents a simplified model of VSC-HVDC transmission system for dynamic simulation study. Normally, simulation analysis in PSCAD/EMTDC software of detailed model of VSC-HVDC connecting OWF to the onshore multi-machine power system requires large computational time due to the switching phenomena of the power converters. Therefore, detailed model of the VSC-HVDC should be simplified in the analysis to diminish complexity and long simulation time. In this thesis, a simplified model of VSC-HVDC transmission system is developed for fast dynamic simulation analysis. The simulation results show that the proposed simplified model of VSC-HVDC system has sufficient accuracy because there is almost no difference among the simulation results for the both simplified and detailed models.

(2) The behaviour of the VSWT-PMSG based OWF differs from the conventional SGs. Conventional SGs can control the frequency fluctuations by governor-free (GF) operation and LFC. In order to participate the primary frequency regulation, the VSWT-PMSG based OWF needs additional power controller and primary reserve. Therefore, this thesis presents a new centralized droop control technique for VSWT-PMSGs based OWF connected through VSC-HVDC transmission system to damp frequency oscillation of the main power grid in which a large scale of WF composed of FSWT-SCIGs is installed. The centralized droop control technique is implemented with the dead band to limit the frequency variation within the permissible limit. The fixed deloaded control strategy is firstly adopted with the centralized droop controller to provide primary reserve. Thus, better frequency regulation performance can be achieved. The validity of the proposed coordinated control scheme is verified by simulation analysis using

PSCAD/EMTDC software on a model system composed of SGs, FSWT-SCIGs based WF, and VSWT-PMSGs based OWF.

(3) However, in the above mentioned schemes for the fixed deloaded operation, output power injected to the grid system from OWF is reduced by a fixed ratio at all times, and hence, the energy loss becomes large. Therefore, this thesis proposes a centralized frequency control scheme with a novel variable deloaded operation for VSWT-PMSGs based OWF connected to the onshore grid through VSC-HVDC transmission system to damp frequency fluctuations of the onshore grid, in which a large-scale WF composed of FSWT-SCIGs and solar PV station are installed. In the frequency control method, the variable deloaded operation is proposed in order to decrease the energy loss, in which deloaded level is variable (from 0% to 10%). The variable deloaded level is achieved by designing a variable gain based on the standard deviation of the frequency fluctuations of the onshore grid. A centralized droop controller with dead band is designed for VSWT-PMSGs to utilize this reserve power to suppress the frequency fluctuations of the onshore grid. The effectiveness of the proposed centralized frequency controller equipped with the variable deloaded function is verified through simulation analysis using PSCAD/EMTDC software on a modified IEEE nine-bus system composed of VSWT-PMSGs-based OWF connected to the onshore system through VSC-HVDC transmission line, FSWT-SCIGs based onshore WF, PV power station, and conventional SGs.

1.6 Outline of the Thesis

Chapter 2 provides the detail of the wind turbine generator system. The general overview and energy extraction from a wind turbine is also described. Then the pitch angle controller models are discussed extensively. Finally, different types of WTGs topologies are presented.

Chapter 3 presents the simplified model of VSC-HVDC transmission system for dynamic simulation study. Detailed design procedure of the proposed simplified model is discussed in this chapter. To evaluate performance of the derived simplified model of VSC-HVDC, simulation analysis is performed on a multi-machine power system model composed of VSWT- PMSGs, VSC-HVDC, and SGs. Comparative analysis between the proposed simplified model and the detailed model of VSC-HVDC is also performed and presented in this chapter.

Chapter 4 introduces a coordinated frequency control method for VSWT-PMSGs based OWF, which is connected to the main onshore grid through VSC-HVDC transmission system. A novel centralized droop controller with constant deloaded operation is designed for VSWT-PMSGs to minimize the frequency fluctuations of the main power system.

The overall design procedure of the proposed centralized frequency control technique, PMSG model along with control system, and power system model are discussed and presented in this chapter. The effectiveness of the proposed centralized frequency controller with constant deloaded operation is verified through simulation analysis on a modified IEEE nine-bus system.

Chapter 5 describes a novel variable deloaded operation of VSWT-PMSGs based OWF to maintain primary reserve, which is connected to onshore grid through VSC-HVDC transmission system. A centralized droop controller with variable deloaded operation is designed for VSWT-PMSGs to utilize this reserve power to suppress the frequency fluctuations of the onshore grid due to the installations of large-scale FSWT-SCIGs based wind farm and PV power station. The effectiveness of the proposed variable deloaded operation and centralized droop controller is verified through simulation analyses on a modified IEEE nine-bus test system.

Finally, Chapter 6 summarizes the findings and concludes the thesis.

Chapter 2

Wind Turbine Model

This chapter describes the detailed modeling of wind turbine. First, a brief overview of wind turbine generation system and power extraction from a practical wind turbine are presented. Then, the pitch angle controllers for both fixed speed and variable speed wind turbine system are discussed. Finally, the different types of wind turbine technologies are discussed.

2.1 Wind Turbine Generator System

A wind turbine generator system is a rotating device that extracts the energy in the wind into the electrical energy. The modern wind turbine generator systems are primarily constructed as system with a wind turbine of horizontal axis rotation, generator along with gear box and rotor break located in nacelle, and tower as depicted in Fig 2.1 [102]. The turbine captures power from wind and drives a generator. The tower supports the nacelle and usually contains the electrical conduits and yaw motor.

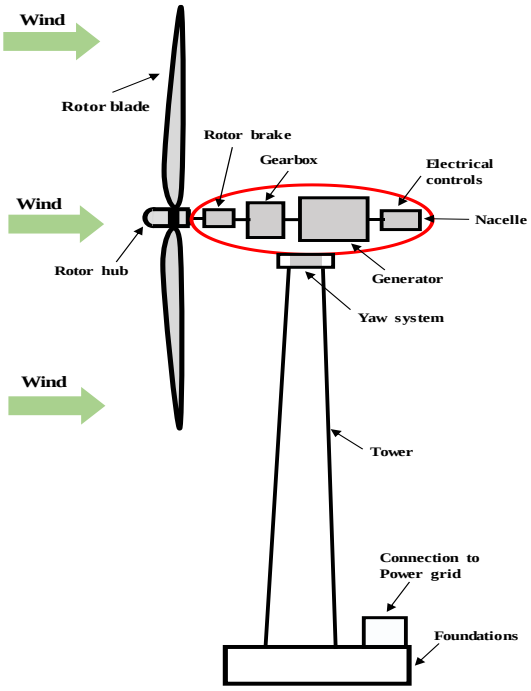

Fig. 2.1. Wind turbine generator system.

Different parts of the wind turbine generator system are shown in Fig 2.2. The modern wind turbine (sometimes called the rotor), mostly has three blades. Wind blowing over the blades causes the blades rotate. Wind speed is measured by using anemometer, and its data is transmitted to the controller. A disc brake can be applied mechanically, electrically, or hydraulically to stop the rotor in emergencies. Wind vane measures wind direction and communicates with the yaw drive to orient the turbine properly with respect to the wind. The yaw drive is used to keep the rotor facing into the wind as the wind direction changes.

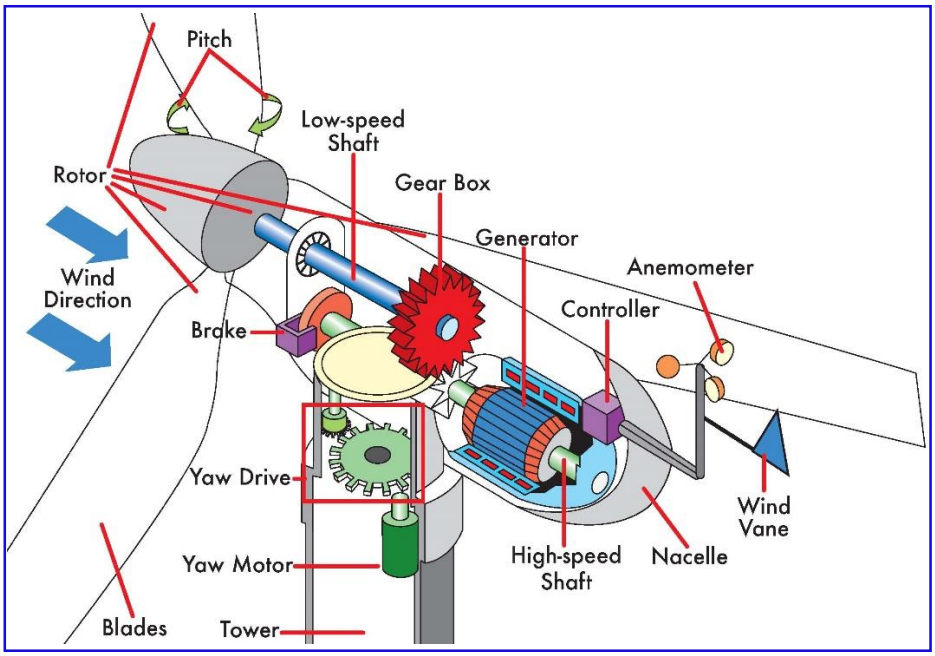

Fig. 2.2. Different parts of wind turbine generator system [103].

The modern wind turbine generator system can operate as fixed speed or variable speed. The fixed speed wind turbines (FSWT) are equipped with a squirrel cage rotor or wound rotor induction generators (referred as FSWT-SCIG). This type of wind turbine is designed to achieve maximum efficiency at one specific wind speed. FSWT-SCIG has often two stator windings which are used at low and high wind speed respectively in order to increase power production. In variable speed wind turbines (VSWT), it is possible to control continuously the rotational speed of the wind turbine according to the wind speed. By this way, the maximum aerodynamic efficiency can be achieved over a wide range of wind speed [104]. The VSWT is typically equipped with a permanent magnet synchronous generator (PMSG) (referred as VSWT-PMSG).

2.2 Wind Power Output

The extracted mechanical power in a wind turbine can be expressed as [40]:

$$P_w = 0.5\rho\pi R^2 V_w{}^3 C_p(\lambda,\beta) \tag{2.1}$$

where, P_w is the captured wind power, ρ is the air density (kg/m^3), R is the radius of the rotor blade (m), V_w is the wind speed (m/s), and C_p is the power coefficient.

The value of C_p can be calculated as follows [105]:

$$C_p(\lambda,\beta) = c_1\left(\frac{c_2}{\lambda_i} - c_3\beta - c_4\right)e^{\frac{-c_5}{\lambda_i}} + c_6\lambda \tag{2.2}$$

$$\frac{1}{\lambda_i} = \frac{1}{\lambda - 0.08\beta} - \frac{0.035}{\beta^3 + 1} \tag{2.3}$$

$$\lambda = \frac{\omega_r R}{V_w} \tag{2.4}$$

$$T_w = \frac{P_w}{\omega_r} \tag{2.5}$$

where, T_w is the wind turbine torque, β is the pitch angle, and λ is the tip speed ratio. Moreover, c_1 through c_6 are the characteristic coefficients of the wind turbine (c_1 = 0.5176, c_2 = 116, c_3 = 0.4, c_4 = 5, c_5 = 21, and c_6 = 0.0068) [106], and ω_r is the rotational speed of the wind turbine (rad/s).

The C_p vs λ characteristics shown in Fig. 2.3 are obtained using Equation (2.2) with different values of the β. When β is equal to zero degrees, the optimum power coefficient (C_{popt}) is 0.48, and the optimum tip speed ratio (λ_{opt}) is 8.1.

In VSWTs, the ω_r is controlled to follow the maximum power point tracking (MPPT). Since the precise measurement of wind speed is difficult, it is better to calculate the maximum power without measuring the wind speed. The MPPT power (P_{MPPT}) for VSWT-PMSG can be expressed as follows [40]:

$$P_{MPPT} = 0.5\rho\pi R^2\left(\omega_r R \Big/ \lambda_{opt}\right)^3 C_{p\_opt} \tag{2.6}$$

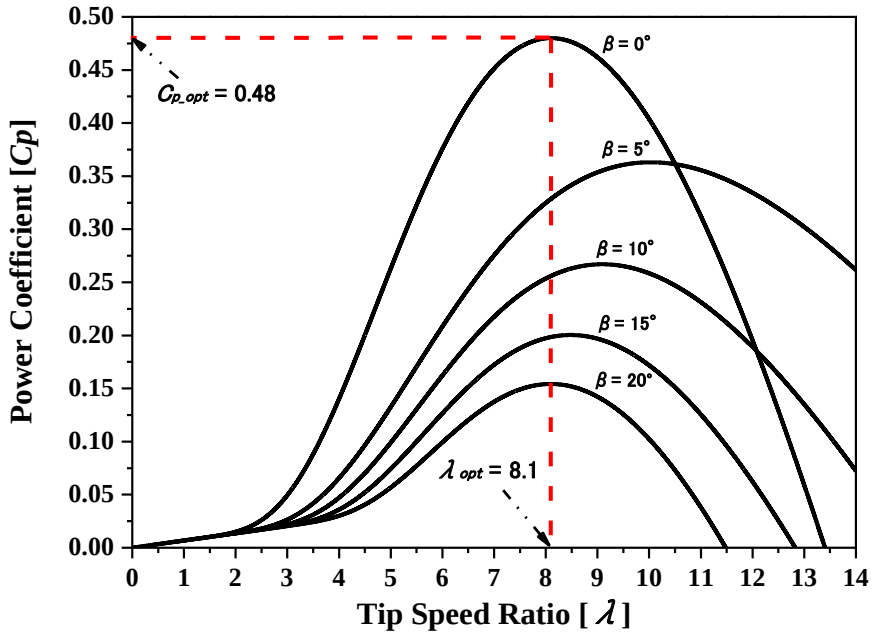

Fig. 2.3. C_p vs λ characteristics of the wind turbine for various pitch angles.

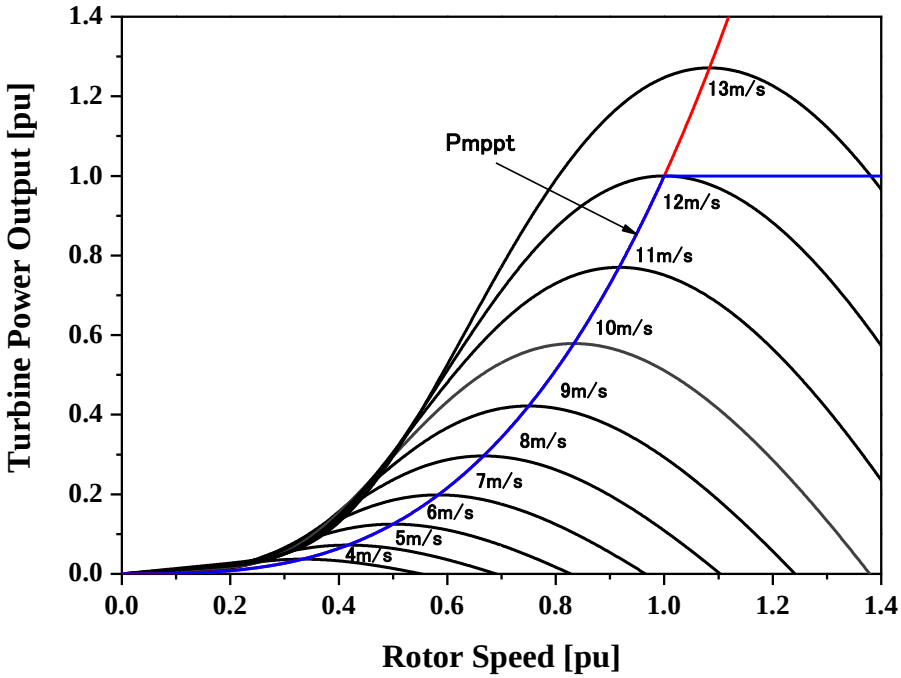

Fig. 2.4. Wind turbine characteristics for PMSG with MPPT line.

Based on this equation, the wind turbine characteristics for PMSG with MPPT is illustrated in Fig. 2.4.

2.3 Pitch Angle Controller Model

Wind power extraction by wind turbines depends on wind speed, and thus, output power of a wind generator always fluctuates due to variations in wind speed. For maintaining the output power of the generator below the rated level, two pitch angle controllers are considered in this thesis for FSWT with squirrel cage induction generator (FSWT-SCIG) and VSWT-PMSG as shown in Figs. 2.5 and 2.6.

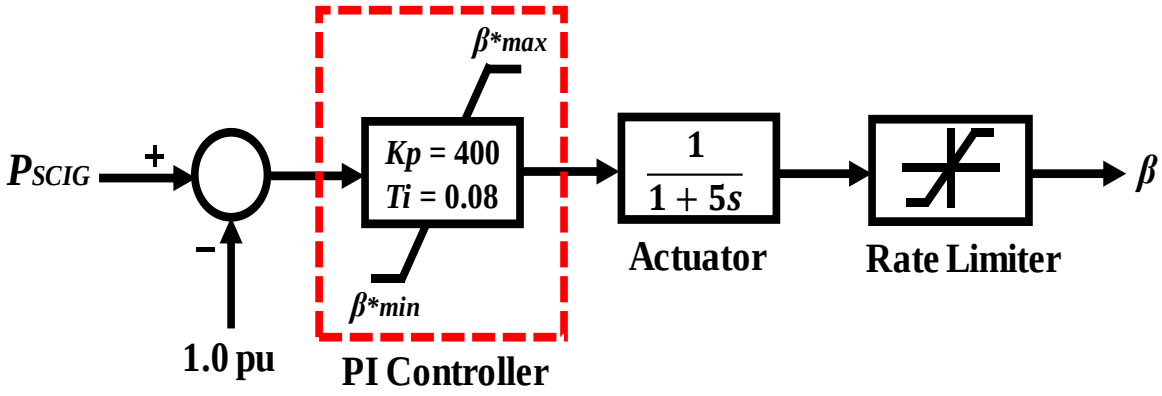

Fig. 2.5. Pitch controller for FSWT-SCIG.

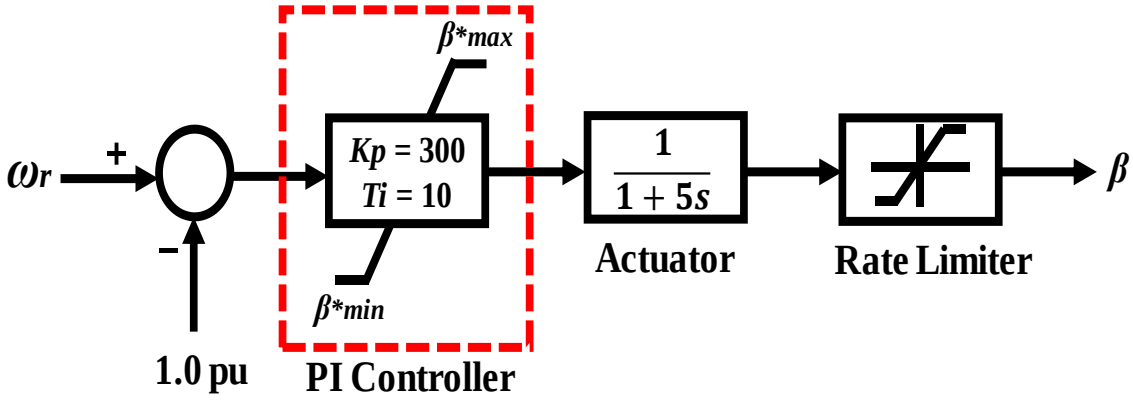

Fig. 2.6. Pitch controller for VSWT-PMSG.

The pitch angle control system for FSWT is used so that the SCIG output does not exceed the rated power, whereas for VSWT, it is used for controlling the rotor speed of PMSG not to exceed the maximum speed (rated ω_r of PMSG). In all of the pitch control systems, a PI controller is used to track the error signal.

2.4 Different Types of Wind Turbine Technology

2.4.1 FSWT-SCIG Technology

The schematic diagram of FSWT-SCIG is depicted in Fig. 2.7. The overall model consists of wind turbine, gearbox, grid-connected SCIG, capacitor bank and soft-starter. The wind turbine captures the wind power at its blades and converts it to the mechanical energy. Finally, this mechanical power is converted to the electrical power of the grid voltage and frequency by SCIG. The rotor speed of a SCIG varies according to the amount of power generated.

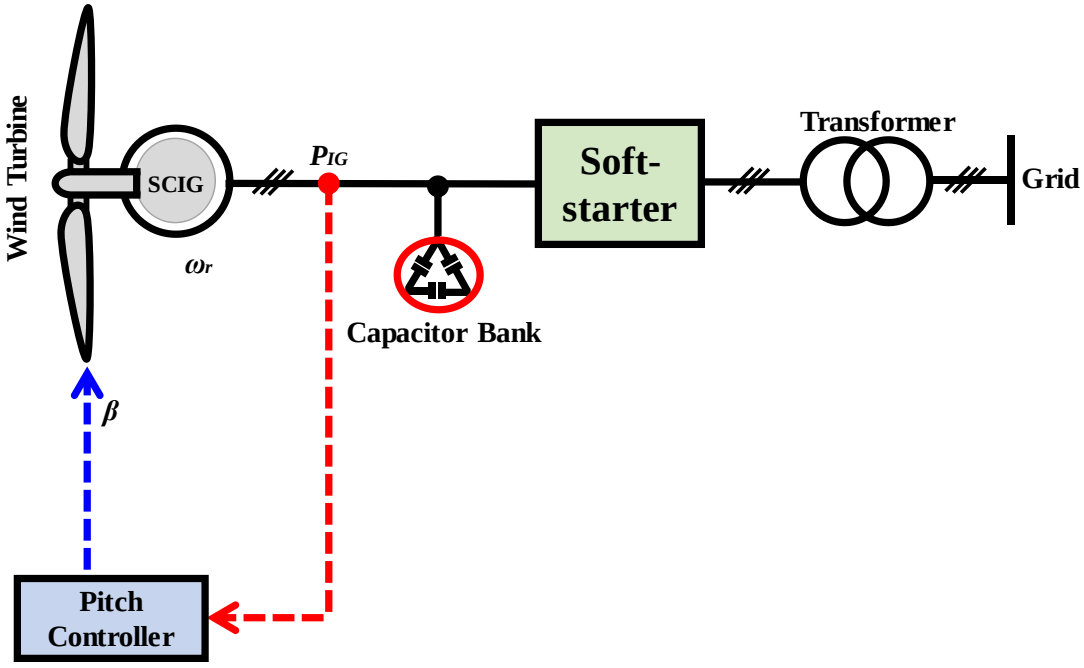

Fig. 2.7. Configuration of FSWT-SCIG.

The rotor speed variations of SCIG are, however, very small, approximately 1 to 2 % of the rated speed. Normally, the rotational speed of the generator is relatively high compared with that of wind turbine. Therefore, the wind turbine speed needs to be stepped up by using a multiple-stage gearbox with an appropriate gear ratio.

The SCIG absorbs reactive power from the grid system. The reactive power compensation is compensated by using the capacitor bank, which should be placed near the generator terminal. Since the SCIG does not have, basically, an ability to control active power output by itself, the active power output is controlled by using the pitch angle controller. The pitch angle controller will be activated when the active power output of SCIG is greater than the rated condition.

The FSWT-SCIG technology is the simplest wind turbine technology which has many superior characteristics such as low cost, operation simplicity, brushless and rugged construction.

However, low aerodynamic efficiency, high mechanical stress during gusty wind speeds, and difficulties in adapting to new grid compliances, such as low voltage ride-through (LVRT) and reactive power support, are the shortcomings of this concept.

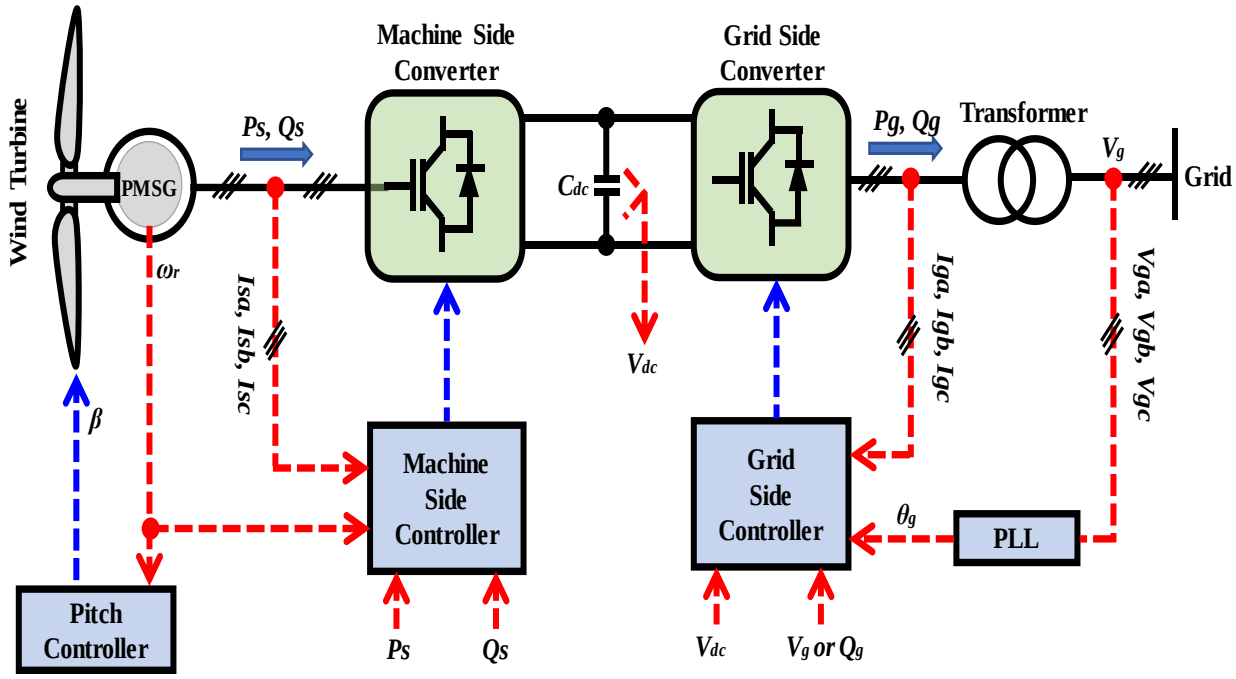

Fig. 2.8. Configuration of VSWT-PMSG.

2.4.2 VSWT-PMSG Technology

The schematic diagram of VSWT-PMSG is shown in Fig. 2.8. A direct-drive PMSG wind turbine uses a synchronous generator whose rotor is excited by permanent magnets. The stator terminal is connected to the grid through a full rating AC/DC/AC converter based on the two levels of insulated gate bipolar transistors (IGBTs). The large number of poles mounted on the rotor allows the generator to operate at low speeds, which means that the gearbox can be omitted, and the generator is directly coupled with the wind turbine. The AC/DC/AC converter is composed of machine side converter (MSC) and grid side converter (GSC). The three phase AC output is converted to the DC voltage by using MSC and finally the DC voltage is converted to the AC voltage of the grid voltage and frequency by using GSC. The full-scale AC/DC/AC converter controls the generated power and the power flow to the grid. In addition, it decouples the electrical grid frequency and the mechanical rotor frequency, and thus the variable speed generation can be possible.

2.5 Chapter Conclusion

In this chapter, an overview of the wind turbine system followed by power extraction is explained. Then the pitch angle controller models for FSWT-SC and VSWT-PMSG are described. Finally, the different types of wind turbine technologies are briefly stated.

Chapter 3

Simplified Model of HVDC Transmission System Connecting Offshore Wind Farm to Onshore Power Grid

This chapter presents a simplified model of voltage source converter based high voltage DC (VSC-HVDC) transmission system for dynamic simulation study. The aim of the simplified model is to diminish the complexity and simulation time of the analysis of grid integrated offshore wind farm (OWF) connected through VSC-HVDC transmission line. This is because simulation analysis of OWF based on the detailed VSC-HVDC model needs very large computation time. To evaluate performance of the derived simplified model of VSC-HVDC, simulation analysis is performed on a multi-machine power system model composed of variable speed wind turbines with permanent magnet synchronous generators (VSWT-PMSGs), VSC-HVDC, and synchronous generators (SGs). Comparative analysis between the proposed simplified model and the detailed model of VSC-HVDC is also performed and presented. The simulation results show that the proposed simplified model of VSC-HVDC has sufficient accuracy for analyzing dynamic characteristics.

3.1 Introduction

Penetration of OWFs into the power system has been increasing significantly since the last decade. OWFs tend toward large capacity to make good use of the stronger winds [26-28]. But grid integration issues of OWFs could seriously impact the operation and stability of their interconnected onshore power system. OWFs are located, in general, several 10s km or more far from the onshore grid connection point. It is a great challenge for both WF developer and transmission system operator (TSO) to transmit hundreds of MW offshore wind power over such a long distance. Most commonly, high voltage AC (HVAC) transmission systems are used for the integration of OWFs to the onshore power grid. However, there can be a case in which HVAC is not suitable from an economical and technical points of view.

On the other hand, VSC-HVDC transmission becomes more attractive and practical to integrate large-scale OWFs into the onshore power grid, due to its high capacity, advanced controllability, lower cable losses, independent and fast control of active and reactive power, and stabilization potential for AC networks [30-35].

The use of VSC-HVDC for connecting OWF to onshore grid has been reported already in some literature [36-39]. In [36, 37], the WF considered is composed of fixed speed induction generators. In [38], SGs are used in the OWF. Doubly fed induction generator (DFIG) is chosen as wind generator for OWF in [39].

However, PMSG is becoming very popular nowadays as variable speed wind generator. In PMSG, the excitation is provided by permanent magnets instead of field winding. Permanent magnet machines are characterized as having large air gaps, which reduce flux linkage even in machines with multi magnetic poles [40]. As a result, low rotational speed generators can be manufactured with relatively small sizes with respect to its power rating. Moreover, gearbox can be omitted due to low rotational speed in PMSG wind generation system, resulting in low cost. Also the amplitude and frequency of the generator voltage can be fully controlled by the converter [41-52]. Therefore, WF composed of VSWT-PMSG is considered in this study.

Simulation analysis in PSCAD/EMTDC software of detailed model of VSC-HVDC connecting OWF to the onshore multi-machine power system requires large computation time due to the switching phenomena of the power converters. Therefore, detailed model of the VSC-HVDC should be simplified in the analysis to diminish complexity and long simulation time.

In this chapter, a simplified model of VSC-HVDC transmission system is developed for fast dynamic simulation analysis. Real wind speed data measured in Hokkaido Island, Japan, is used in the simulation analyses to obtain the realistic responses. Also, comparative analysis of dynamic characteristic between the proposed simplified and the detailed models is performed by using PSCAD/EMTDC software.

3.2 Power System Model

Fig. 3.1 depicts the power system model considered in the analysis, which is composed of nine-bus main system and two WFs. The nine-bus system consists of two thermal power plants (SG1 rated at 300MVA and SG2 rated at 200MVA) and a hydro power plant (SG3 rated at 100MVA). SG1 is operated under load frequency control (LFC). SG2 and SG3 are operated under governor free (GF) control. LFC is used to control frequency fluctuation with a long period more than a few minutes, and GF is used to control fluctuation with a short period less than a minute.

The IEEE type AC4A excitation system model shown in Fig. 3.2 [109] is used for all SGs. The parameters of IEEE type AC4A excitation system model are taken from [109]. Fig. 3.3 shows

the thermal governor model used in SG1 and SG2 [110]. The hydro governor model used for SG3 is shown in Fig 3.4 [110]. The values of 65M and 77M are presented in Table 3.1.

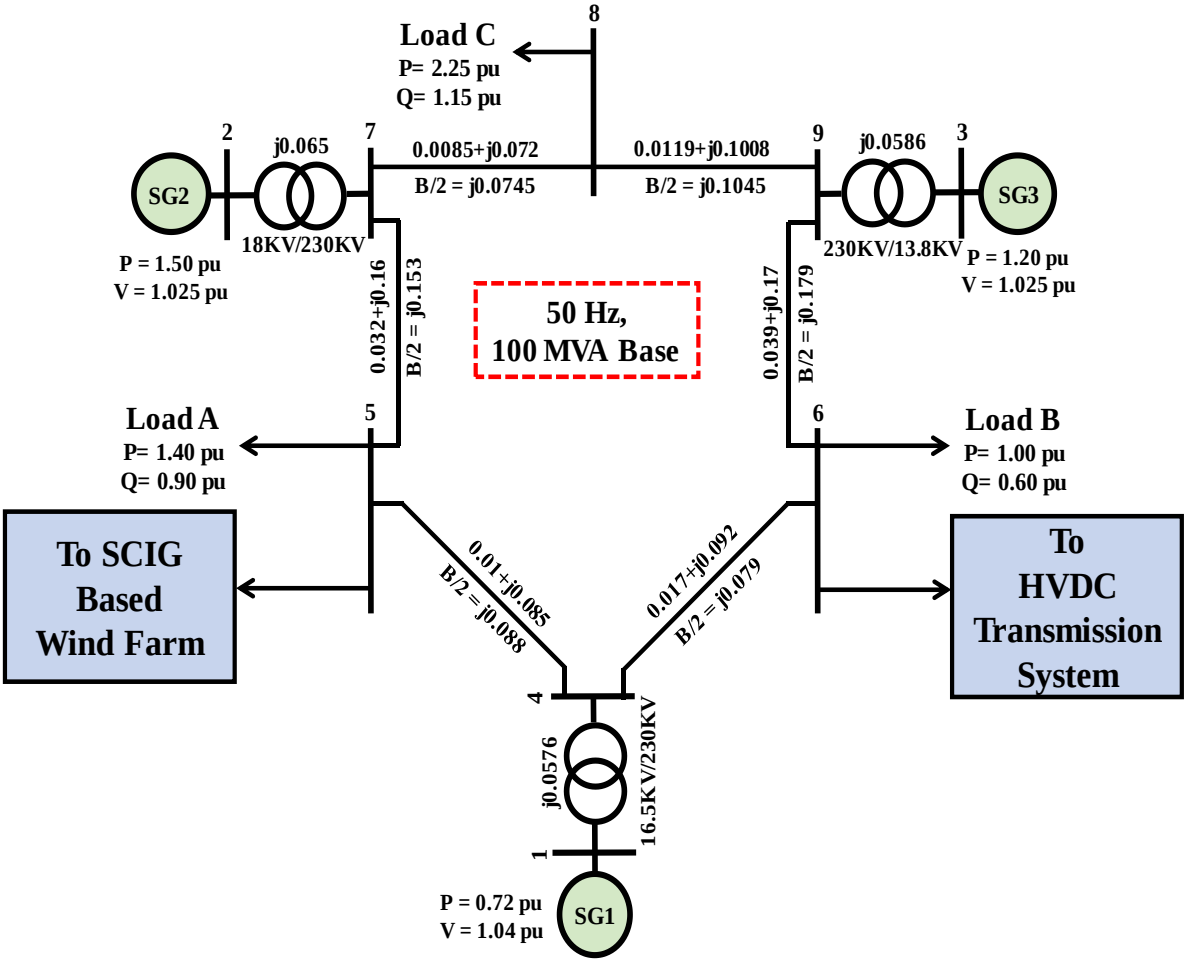

Fig. 3.1. Power system model.

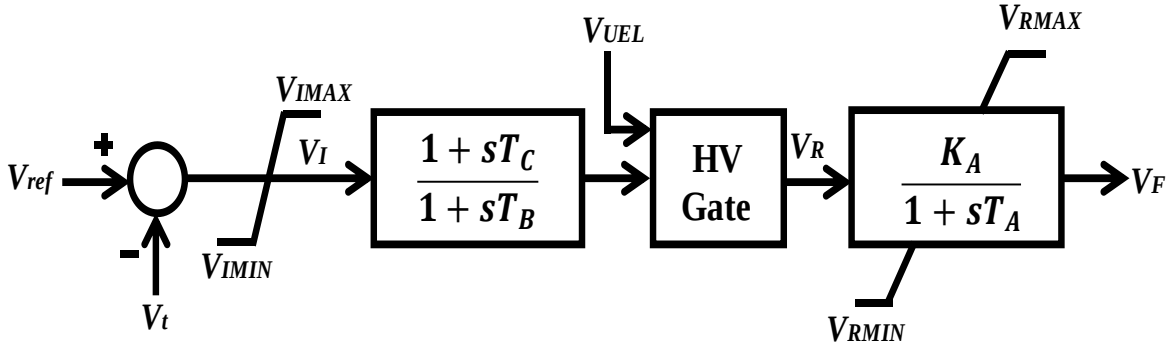

Fig. 3.2. IEEE type AC4A excitation system model.

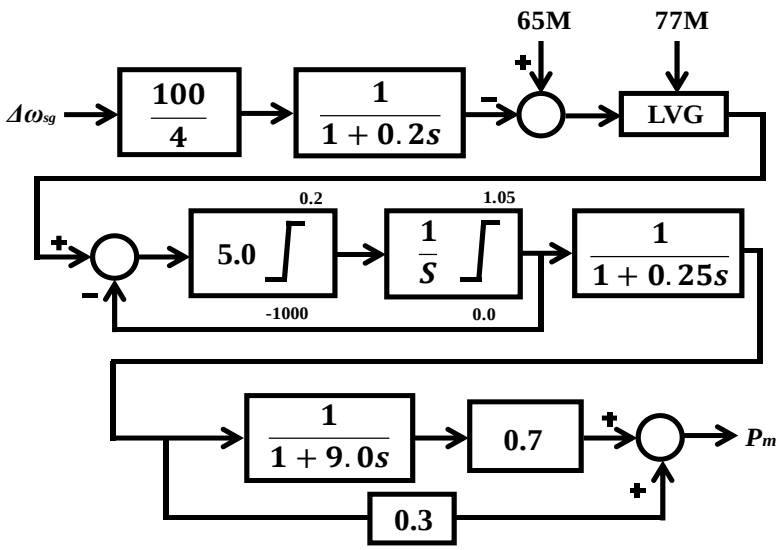

Fig. 3.3. Thermal governor model.

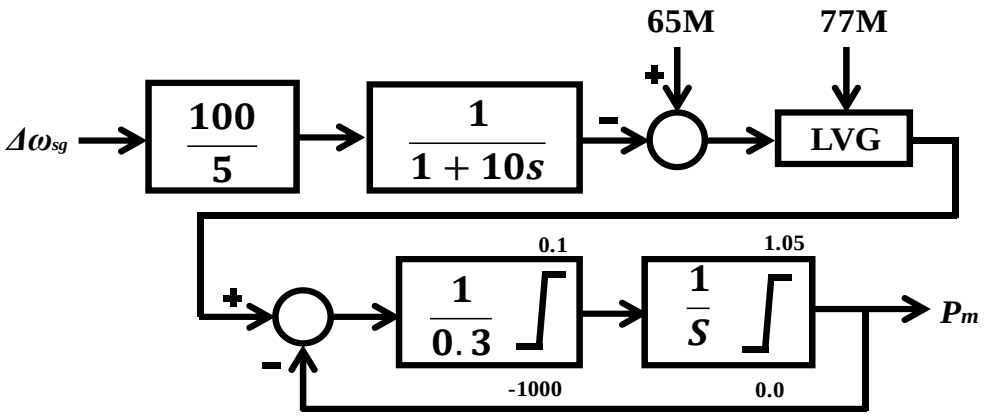

Fig. 3.4. Hydro governor model.

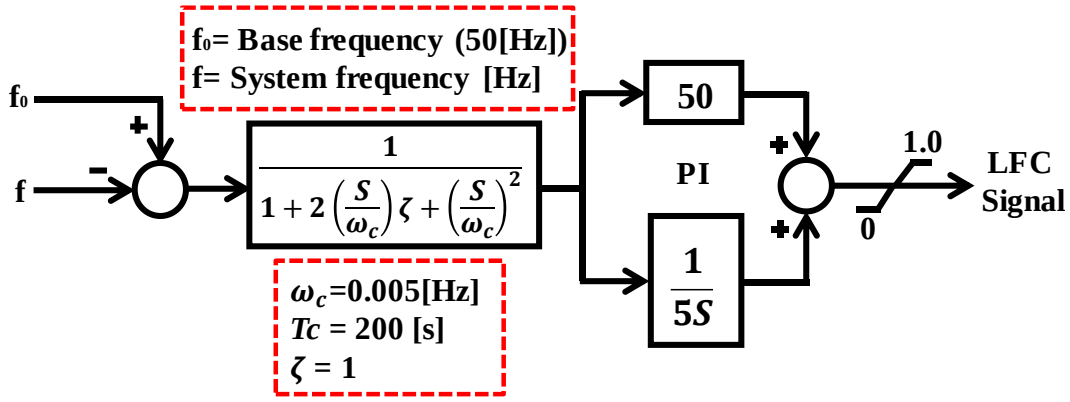

Fig. 3.5. LFC model.

In Figs. 3.3 and 3.4, $\Delta\omega_{sg}$: the revolution speed deviation [pu], 65M: the initial output [pu], 77M: the load limits (65M + rated MW output × PLM [%]), PLM: the spare governor operation

[%], P_m: the turbine output [pu]. Fig. 3.5 shows the LFC model used in this study. The LFC sends the output value signal to the power plant (SG1) after detecting frequency deviations. Then, governor output value (65M) of the power plant is changed by LFC signal, and the power plant output is changed.

Table 3.1. Values of 65m and 77M.

SG1 (Thermal)	***Frequency control***	***65M***	***77M***
	LFC	LFC signal	1
SG2 (Thermal)	***Frequency control***	***65M***	***77M***
	GF	0.80	0.84
SG3 (Hydro)	***Frequency control***	***65M***	***77M***
	GF	0.80	0.84

Table 3.2. Parameters of conventional SGs and wind generators.

SGs				**PMSG**		**SCIG**	
Parameters	SG1	SG2	SG3	MVA	20 (each)	MVA	20 (each)
Rated Power	300 MVA	200 MVA	100 MVA	R_{st}	0.02 pu	R_1	0.01 pu
Voltage	16.5 kV	18 kV	13.8 kV	L_{dst}	0.96 pu	X_1	0.1 pu
R_a	0.003 pu	0.003 pu	0.003 pu	L_{qst}	0.76 pu	X_m	3.5 pu
X_l	0.1 pu	0.1 pu	0.1 pu	Ψ_m	1.4 pu	R_{21}	0.035 pu
X_d	2.11 pu	2.11 pu	1.20 pu	H	3.0 s	R_{22}	0.014 pu
X_q	2.05 pu	2.05 pu	0.700 pu			X_{21}	0.03 pu
$X`_d$	0.25 pu	0.25 pu	0.24 pu			X_{22}	0.089 pu
$X``_d$	0.21 pu	0.21 pu	0.20 pu			H	1.5 s
$X``_q$	0.21 pu	0.21 pu	0.20 pu				
$T`_{do}$	6.8 s	7.4 s	7.2 s				
$T``_{do}$	0.033 s	0.033 s	0.031 s				
$T``_{qo}$	0.030 s	0.030 s	0.030 s				
H	4.0 s	4.5 s	4.3 s				

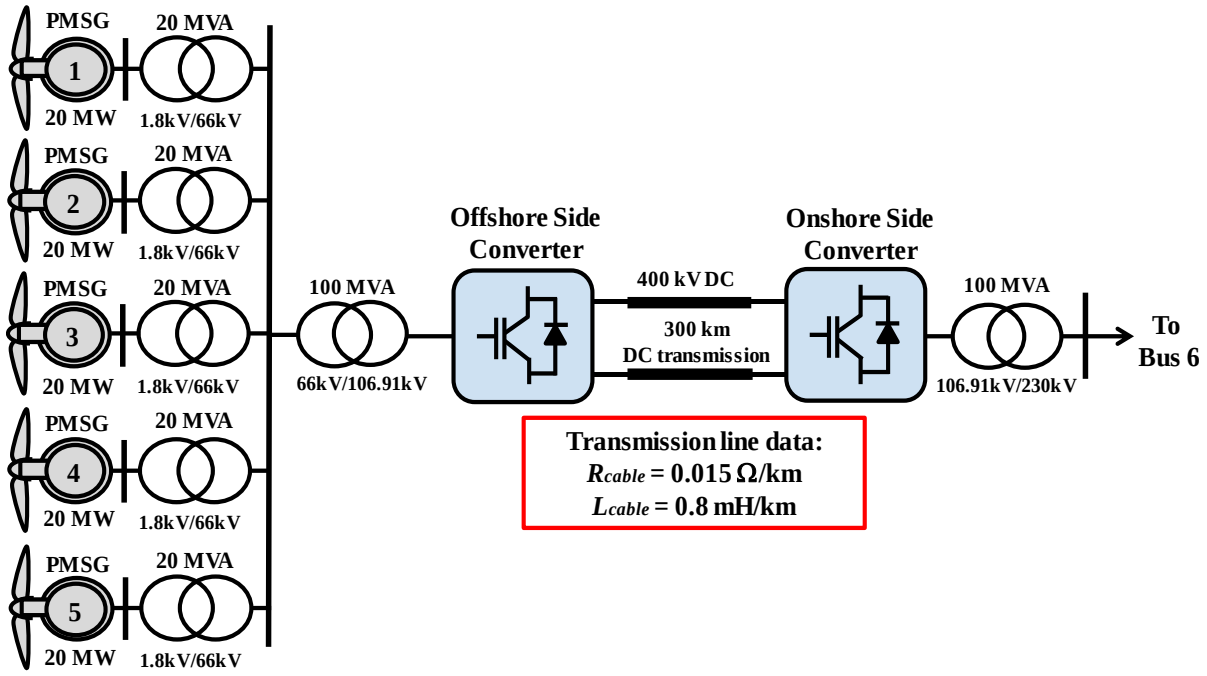

Fig. 3.6. Layout of OWF connected to the main power system through 400 kV VSC-HVDC transmission system.

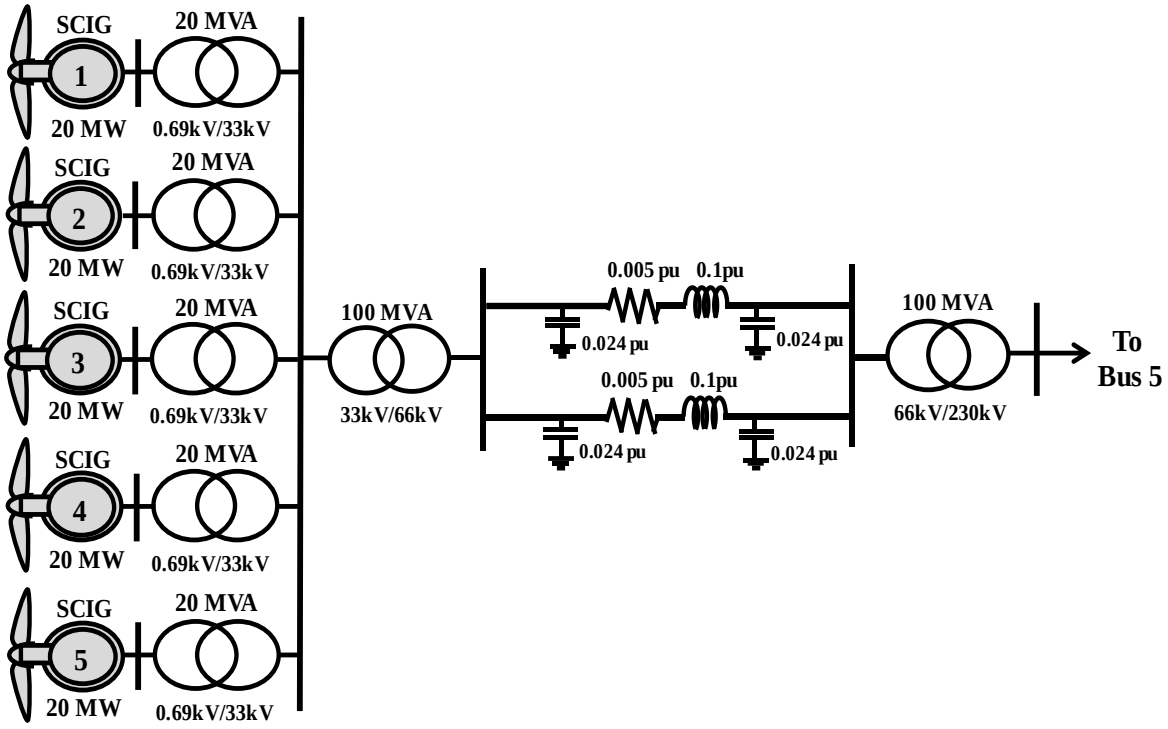

Fig. 3.7. Layout of FSWT-SCIGs based WF.

An OWF is connected to bus 6 through 400kV VSC-HVDC transmission system as depicted in Fig. 3.6. The length of the HVDC transmission line is 300km. The OWF is composed of five VSWT-PMSGs (rated at 20MW each). The simplified model of VSWT-PMSG and its control system presented in [105] are used in this study. Another WF is connected to bus 5 of the main system as depicted in Fig. 3.7. This WF is composed of five fixed speed wind turbine with squirrel cage induction generators (FSWT-SCIGs). The capacity of each FSWT-SCIG is 20MW. It is connected to the grid system through transformers and double circuit transmission line. Each VSWT-PMSG and FSWT-SCIG represents aggregated model. The aerodynamic model of wind turbine is described in Chapter 2. The parameters of conventional SGs, PMSG and SCIG are presented in Table 3.2 [105, 111].

3.3 Modeling and Control Strategy of PMSG

The overall block diagram of VSWT-PMSG model is shown in Fig. 3.8. In this study, the simplified model is used to decrease the simulation time [105].

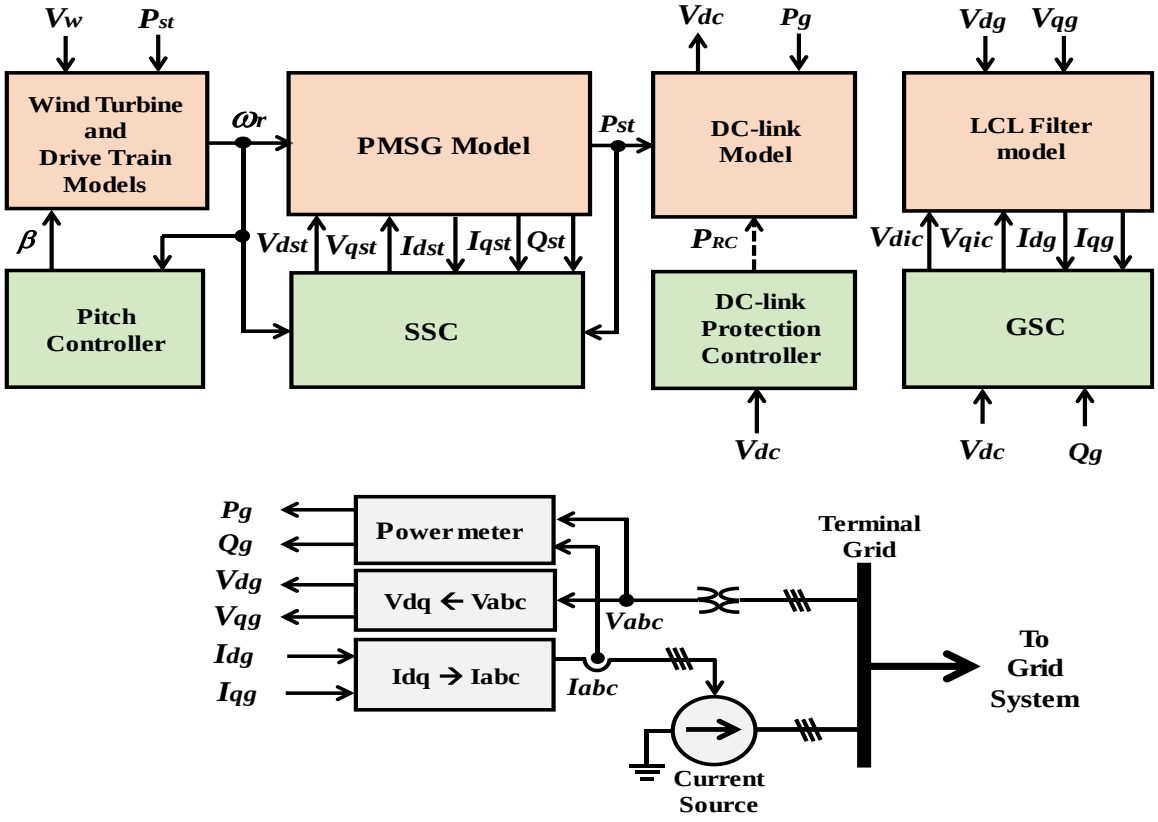

Fig. 3.8. Simplified model of VSWT-PMSG.

The model consists of mechanical part, electrical part, and control system part. The mechanical part includes wind turbine and drive train models; the electrical part includes PMSG, DC-Link circuit, and LCL filter models; and the controller system part includes pitch controller, DC-Link circuit protection controller, stator side controller (SSC), grid side controller (GSC), and the interface with grid system. The interface inputs the terminal grid voltage to the simplified model and injects the output current from the simplified model to the grid system through a three phase current source [105].

3.3.1 Stator Side Controller (SSC)

The block diagram of SSC is depicted in Fig. 3.9, which controls the active and reactive power of PMSG by controlling the q-axis stator current (I_{qst}) and the d-axis stator current (I_{dst}), respectively. SSC consists of four conventional PI controllers to compensate different error signals. Power reference (P_{ref}) is obtained from MPPT controller with the power losses reduced. The reactive power reference (Q_{st}*) is set to zero for unity power factor operation.

3.3.2 Grid Side Controller (GSC)

The block diagram of GSC is shown in Fig. 3.10, which controls the DC-Link voltage (V_{dc}) and the reactive power delivered to the grid system (Q_g) by controlling the q-axis current (I_{qg}) and the d-axis current (I_{dg}) of LCL filter output current, respectively. The four PI controllers are used to track the different error signals.

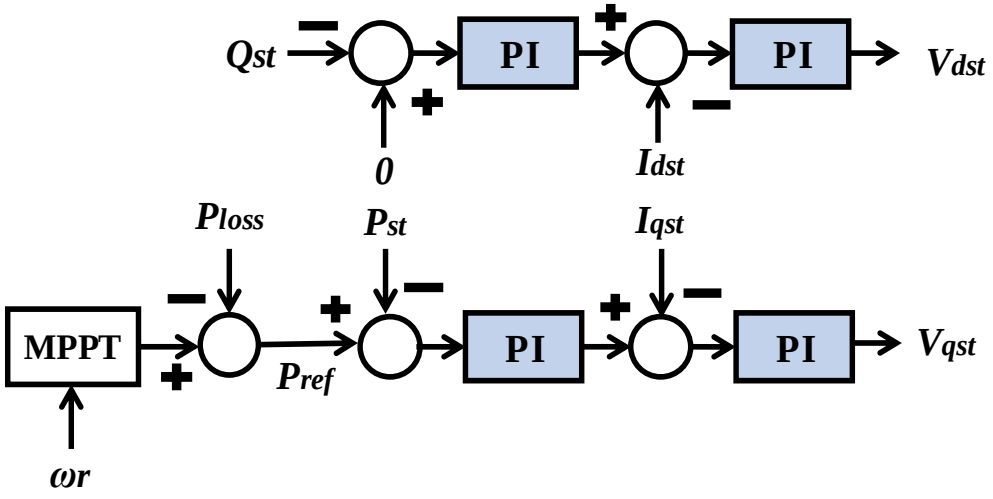

Fig. 3.9. Block diagram of SSC.

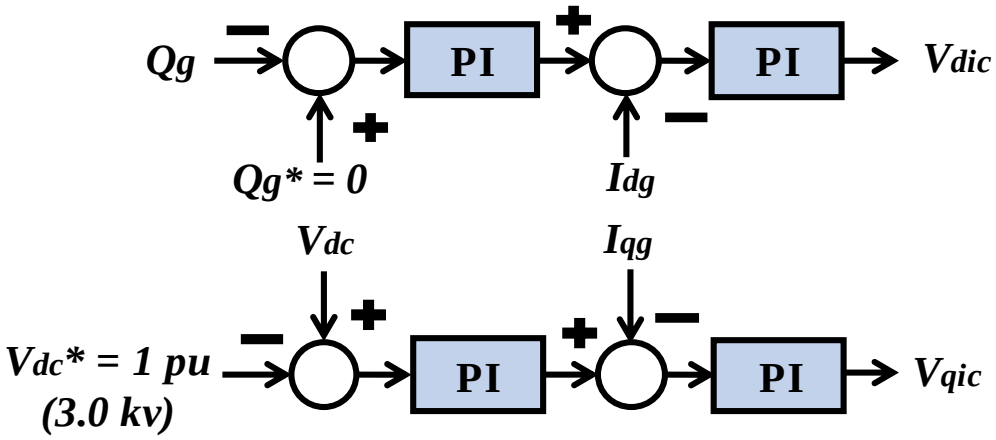

Fig. 3.10. Block diagram of GSC.

3.4 VSC-HVDC Transmission System Model

3.4.1 Detailed Model of VSC-HVDC System

Block diagram of the detailed model of VSC-HVDC system along with its control system is shown in Fig. 3.11. It consists of rectifier and inverter based on the two levels of Insulated Gate Bipolar Transistor (IGBT) which are controlled by Rectifier Controller (RC) and Inverter Controller (IC). The Pulse Width Modulation (PWM) technique is used in the detailed model of VSC-HVDC system for both inverter and rectifier. The carrier frequency is 3.0 KHz.

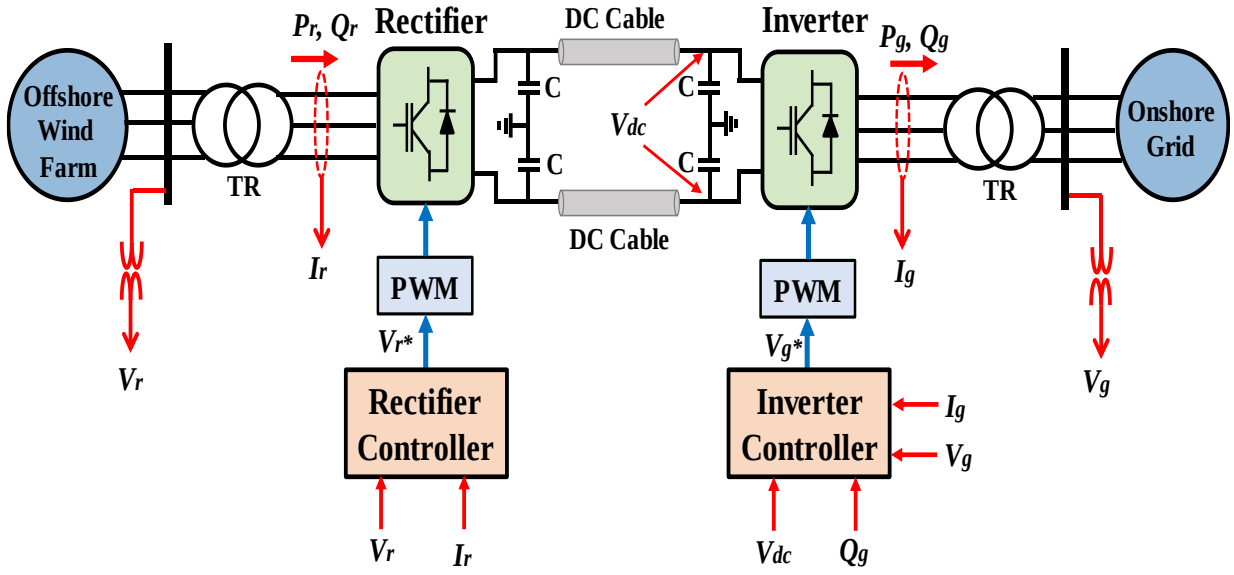

Fig. 3.11. Detailed model of VSC-HVDC system.

Three phase AC voltage generated by the OWF is rectified to DC voltage through the rectifier. Three phase current (*Ir*), voltage (*Vr*), active power (*Pr*), and reactive power (*Qr*) are detected on the offshore side AC system. The rectified DC voltage is transmitted to the onshore side. The transmitted DC voltage is converted again into AC voltage through the onshore side inverter. The grid current (*Ig*), grid voltage (*Vg*), and reactive power (*Qg*) are detected on the onshore side AC system.

3.4.1.1 Rectifier Controller System

Block diagram of the RC is illustrated in Fig. 3.12. The aim of the RC is to ensure the normal operation of VSC-HVDC connection based OWF. The rectifier station must establish an AC voltage of stable amplitude and frequency for the local grid of OWF. The voltage magnitude and phase of OWF are controlled by d-axis current (*Ird*) and q-axis current (*Irq*) of VSC-HVDC rectifier system. The voltage magnitude reference is chosen as 1.0 pu and voltage phase reference is set to 0.0 degree for stable operation of OWF.

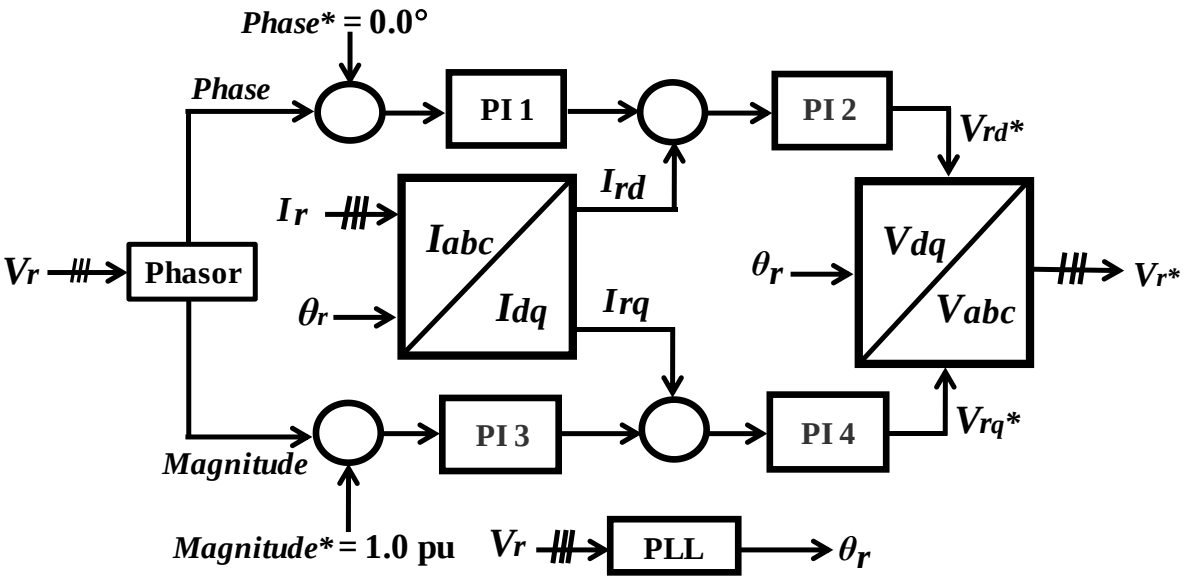

Fig. 3.12. Rectifier controller system.

3.4.1.2 Inverter Controller System

Fig. 3.13 shows the IC. The controller is used to control the reactive power (*Qg*) delivered to the onshore grid and keep the dc-link voltage (*Vdc*) constant by using d-axis (*Igd*) and q-axis

(I_{gq}) currents of VSC-HVDC inverter system respectively. The reactive power reference is set to 0.0 pu for unity power factor operation.

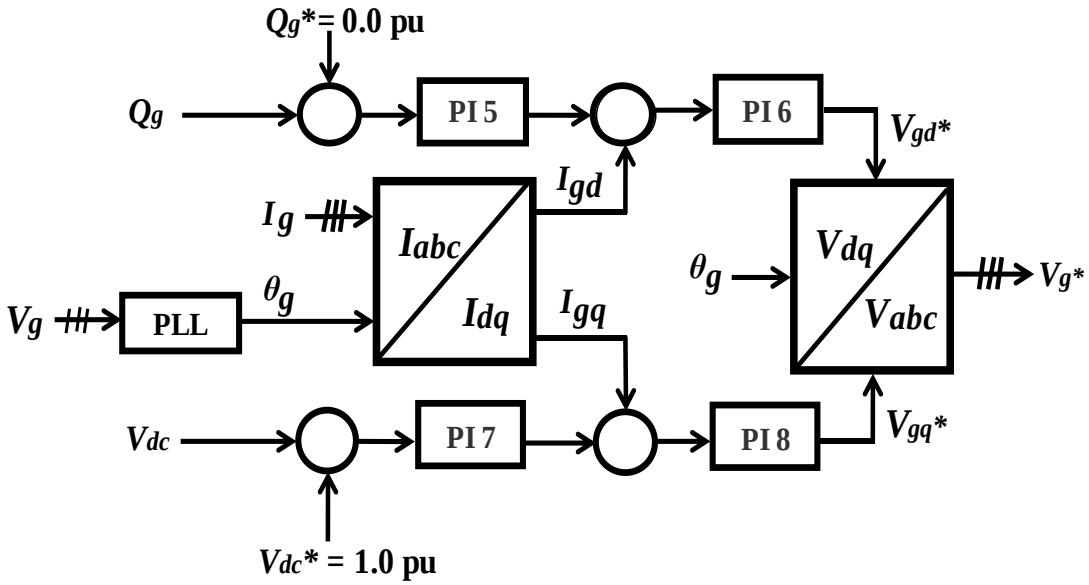

Fig. 3.13. Inverter controller system.

3.4.2 Proposed Simplified Model of VSC-HVDC System

The main objective of the proposed simplified model of VSC-HVDC is to reduce complexity of the detailed model and computation time for simulation analysis. The accuracy level of dynamic characteristics in this context refers to the ability of the simplified model to characterize active and reactive power output in the both offshore side and onshore side, and dc-link voltage performances under wind speed variations.

A configuration of simplified model of VSC-HVDC system with its control system is depicted in Fig. 3.14. The controlled voltage sources are used both in offshore side and onshore side instead of rectifier and inverter to remove the complexity of the switching devices. As a result of that, the simulation time will be reduced significantly.

3.4.2.1 Rectifier Controller System

The rectifier side voltage source is controlled by RC as illustrated in Figs. 3.12

3.4.2.2 Inverter Controller System

The inverter side voltage source is controlled by IC as illustrated in Figs. 3.13.

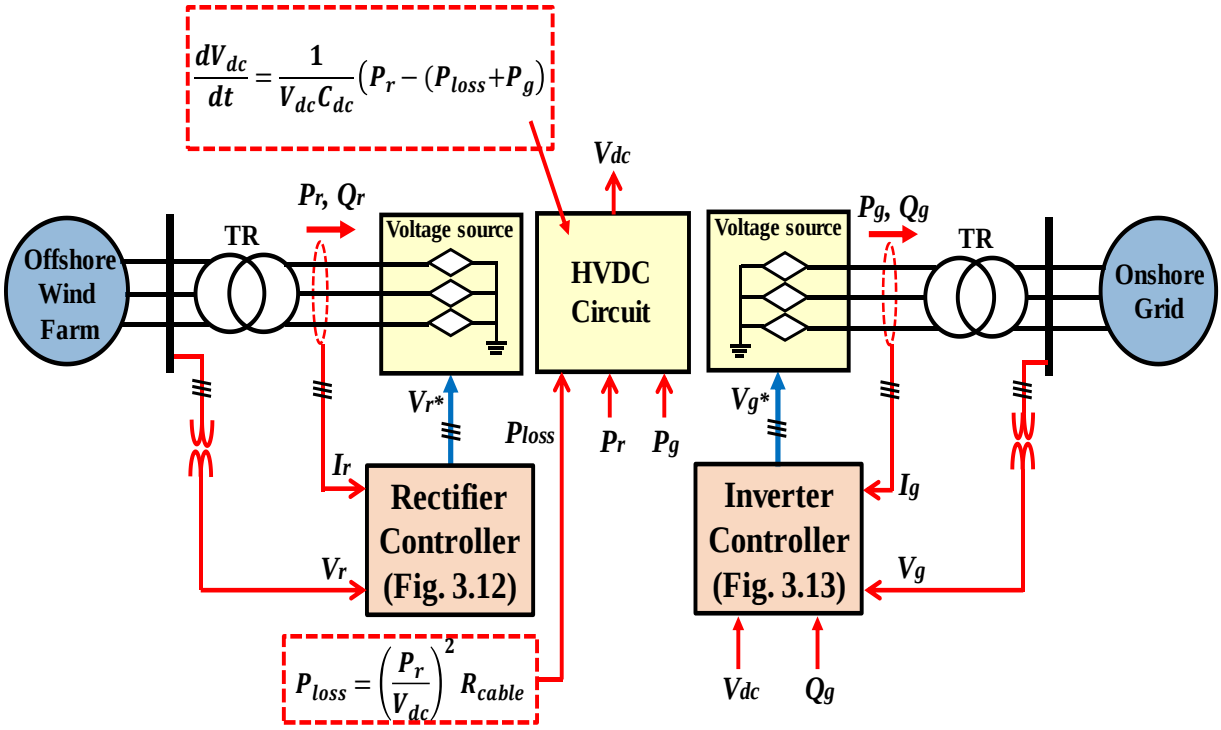

Fig. 3.14. Simplified model of VSC-HVDC system.

3.4.2.3 DC-Link Model

The portion of the HVDC circuit is expressed based on the power balance [112], which means that the power supplied from the OWF must be equal to the sum of the power received by the grid and transmission line loss. In Fig. 3.14, *Vdc* is the DC-Link circuit voltage, *Cdc* is the DC-Link capacitor, *Pr* is the supplied power from the OWF, *Pg* is the grid side power, and *Ploss* is the power loss.

3.5 Simulation Results

Simulation analysis is performed on the model system depicted in Fig. 3.1 by using PSCAD/EMTDC software. The simulation time period is taken 600 s. The rated frequency is 50 Hz. The personal computer configuration for the simulation study is Intel (R) Core (TM) i7-4770M CPU@3.40GHz Ram 8GB. Since the simplified model does not represent the harmonics, much larger time step (100 microseconds) can be used in the simulation analyses.

The real wind speed data used in this study are depicted in Figs. 3.15 and 3.16, which were measured in Hokkaido Island, Japan. Comparative analysis between the detailed and simplified models of VSC-HVDC system has been performed and results are shown in Figs. 3.17 to 3.24.

The active power output of each VSWT-PMSG and FSWT-SCIG are illustrated in Figs. 3.17 and 3.18.

The total active and reactive powers of offshore side and onshore side of VSC-HVDC are depicted in Figs. 3.19 and 3.20. Fig. 3.21 shows the voltage (Vdc) in the VSC-HVDC transmission system. It is seen that the DC transmission voltage of VSC-HVDC system is almost constant at rated DC voltage (400kV). Fig. 3.22 shows the total active and reactive power output of SCIGs based WF.

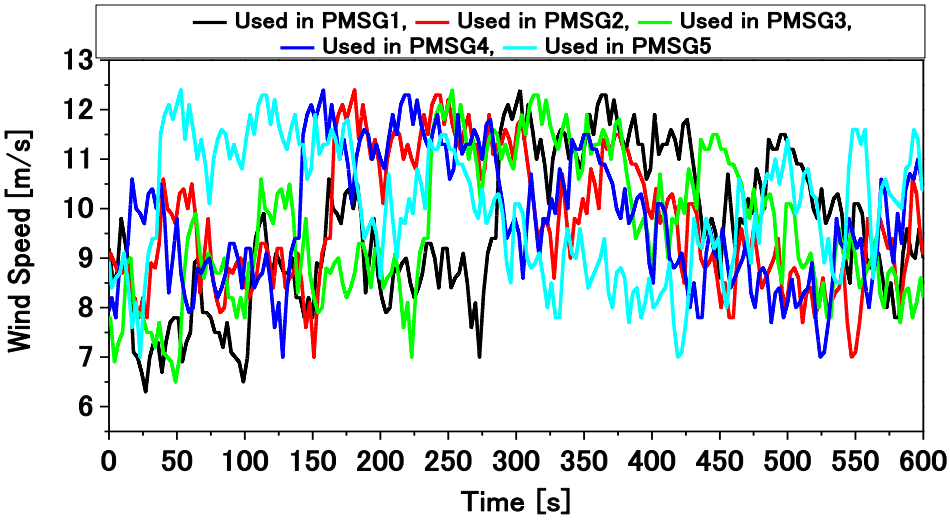

Fig. 3.15. Wind speeds used in VSWT-PMSGs.

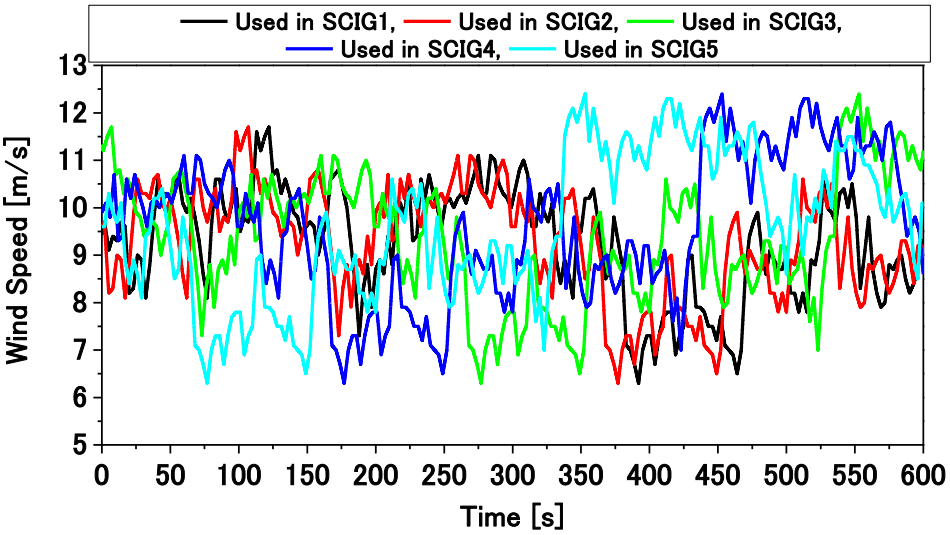

Fig. 3.16. Wind speeds used in FSWT-SCIGs.

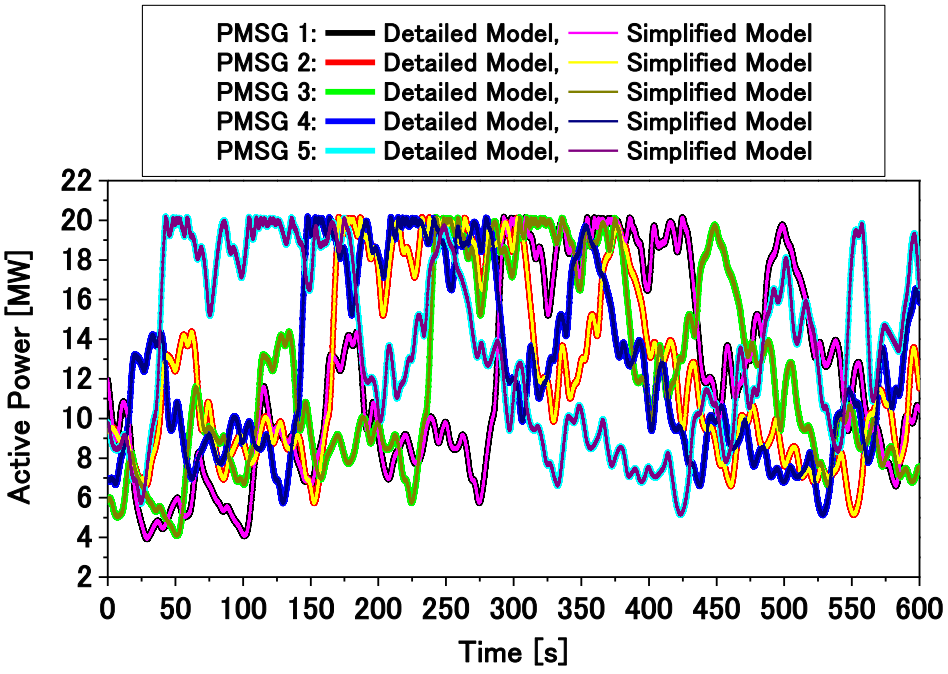

Fig. 3.17. Active power output VSWT-PMSGs.

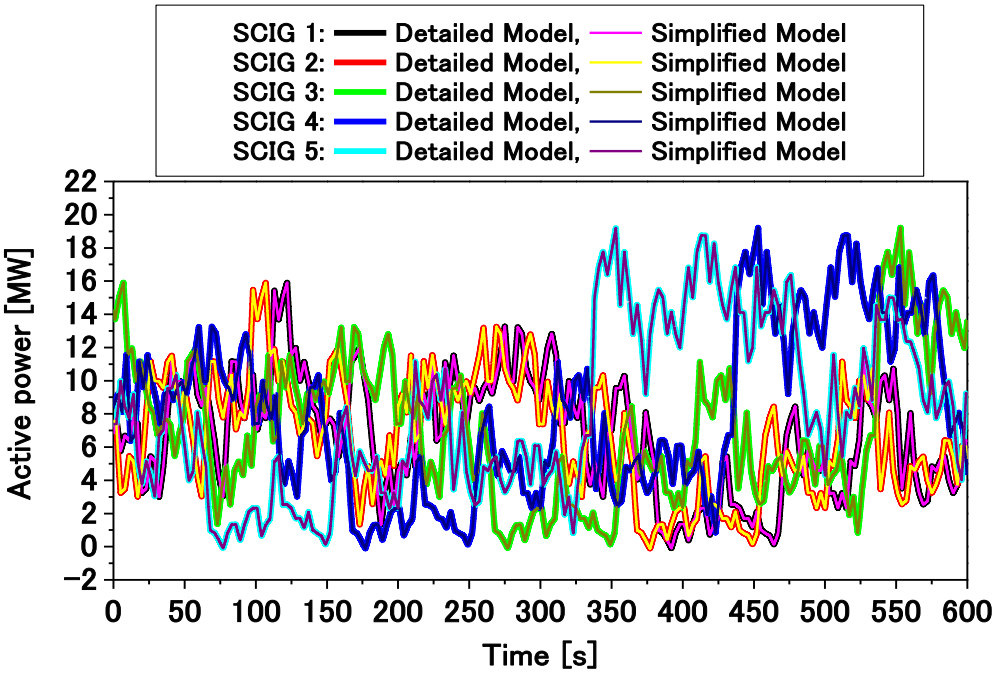

Fig. 3.18. Active power output FSWT-SCIGs.

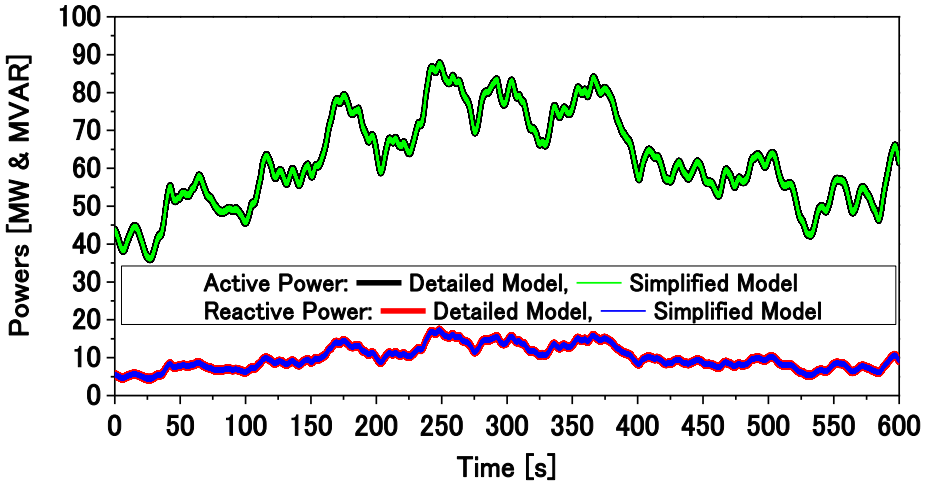

Fig. 3.19. Power input to offshore side of VSC-HVDC.

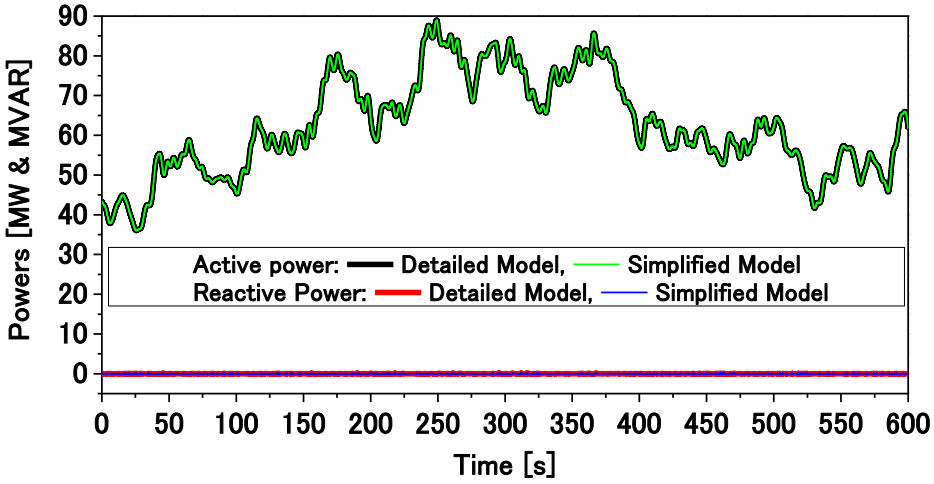

Fig. 3.20. Power output from onshore side of VSC-HVDC.

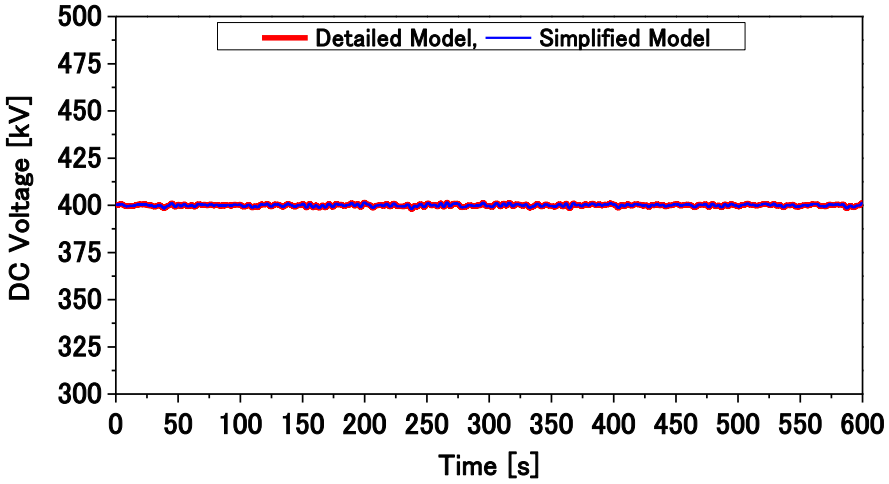

Fig. 3.21. V_{dc} in VSC-HVDC transmission line.

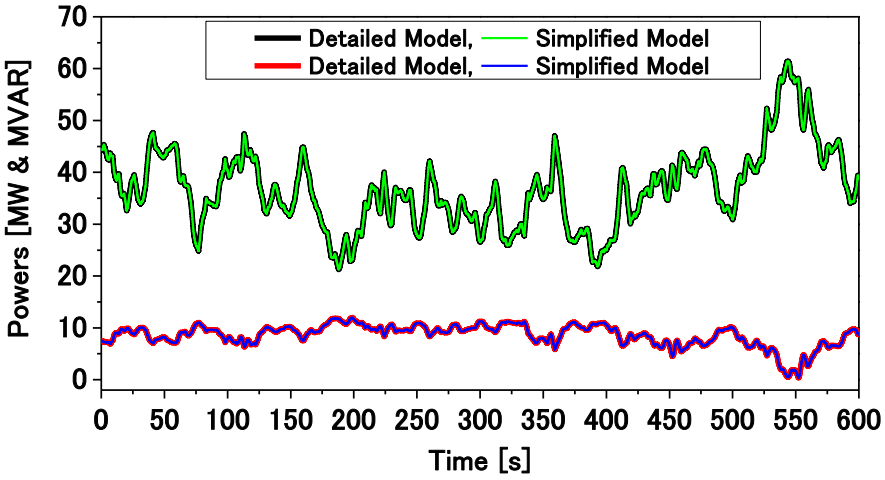

Fig. 3.22. Total active and reactive power output of FSWT-SCIGs based WF.

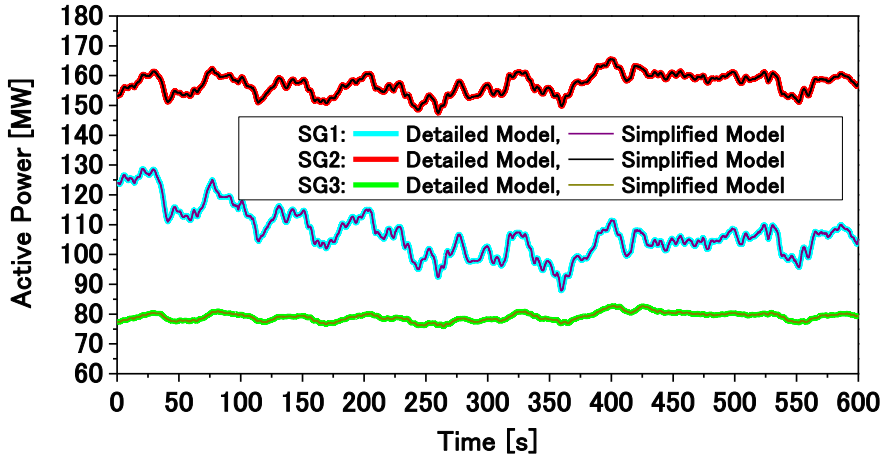

Fig. 3.23. Active power output of conventional SGs.

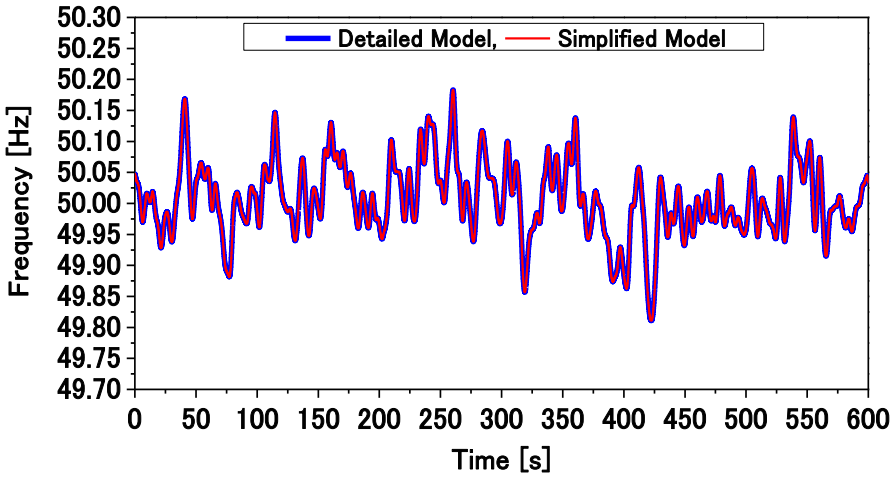

Fig. 3.24. Frequency response of the onshore power system.

Finally, the active power output of conventional SGs and frequency response of the onshore power system are illustrated in Figs. 3.23 and 3.24. It is seen that the conventional SGs adjust their active power output according to the fluctuating power injected from the VSC-HVDC based OWF.

From the simulation analyses, it can be concluded that the simplified model has sufficient accuracy. Moreover, the simulation time of the simplified model is much shorter than that of the detailed model of VSC-HVDC system as presented in Table 3.3.

Table 3.3. Computation Time of Each Model.

Simulation Duration	**Computation Time**	
	Detailed model	***Simplified model***
600 sec	59.2 hours	32 minutes
Time Step	10 μsec	100 μsec

3.6 Chapter Conclusion

In this chapter, a new simplified model of HVDC transmission system connecting OWF to onshore grid is proposed. Comparative analyses of dynamic characteristics between the simplified and detailed models have been performed in order to confirm the validity of the proposed simplified model of VSC-HVDC system. The simplified model of VSC-HVDC system has sufficient accuracy because there is almost no difference among the simulation results for the both simplified and detailed models. Moreover, the simulation time can be reduced significantly by using the proposed simplified model of VSC-HVDC system. Therefore, the proposed simplified model can be used effectively to analyze the power system with VSC-HVDC based OWF.

Chapter 4

Frequency Regulation of Power System by Constant Deloaded PMSG-based Offshore Wind Farm using Centralized Droop Controller

In this chapter, a new coordinated frequency control method is proposed for variable speed wind turbines with permanent magnet synchronous generators (VSWT-PMSGs) based offshore wind farm (OWF), which is connected to the main onshore grid through voltage source converter (VSC) based high voltage DC (HVDC) transmission system. The purpose of the proposed system is to damp the frequency oscillations of onshore grid due to the installation of large-scale fixed speed wind turbines with squirrel cage induction generators (FSWT-SCIGs) based wind farm (WF) and photovoltaic (PV) power station. A novel centralized droop controller with dead band is designed for VSWT-PMSGs to decrease the frequency fluctuations of the onshore main power system. In the proposed system, primary frequency reserve is implemented by deloaded operation of VSWT-PMSGs in the OWF. The effectiveness of the proposed centralized frequency controller is verified through simulation analysis on a modified IEEE nine-bus model system in PSCAD/EMTDC software.

4.1 Introduction

Penetration of large-scale renewable power sources like PV station and WF to the power grid has increased significantly. Accordingly, the operation of power system is becoming critical, because some of the conventional synchronous generators (SGs) need to be retired due to the penetration. The frequency oscillations of the power system due to large installations of renewable power sources is a key anxiety [62]. Large WFs like OWFs are, however, expected to contribute to the system frequency stabilization and new grid codes demand that the OWFs should work like conventional plants [41].

Usually, the characteristics of VSWT-PMSG based OWFs are different from that of the conventional power plants. Conventional SGs are able to control the frequency oscillations by load frequency control (LFC) and governor free (GF) operation. To contribute to the primary frequency

regulation in a similar way to conventional SGs, the VSWT-PMSG based OWFs require additional active power control loop and primary reserve.

On the other hand, OWF is, in general, far from the onshore grid connection point by several tens of km or more, and usually high voltage AC (HVAC) transmission system is used for connecting the OWF to the onshore power grid. However, HVAC system is not appropriate to very long transmission line from technical and economical points of view. Instead, VSC-HVDC transmission system is more attractive and practical for connecting large-scale OWF with the onshore power grid due to its advanced controllability, stabilization potential for AC networks, and high capacity [31].

Therefore, in this chapter, a coordinated frequency control method is proposed for VSWT-PMSG based OWF connected to the onshore grid through HVDC transmission line to reduce frequency variations of the onshore main power system. The centralized droop control technique is implemented with the dead band to limit the frequency variation within the permissible limit. In addition, the deloaded control strategy is adopted with the centralized droop controller to provide primary reserve. Deloaded operation is performed by controlling the speed of VSWT-PMSG and by modifying the maximum power point tracking (MPPT) power. Thus, better frequency regulation performance can be achieved. Real wind speed data measured in Hokkaido, Japan, is used in the simulation analyses to obtain the realistic responses.

The effectiveness of the proposed centralized frequency controller is verified through simulation analysis on a modified IEEE nine-bus model system composed of VSWT-PMSGs-based OWF connected to the main system through VSC-HVDC transmission line, FSWT-SCIGs-based onshore WF, PV power station, and conventional SGs.

4.2 Frequency Regulation of Power System by Rotor Speed Control-based Deloaded Operation of VSWT-PMSG

4.2.1 Power System Model

The power system model used in the analysis is shown in Fig. 4.1, which is composed of nine-bus main system and two WFs. The nine-bus system consists of two thermal power plants (SG1 rated at 300 MVA and SG2 rated at 200 MVA) and a hydro power plant (SG3 rated at 100 MVA). SG1 is operated under LFC. SG2 and SG3 are operated under GF control. An OWF is connected to bus 6 through 400kV VSC-HVDC transmission system as depicted in Fig. 4.2. The

length of the HVDC transmission line is 300 km. The OWF is composed of five VSWT-PMSGs (rated at 20 MW each). The second WF is connected to bus 5 of the main system as depicted in Fig. 4.3. This WF is composed of five FSWT-SCIGs. The capacity of each FSWT-SCIG is 20 MW. It is connected to the grid system through transformers and double circuit transmission line. Each VSWT-PMSG and FSWT-SCIG represents aggregated model. The aerodynamic model of wind turbine are already discussed in Chapter 2. Also, the parameters of SGs, PMSGs and SCIGs are discussed in Chapter 3.

The IEEE type AC4A excitation system model shown in Fig. 4.4 [109] is used for all SGs. The parameters of IEEE type AC4A excitation system model is taken from Ref. [109]. Fig. 4.5 shows the thermal governor model used in SG1 and SG2 [110]. The hydro governor model used for SG3 is shown in Fig 4.6 [110]. The values of 65M and 77M are presented in Table I.

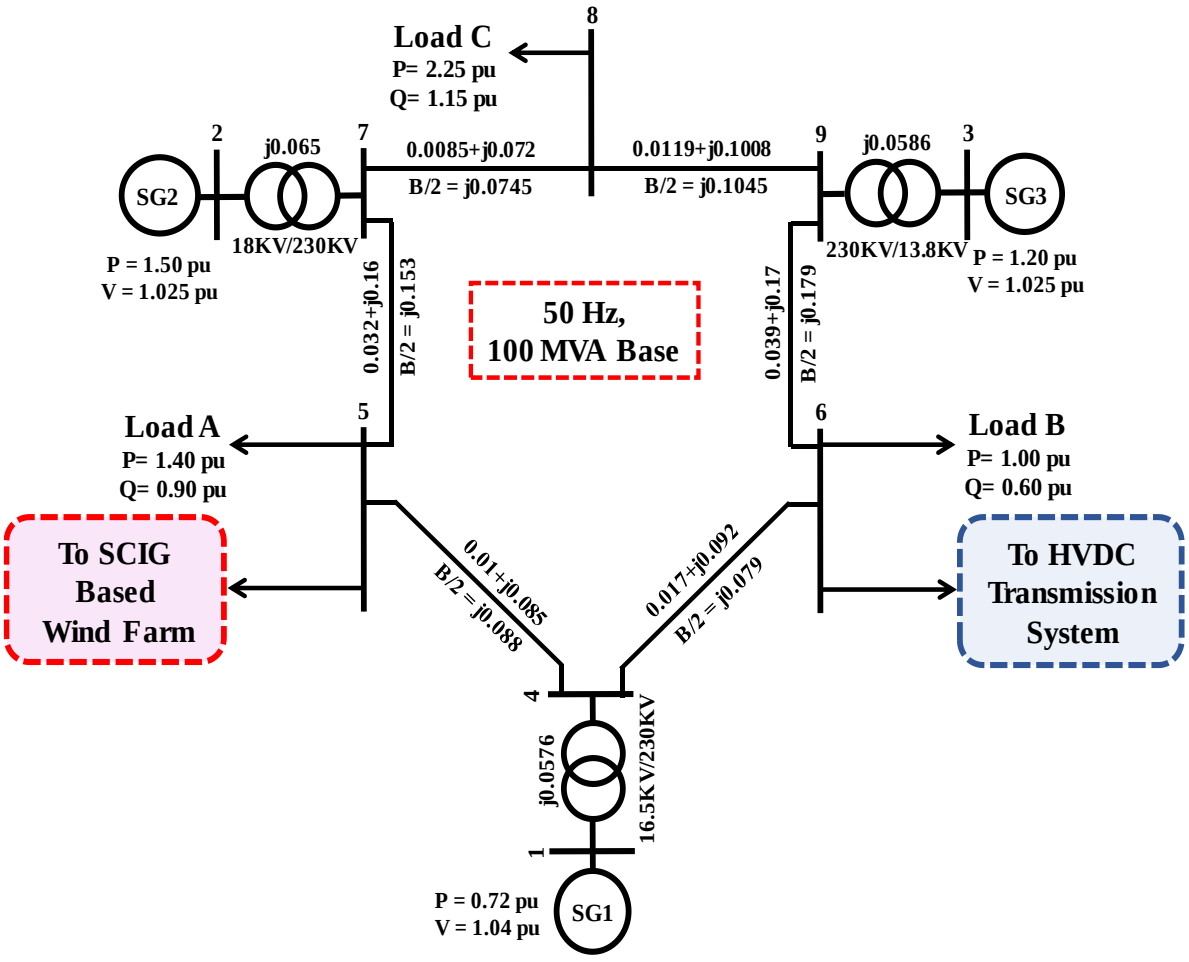

Fig. 4.1. Power system model.

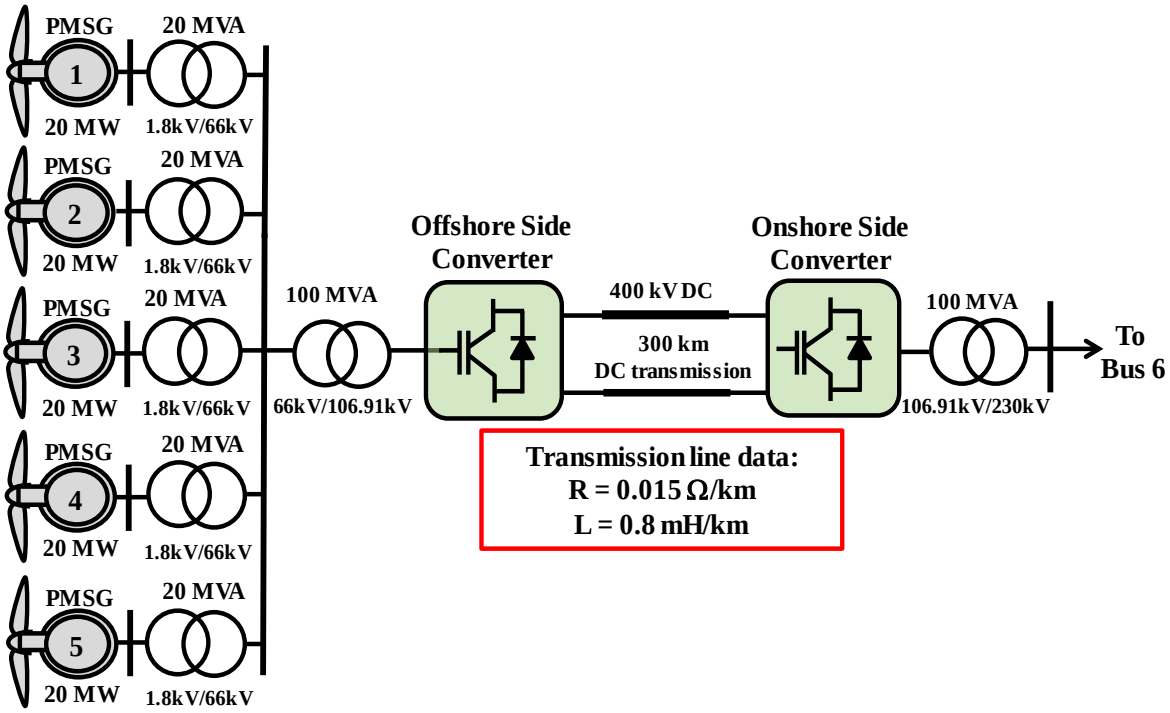

Fig. 4.2. Configuration of VSWT-PMSG based OWF connected through VSC-HVDC transmission system.

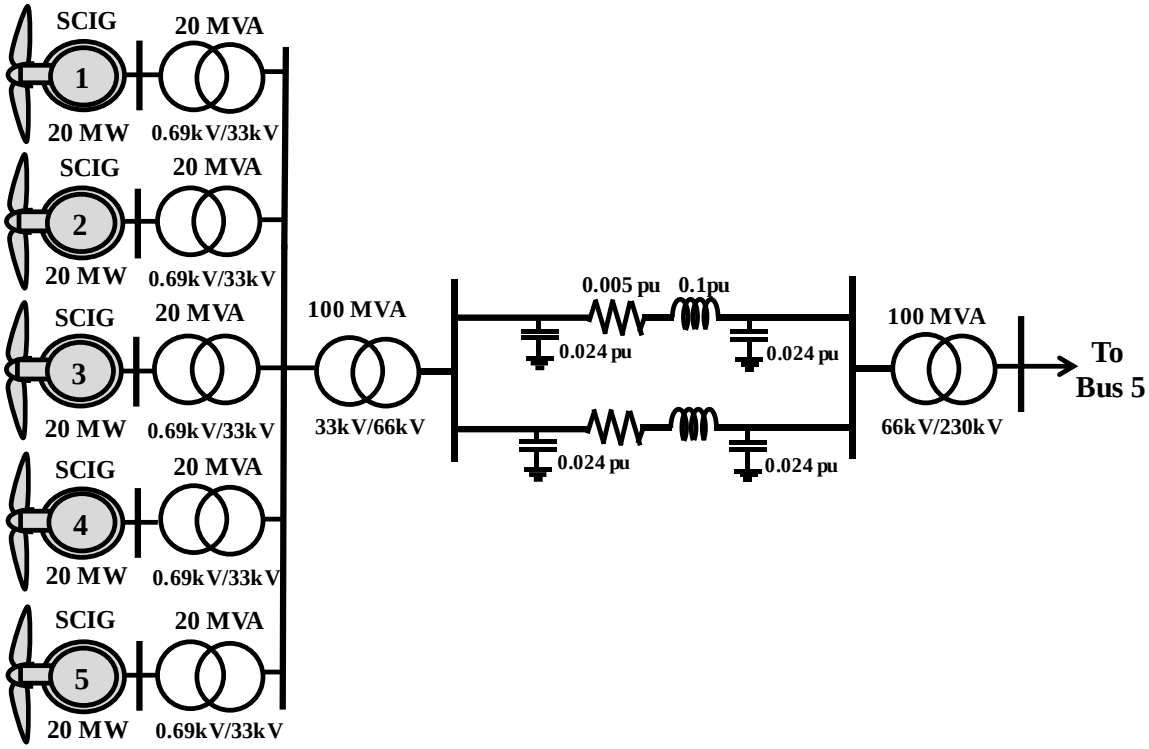

Fig. 4.3. Configuration of FSWT-SCIGs based onshore wind farm.

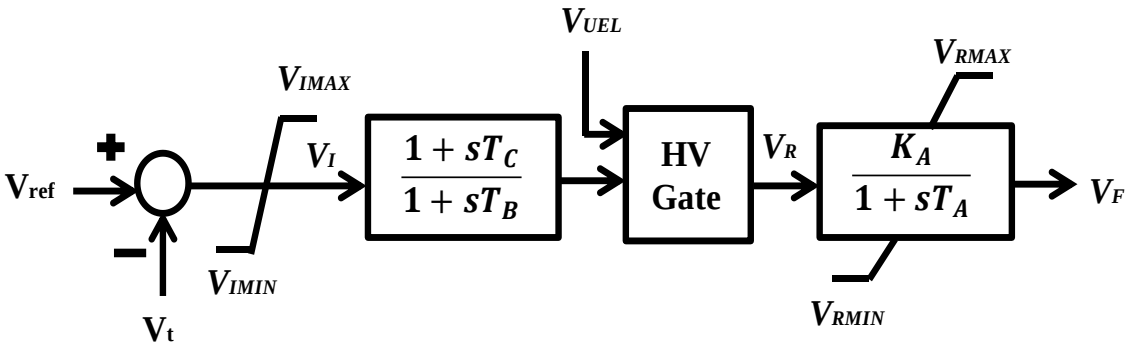

Fig. 4.4. IEEE type AC4A excitation system model.

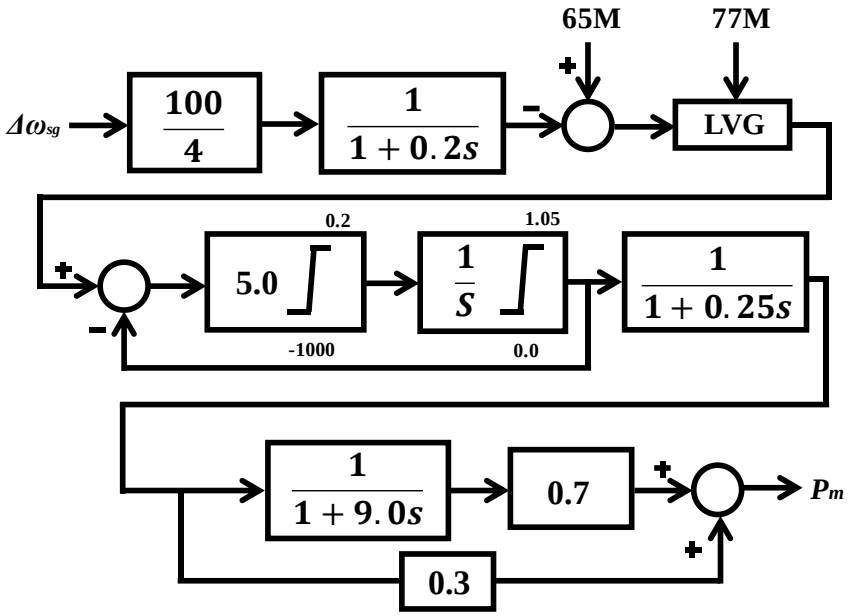

Fig. 4.5. Thermal turbine governor model.

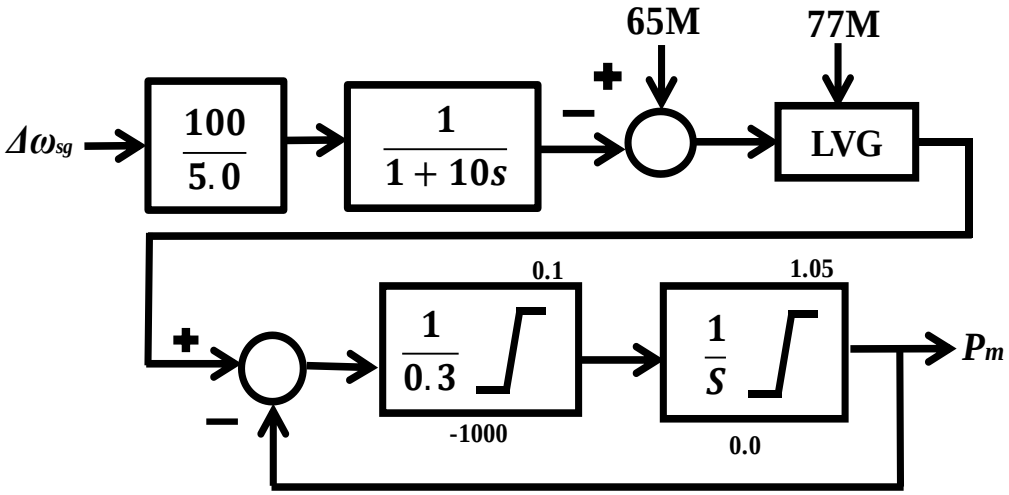

Fig. 4.6. Hydro turbine governor model.

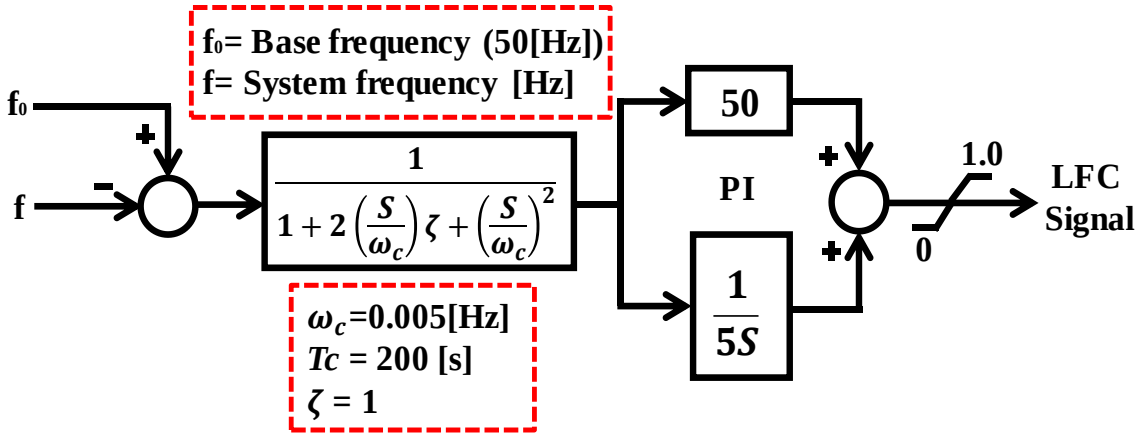

Fig. 4.7. LFC model.

Table 4.1. Values of 65M and 77M

SG1 (Thermal)	***Frequency control***	***65M***	***77M***
	LFC	LFC signal	1
SG2 (Thermal)	***Frequency control***	***65M***	***77M***
	GF	0.80	0.84
SG3 (Hydro)	***Frequency control***	***65M***	***77M***
	GF	0.80	0.84

In Figs. 4.5 and 4.6, $\triangle\omega_{sg}$: the revolution speed deviation [pu], 65M: the initial output [pu], 77M: the load limits (65M + rated MW output × PLM [%]), PLM: the spare governor operation [%], Pm: the turbine output [pu].

Fig. 4.7 shows the LFC model used in this study. The LFC sends the output value signal to the power plant (SG1) according to frequency deviations. Then, governor output value (65M) of power plant is changed by LFC signal, and the power plant output is changed.

4.2.2 Modeling and Control Strategy of PMSG

The overall block diagram of VSWT-PMSG model is shown in Fig. 4.8. In this study, the simplified model is used to decrease the simulation time [105]. The model consists of mechanical part, electrical part, and control system part. The mechanical part includes wind turbine and drive train models; the electrical part includes PMSG, DC-Link circuit, and LCL filter models; and the controller system part includes pitch controller, DC-Link circuit protection controller, stator side controller (SSC), grid side controller (GSC), and the interface with grid system. The interface

inputs the terminal grid voltage to the simplified model and injects the output current from the simplified model to the grid system through a three phase current source [105].

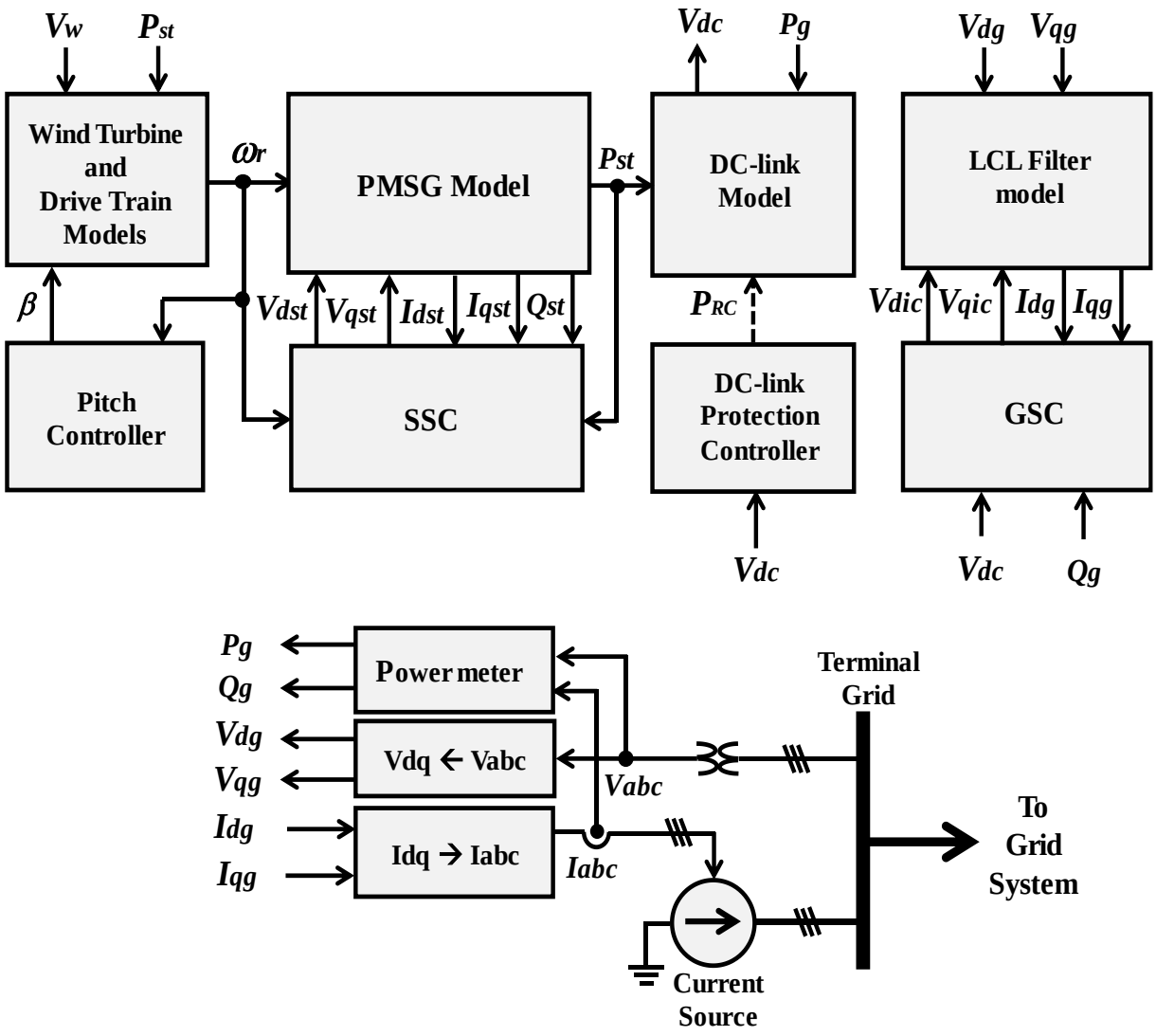

Fig. 4.8. Simplified model of VSWT-PMSG.

4.2.2.1 Stator Side Controller (SSC)

The block diagram of SSC is depicted in Fig. 4.9, which controls the active and reactive power of PMSG by controlling the q-axis stator current (I_{qst}) and the d-axis stator current (I_{dst}), respectively. SSC consists of four conventional PI controllers to compensate different error signals. The reactive power reference (Q_{st}*) is set to zero for unity power factor operation. The calculation method of active power reference (P_{ref}) will be discussed in section 4.2.3.

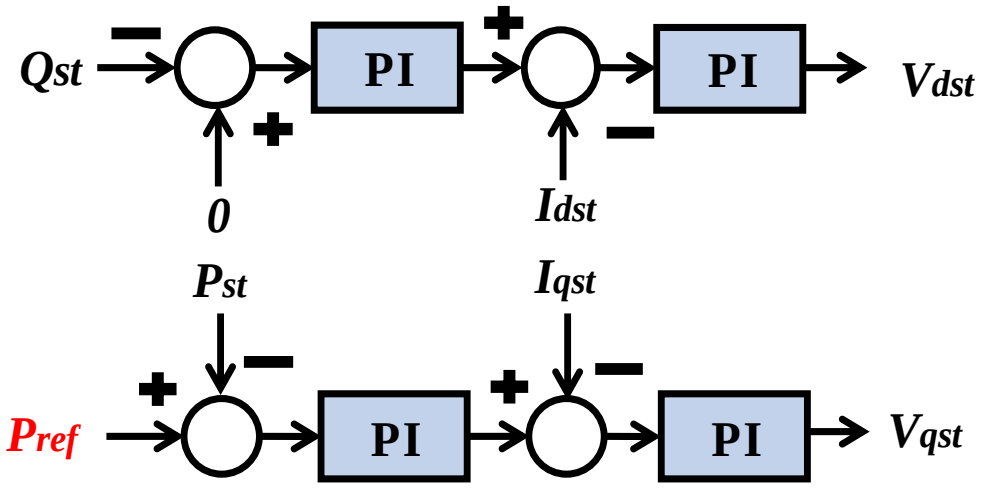

Fig. 4.9. Conventional stator side controller.

4.2.2.2 Grid Side Controller (GSC)

The block diagram of GSC is shown in Fig. 4.10, which controls the DC-Link voltage (V_{dc}) and the reactive power delivered to the grid system (Q_g) by controlling the q-axis current (I_{qg}) and the d-axis current (I_{dg}) of LCL filter output current, respectively. The four PI controllers are used to track the different error signals.

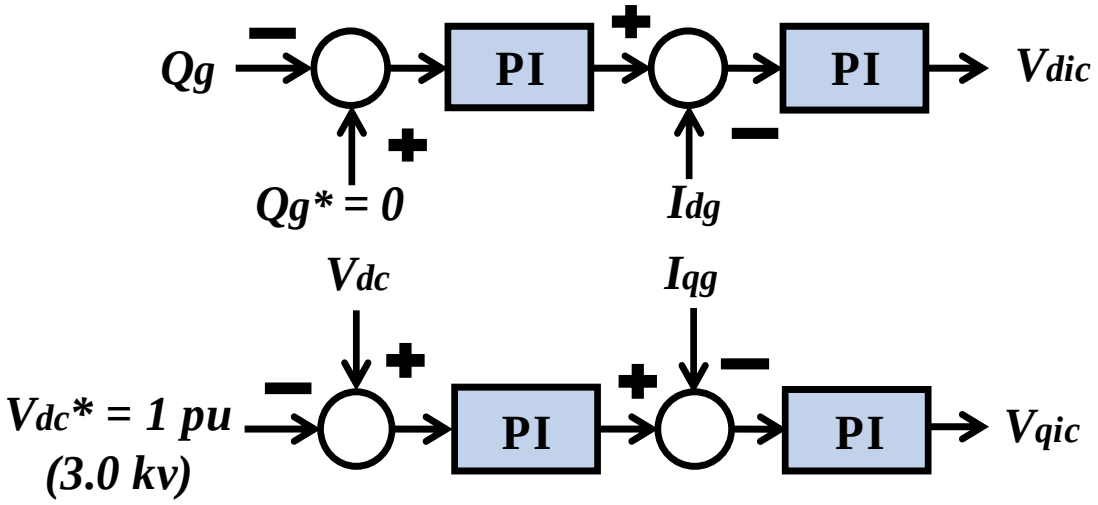

Fig. 4.10. Conventional grid side controller.

4.2.3 Proposed Coordinated Frequency Controller

Generally, frequency control in a power system is performed by conventional power plants. The thermal units perform primary frequency control, while secondary frequency control is

performed by LFC. Frequency regulation is a key factor for integrating large-scale WF into the power system and WF should also take responsibility to damp power system frequency variation.

4.2.3.1 Deloaded Operation

Due to the uncontrollability of the wind speed, it is inherently non-capable for VSWT-PMSG to provide primary reservation. As, with the help of modified control strategies, the VSWT-PMSG can generate less active power than its available MPPT output, however, the difference between the actual active power and available MPPT active power can be used as a primary reserve. To obtain the reserve active power, the VSWT-PMSG should operate in a deloaded mode instead of in MPPT mode.

From the aerodynamic power equation of wind turbine generator (WTG) of Eq. (4.1), the power vs. rotor speed characteristics of wind turbines are nonlinear [105].

$$P_w = 0.5\rho\pi R^2 V_w{}^3 C_p(\lambda,\beta) \tag{4.1}$$

$$C_p(\lambda,\beta) = c_1\left(\frac{c_2}{\lambda_i} - c_3\beta - c_4\right)e^{\frac{-c_5}{\lambda_i}} + c_6\lambda \tag{4.2}$$

$$\frac{1}{\lambda_i} = \frac{1}{\lambda - 0.08\beta} - \frac{0.035}{\beta^3 + 1} \tag{4.3}$$

$$\lambda = \frac{\omega_r R}{V_w} \tag{4.4}$$

Where, P_w is the captured wind power, ρ is the air density (kg/m^3), R is the radius of the rotor blade (m), V_w is the wind speed (m/s), and C_p is the power coefficient. β is the pitch angle, and λ is the tip speed ratio. c_1 through c_6 are the characteristic coefficients of the wind turbine.

Fig. 4.11 shows the power vs. speed curve based on Eq. 4.1. Due to the non-linear characteristics of wind turbine, the wind turbine exhibits maximum power at a specific rotor speed. As previously mentioned, for frequency control of the power system it is necessary that the WTGs have sufficient power reserve.

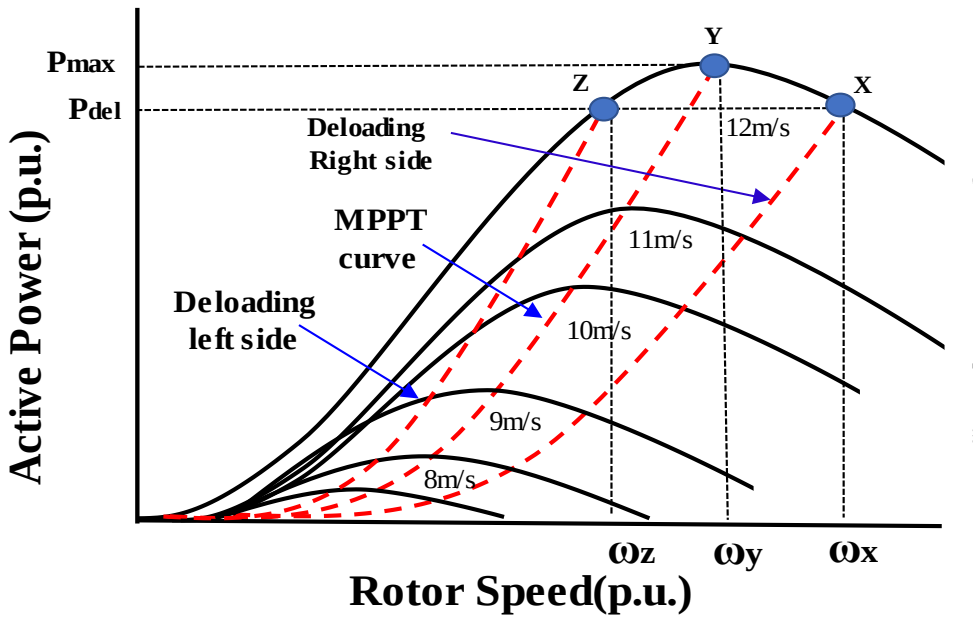

Fig. 4.11. MPPT and deloaded power curve of VSWT.

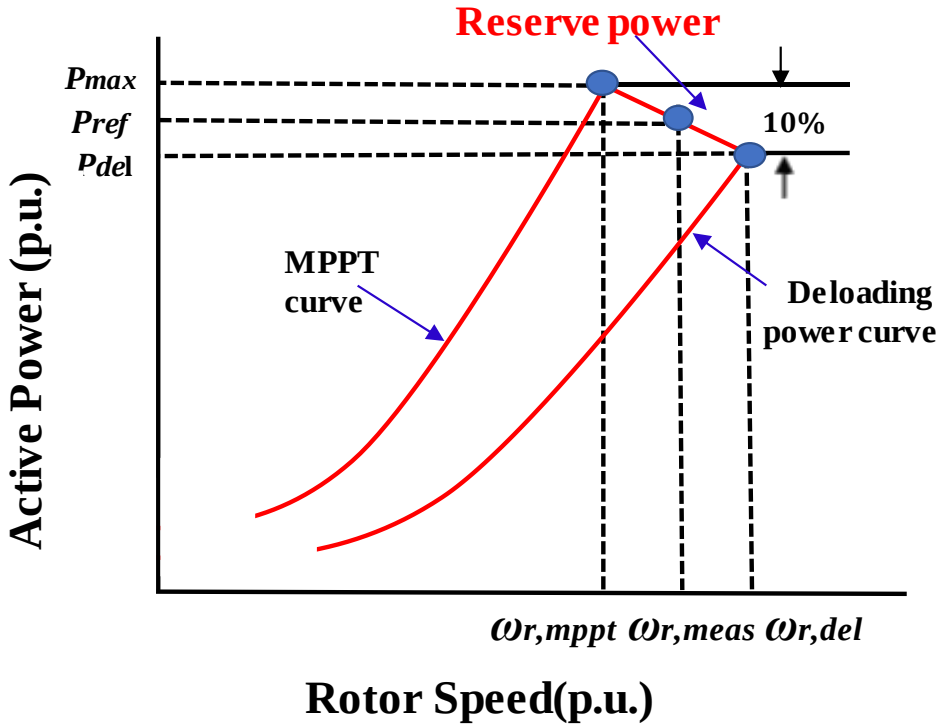

Fig. 4.12. Power margin for 10% deloading.

In this work, a 10% wind power margin is preserved through rotor speed control of PMSG. The deloading operation can be performed by shifting the operating point either in the left-hand side (under speeding) or right-hand side (over speeding) of MPPT point as shown in Fig. 4.11. Over speeding technique by shifting the operating point to the right-hand side is used in this study to get a 10% power reserve. Because deloading operation of over speeding can improve the small signal stability [113].

For a 10% deloaded VSWT-PMSG, the deloaded power output, $P_{del} = 0.9P_{mppt}$, where, P_{mppt} is the maximum power at MPPT point. As an example, at a wind speed of 12 m/s, under MPPT condition the VSWT-PMSG used in this work delivers P_{mppt} = 1.0 pu. The rotor speed corresponding to this power output is $\omega_{r,mppt}$ = 1 pu. If the WTG is 10% deloaded at that wind speed, power output would fall to P_{del} = 0.90 pu, with rotor speed rising to $\omega_{r,del}$ = 1.18 pu.

The deloaded power reference ($P_{ref,del}$) of the VSWT-PMSG for any rotor speed is calculated by using Fig. 4.12 as [94]:

$$P_{ref,del} = P_{del} + \left(P_{mppt} - P_{del}\right)\frac{\omega_{r,del} - \omega_{r,meas}}{\omega_{r,del} - \omega_{r,mppt}} \tag{4.5}$$

Where, $\omega_{r,meas}$ is the actual rotor speed of VSWT-PMSG.

4.2.3.2 Centralized Droop Control

Configuration of centralized droop control system is illustrated in Fig. 4.13. In this droop control technique, a dead band is embedded. The frequency controller of VSWT-PMSG is only activated when the frequency variation is outside the predefined limit (|a| = 0.075). The droop gain (K_{droop}) is chosen on trial and error basis to obtain the optimum performance from the centralized droop controller. For better frequency control, sufficient power reserve should be maintained by using deloaded technique as discussed earlier.

The droop control includes providing an output power term proportional to the deviations of frequency.

$$\Delta P_{droop} = K_{droop}\Delta f \tag{4.6}$$

The reference active power (P_{ref}) for each PMSG is expressed as:

$$P_{refn}(n=1,2,...5) = P_{refTotal} \times \frac{P_{ref,del}(n=1,2,..5)}{P_{ref,del}1 + P_{ref,del}2 + P_{ref,del}3 + P_{ref,del}4 + P_{ref,del}5} \quad (4.7)$$

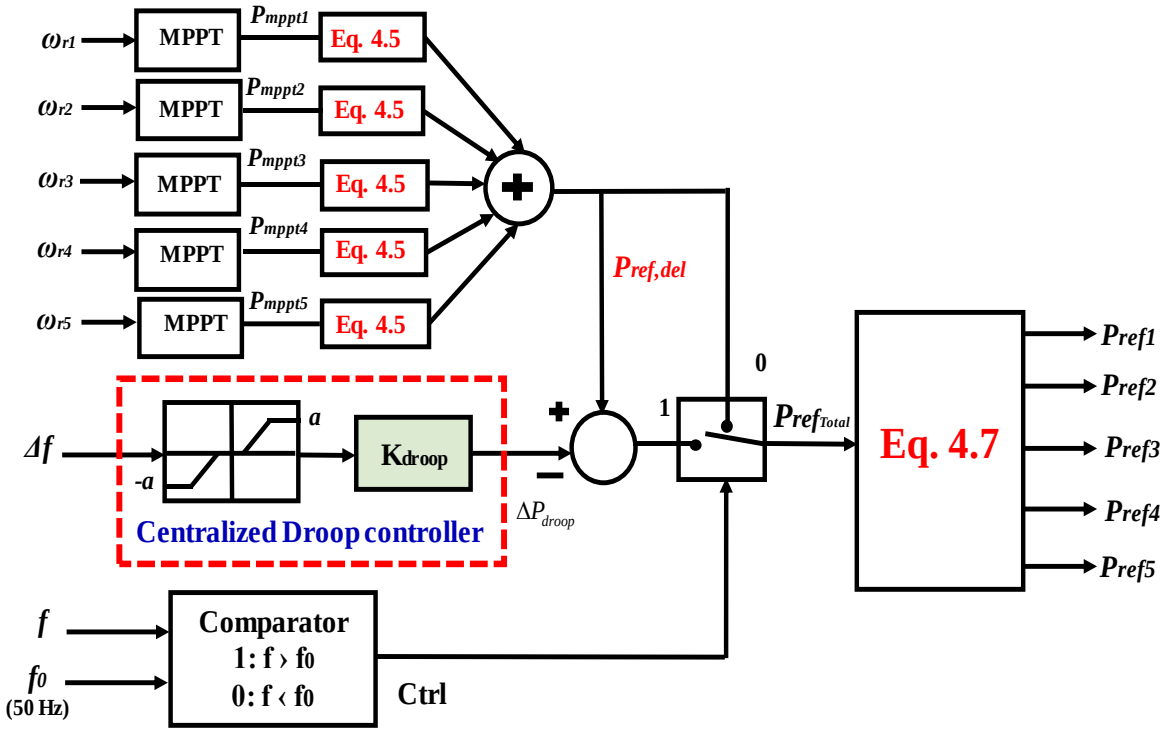

Fig. 4.13. Centralized frequency controller.

4.2.4 Modeling of HVDC System

In this work, a simplified model of VSC-HVDC system is used instead of detailed model to diminish the complexity and reduce the large computing time [112]. Fig. 4.14 illustrates the system configuration of the simplified model of VSC-HVDC system with its control system. The system is consisting of the two main part, one is a converter on the offshore side and the other is an inverter on the onshore side, which are modelled using voltage sources instead of detailed switching circuit with insulated gate bipolar transistors (IGBTs) [105]. Three phase AC voltage generated by OWF is rectified to DC voltage through the converter. Three phase current (I_r), voltage (V_r), active power (P_r), and reactive power (Q_r) are detected on the offshore side AC system. The rectified DC voltage is transmitted to the onshore side. The transmitted DC voltage is converted again into AC voltage through the onshore side inverter. The converter is controlled by the converter controller (CC) and

the inverter is controlled by the inverter controller (IC). Comparative analyses between the VSC-HVDC simplified model and the detailed model using IGBT based switching circuits are presented in Chapter 3 [112] and it is concluded the simple model is very accurate.

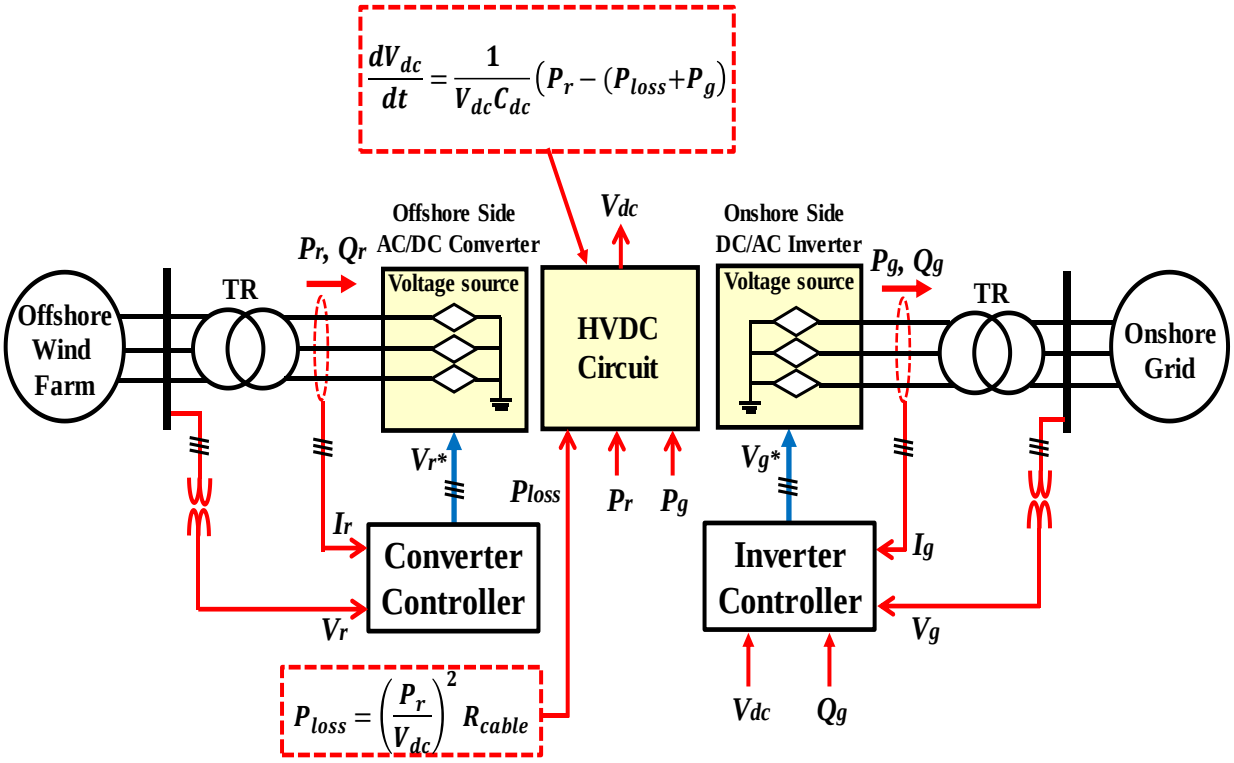

Fig. 4.14. Schematic diagram of VSC-HVDC system.

. 4.2.4.1 Converter Controller (CC)

The block diagram of CC is depicted in Fig. 4.15. The main objective of the CC is to ensure the normal operation of VSC-HVDC connection based OWF. The converter station must establish an AC voltage of stable amplitude and frequency for the local grid of OWF. The voltage magnitude and phase of OWF are controlled by q-axis current (*Irq*) and d-axis current (*Ird*) of VSC-HVDC rectifier system. The voltage magnitude reference (*Magnitude**) is chosen as 1.0 pu and voltage phase reference (*Phase**) is set to 0.0 degree.

4.2.4.2 Inverter Controller (IC)

The block diagram of IC is illustrated in Fig. 4.16. The aim of the IC is to control the reactive power (Q_g) delivered to the onshore grid and keep the DC-Link voltage (Vdc) constant by using d-axis (Igd) and q-axis (Igq) currents of VSC-HVDC inverter system, respectively. The reactive power reference (Q_g*) is set to 0.0 pu for unity power factor operation and DC-Link voltage

reference (V_{dc}*) is set to 1.0 pu.

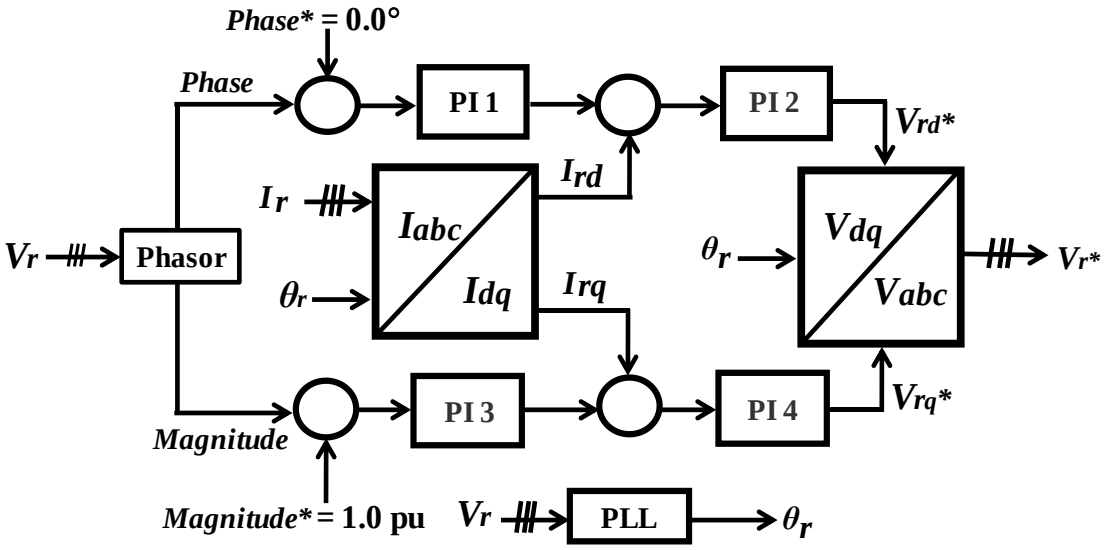

Fig. 4.15. Block diagram of CC.

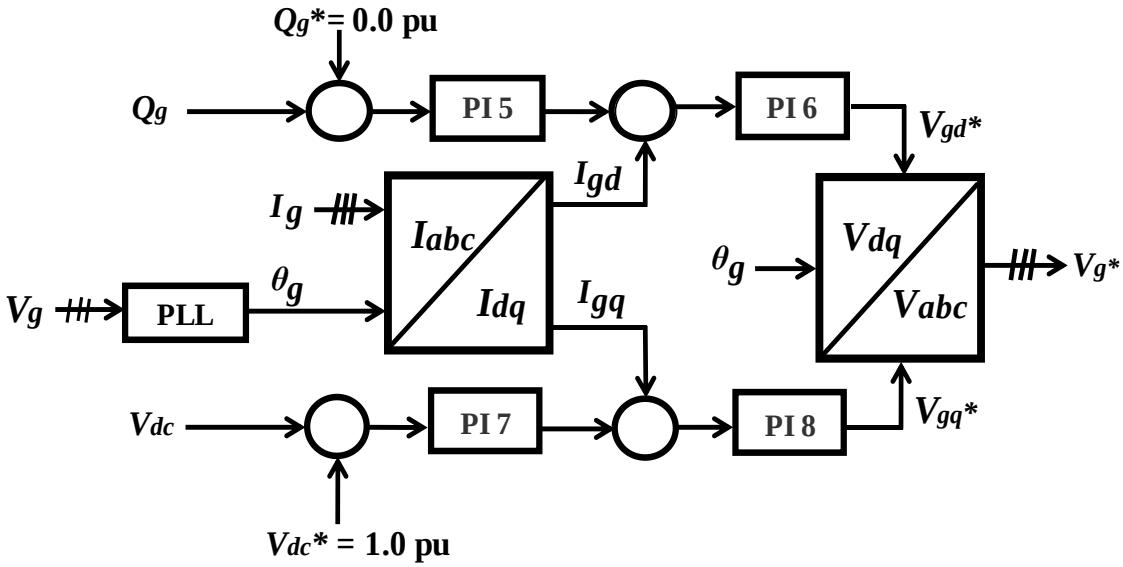

Fig. 4.16. Block diagram of IC.

4.2.4.3 DC-Link Model

The portion of the HVDC circuit can be expressed based on the power balance [112] as shown in the red dotted line block of Fig.14, which means that the power supplied from the OWF must be equal to the sum of the power received by the grid and transmission line loss. In Fig. 4.14, V_{dc}

is the DC-Link circuit voltage, *Cdc* is the DC-Link capacitor, *Pr* is the supplied power from the OWF, *Pg* is the grid side power, and *Ploss* is the power loss.

4.2.5 Simulation Results

The power system model shown in Fig. 4.1 is used for simulation study. The simulation analysis is performed by using PSCAD/EMTDC software. The rated frequency is 50 Hz. The simulation period is taken 800 s. Two cases are considered in this study. In Case 1, the simulation analysis is performed without any frequency controller in the OWF, whereas simulation analysis is performed with the proposed centralized frequency controller in Case 2. The real wind speed data measured in Hokkaido Island, Japan, are used for both SCIG and PMSG based WF as illustrated in Figs. 4.17 and 4.18. The total active and reactive powers of offshore side and onshore side of VSC-HVDC are depicted in Figs. 4.19 and 4.20. It is seen that the active power output in Case 2 is 10% less than that in Case 1. This is because, in Case 2 deloaded operation is performed.

Fig. 4.21 shows the total active and reactive power output of FSWT-SCIGs based WF. As the SCIGs are directly connected to the grid, there is almost no difference in active and reactive powers between two cases. Fig. 4.22 depicts the active power output of conventional SGs. The SGs are providing higher active power in Case 2 than in Case 1 since the deloaded operation is performed in the OWF in Case 2.

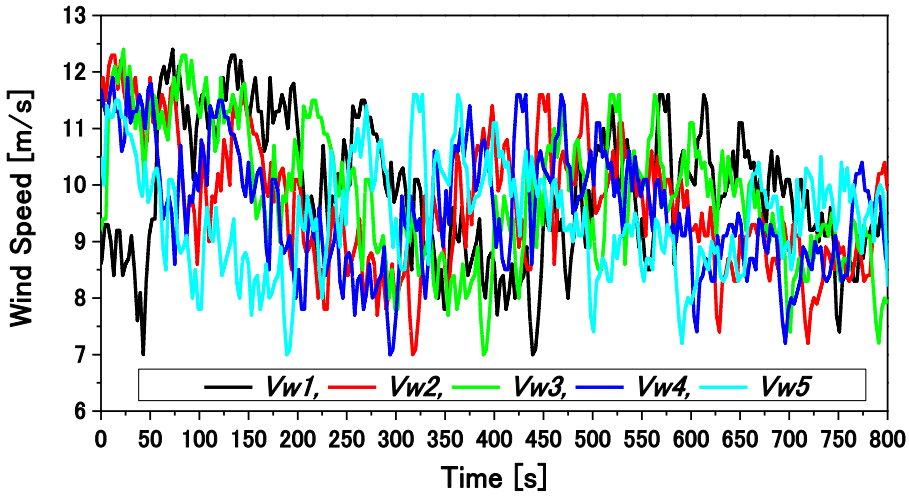

Fig. 4.17. Wind speeds applied to VSWT-PMSGs.

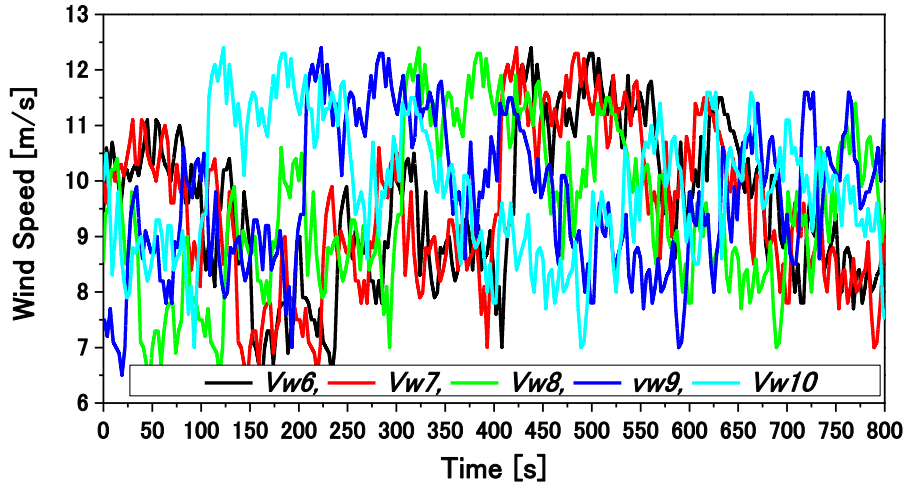

Fig. 4.18. Wind speeds applied to FSWT-SCIGs.

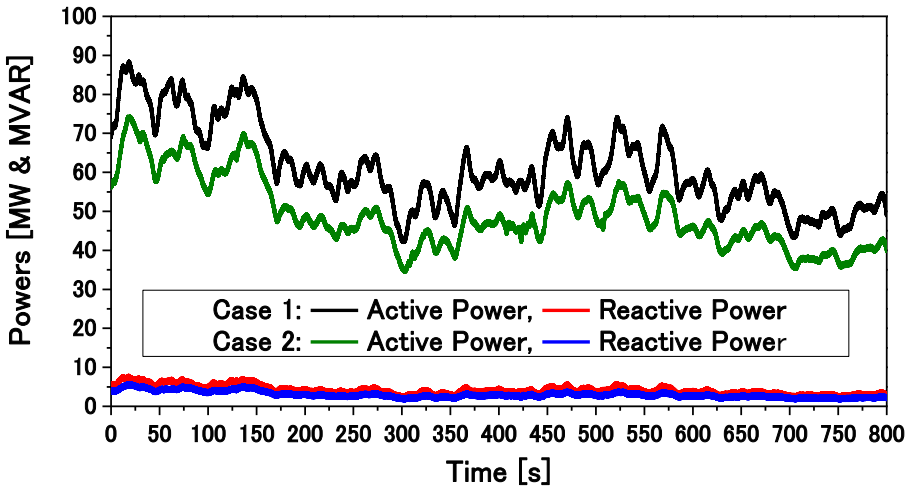

Fig. 4.19. Power input to offshore side of VSC-HVDC.

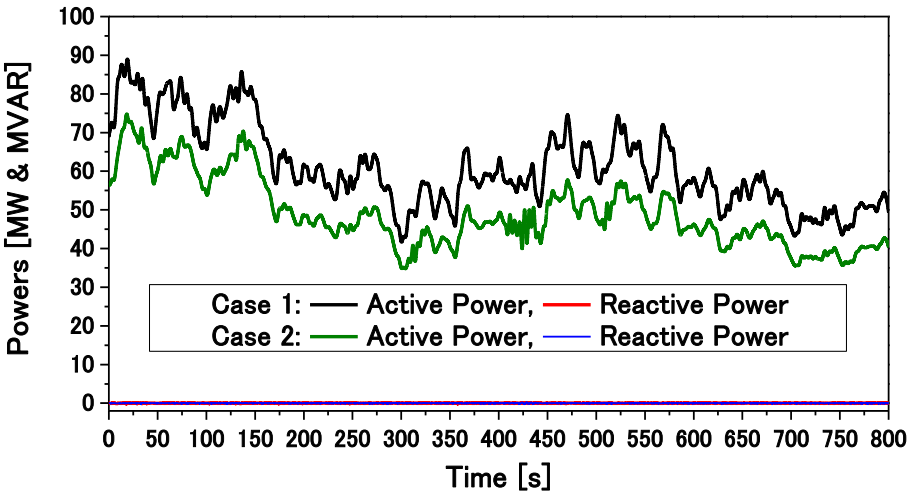

Fig. 4.20. Power output from onshore side of VSC-HVDC.

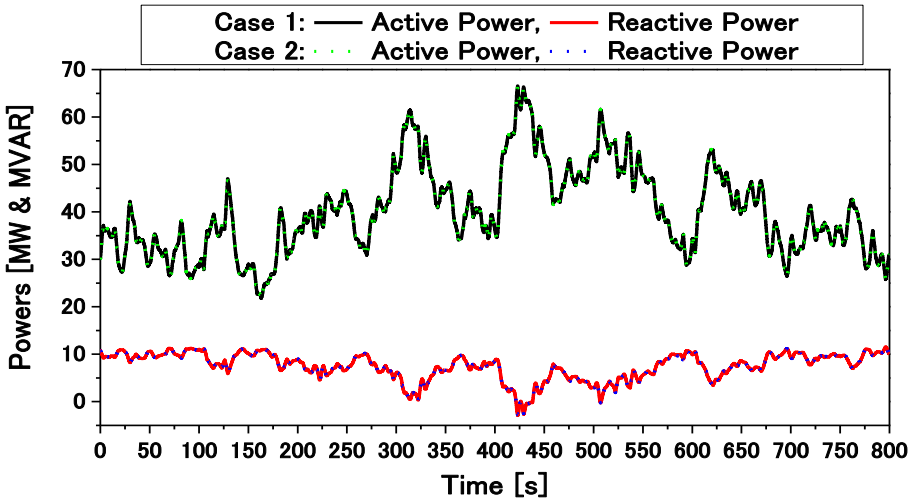

Fig. 4.21. Total active and reactive power output of FSWT-SCIGs based WF.

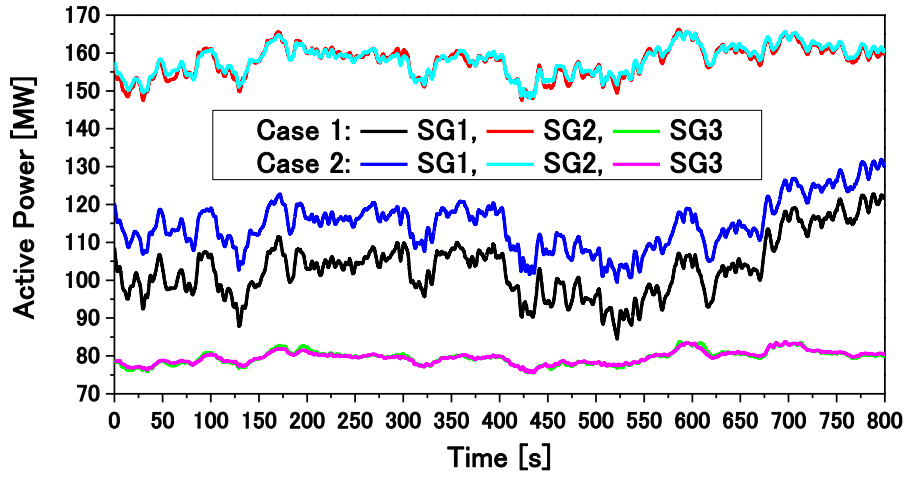

Fig. 4.22. Active power output of conventional SGs.

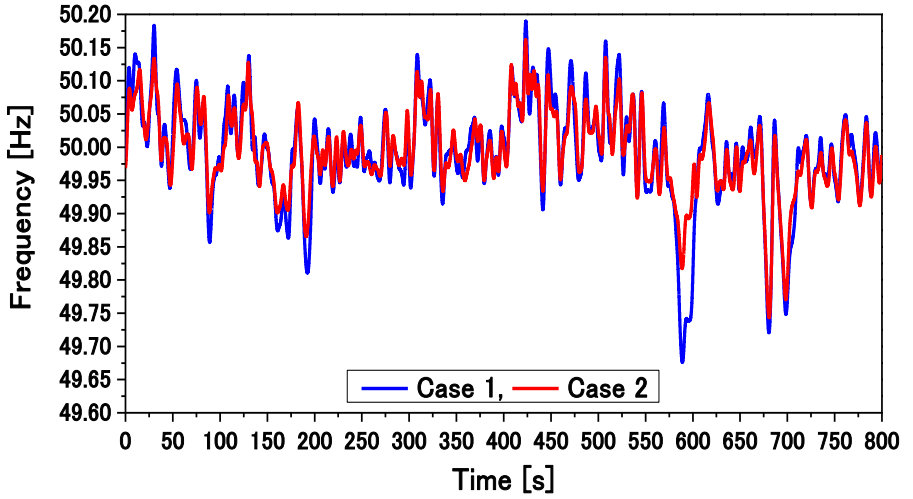

Fig. 4.23. Frequency response of the main power system.

The frequency response of the power system is depicted in Fig. 4.23. Due to the centralized droop control and deloaded operation, the frequency response of the power system is more stable in Case 2 than in Case 1.

From Table 4.2, it can be seen that the frequency deviation and the standard deviation of system frequency are smaller in Case 2 than in Case 1. Therefore, frequency fluctuations can be damped effectively by using the proposed centralized frequency control strategy.

Table 4.2. Comparison of frequency deviation and standard deviation of system frequency in both cases

	Case 1	***Case 2***
Maximum Frequency Deviation, +Δf [Hz]	0.1897	0.1616
Minimum Frequency Deviation, -Δf [Hz]	-0.3239	-0.2567
Standard Deviation, σ [Hz]	0.0739	0.0609

4.3 Frequency Regulation of Hybrid Power System by Deloaded Operation of VSWT-PMSG

4.3.1 Hybrid Power System Model

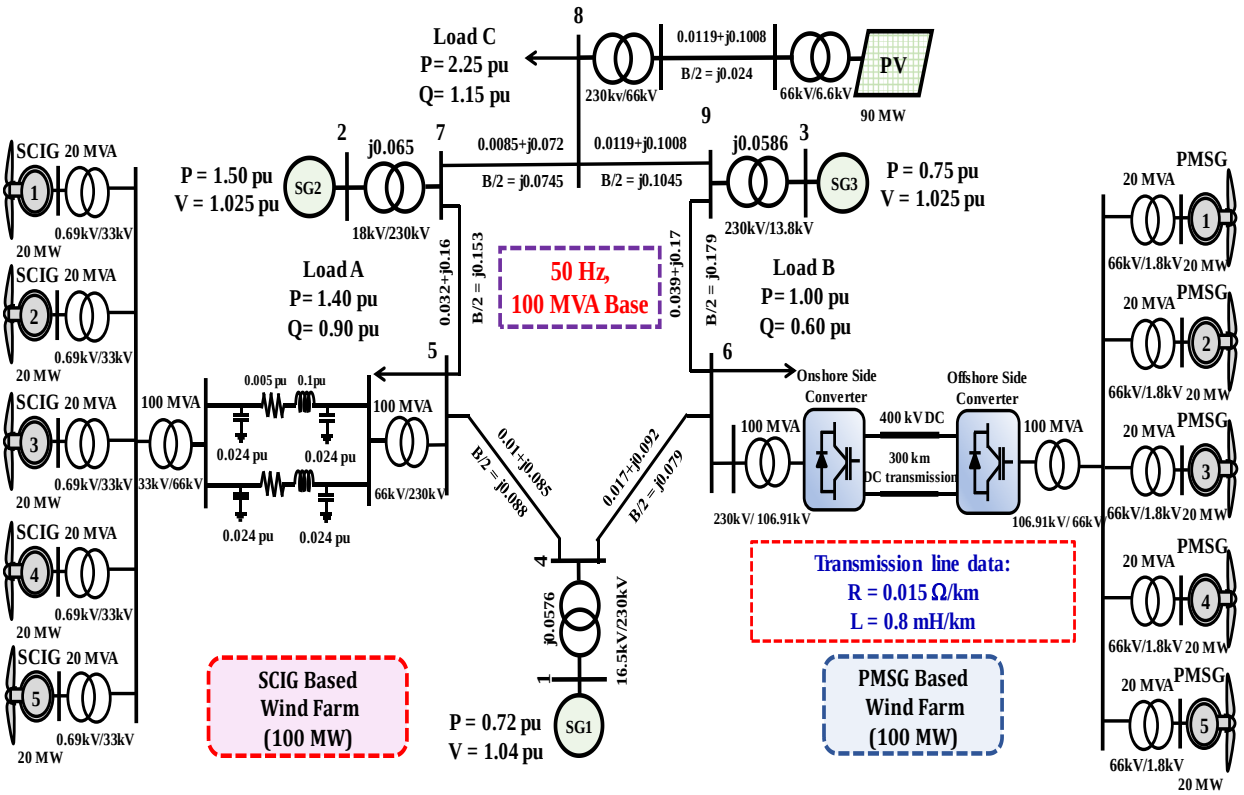

Fig. 4.24. Hybrid power system model.

The study in this section is using the same power system model as shown in Fig. 4.1. But a PV station is also connected at bus 8 which is illustrated in Fig. 4.24. The capacity of PV station is 90 MW and its model is taken from [114].

4.3.2 Modeling and Control Strategy of PMSG

The study in this section is using the same simplified model of PMSG as that discussed in Section 4.2.2. In this case the *Pref* is taken from Fig. 4.25.

4.3.3 Proposed Centralized Frequency Controller

4.3.3.1 Deloaded operation

As the wind speed applied to PMSG is continuously varied, it cannot provide primary reserve. However, with some additional control loop, the VSWT-PMSG can provide reserve power by decreasing its output less than its available MPPT power. Thus, the primary reserve can be defined as the difference between available MPPT output and generated actual active power.

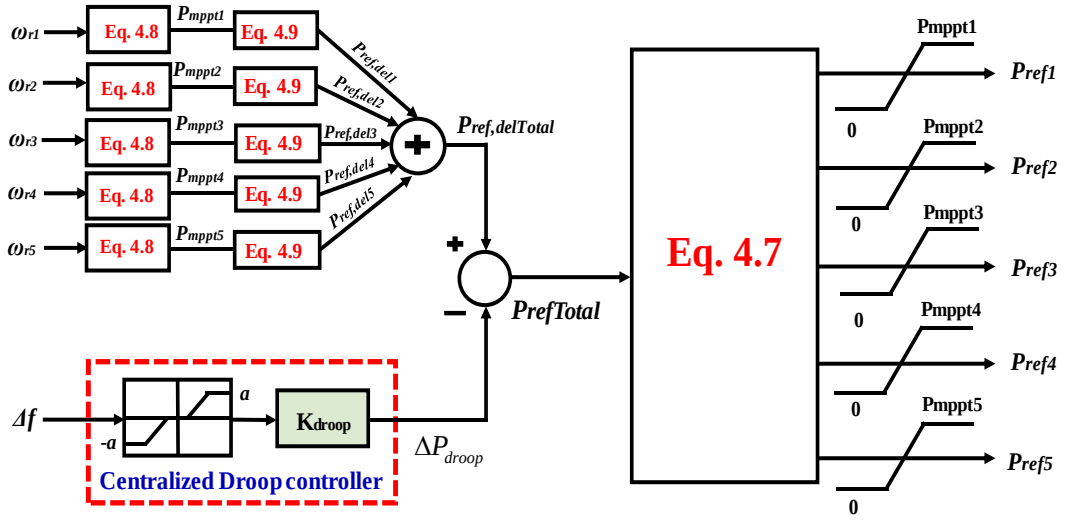

Fig. 4.25: Centralized frequency controller

The MPPT power (P_{MPPT}) for VSWT-PMSG can be expressed as follows [40]:

$$P_{MPPT} = 0.5\rho\pi R^2 \left(\omega_r R / \lambda_{opt} \right)^3 C_{p\_opt} \tag{4.8}$$

Fig. 4.25 depicts the schematic diagram of centralized frequency control system. To achieve the active power reserve margin, the VSWT-PMSG must operate in a deloaded mode instead of in MPPT mode. In this work, 10% power is reserved. So, reference deloaded active power can be written as:

$$P_{ref,del}=0.9*P_{mppt} \tag{4.9}$$

4.3.3.2 Centralized Droop Control

The study in this section is using the same centralized droop control technique as that discussed in Section 4.2.3.2. The limiter is used in the last stage so that the output reference of each VSWT-PMSG will not be greater than the MPPT output.

4.3.4 Modeling of HVDC System

The study in this section is using the same simplified model of VSC-HVDC system as that discussed in Section 4.2.4.

4.3.5 Simulation results

Simulation study is conducted on a power system model depicted in Fig. 4.24. The rated frequency is 50 Hz.

Two cases are considered in this work. They are:

Case 1: Without any deloaded operation and droop controller in the VSWT-PMSGs.

Case 2: With proposed centralized frequency controller in the VSWT-PMSGs.

The actual wind speed data measured in Hokkaido Island, Japan, are used for both PMSG and SCIG based WF as depicted in Figs. 4.26 and 4.27. Figs. 4.28 and 4.29 show the total active power profile of OWF (VSWT-PMSGs) and onshore side of VSC-HVDC transmission system. It is seen that the active power output at some point is smaller in Case 2 than Case 1. This is because the deloading operation is activated in Case 2. In addition, at some point the active power output in Case 2 is equal or close to Case 1. This is because the deloaded power (10 %) is used by the droop controller (ΔP_{droop}) to remove the frequency fluctuations.

The total active power profile of FSWT-SCIGs and PV power station are depicted in Figs. 4.30 and 4.31. As the SCIGs and PV plant are directly connected to the grid, there is almost no difference in active power between two cases.

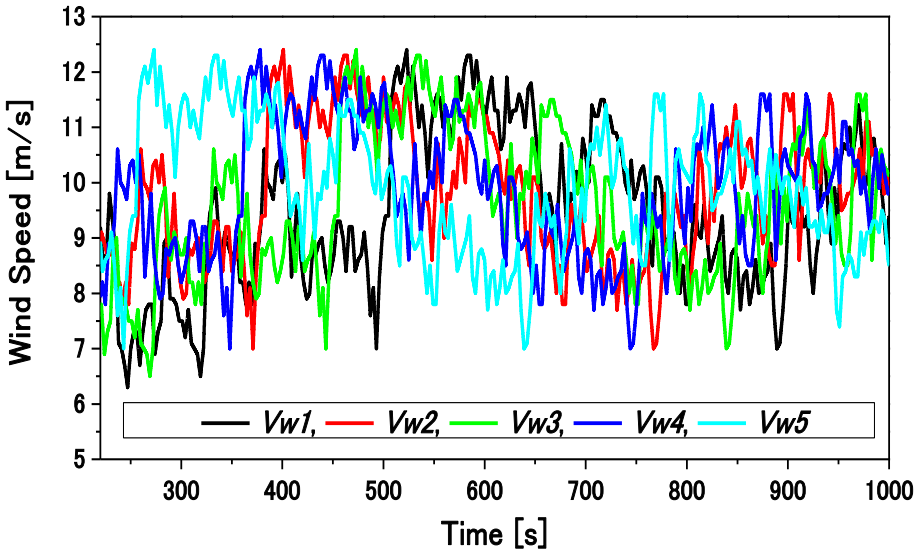

Fig. 4.26: Wind speeds data (VSWT-PMSG).

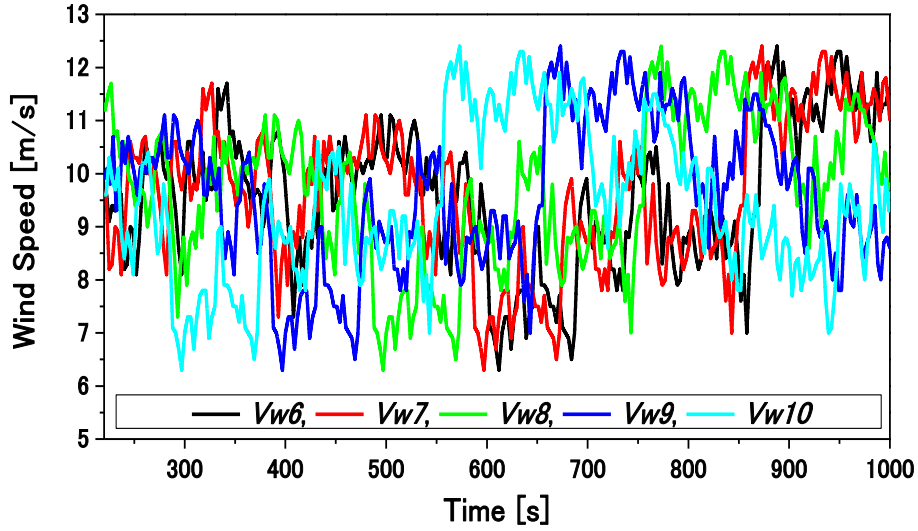

Fig. 4.27: Wind speeds data (FSWT-SCIGs).

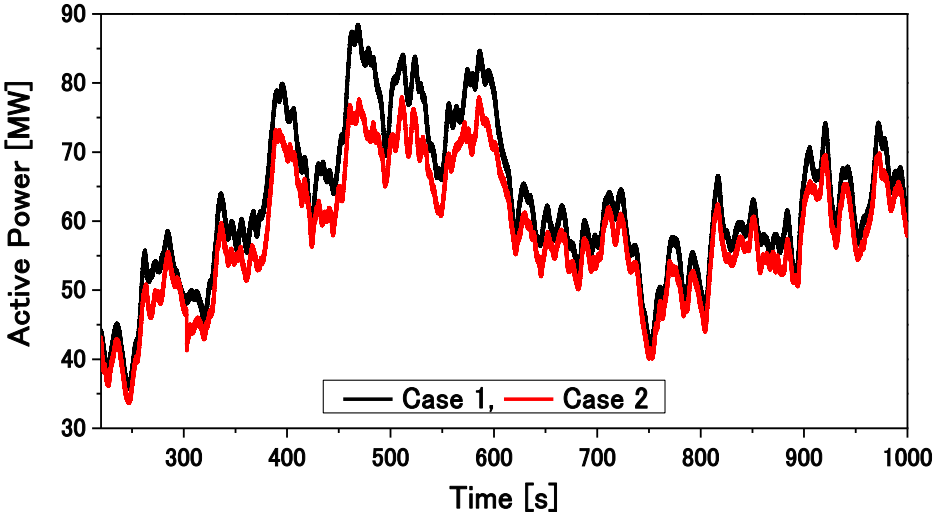

Fig. 4.28: Active power profile of VSWT-PMSGs.

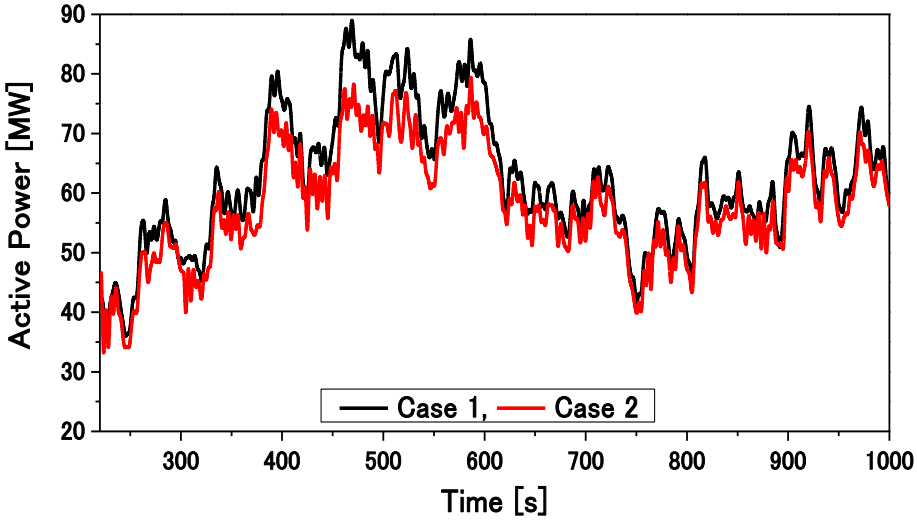

Fig. 4.29: Active Power profile from onshore side of VSC-HVDC transmission system.

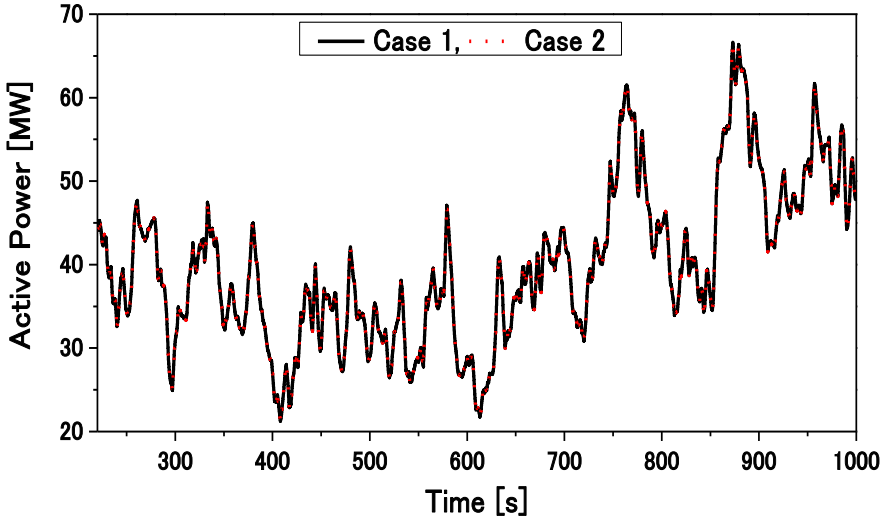

Fig. 4.30: Active Power profile of FSWT-SCIGs.

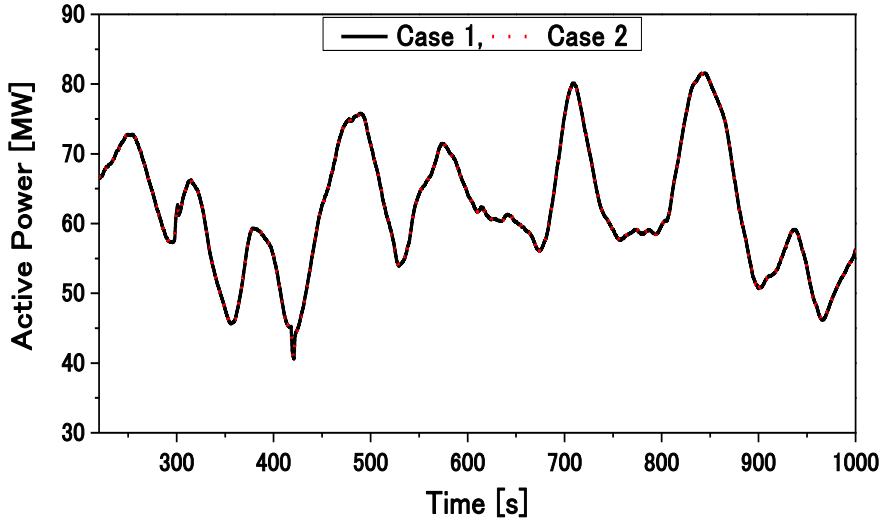

Fig. 4.31: Active Power profile of PV power station.

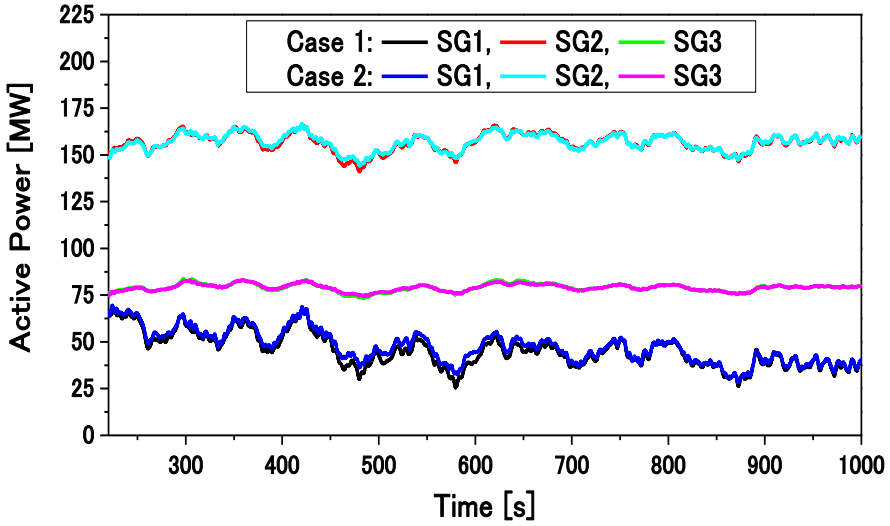

Fig. 4.32: Active power profile of conventional SGs.

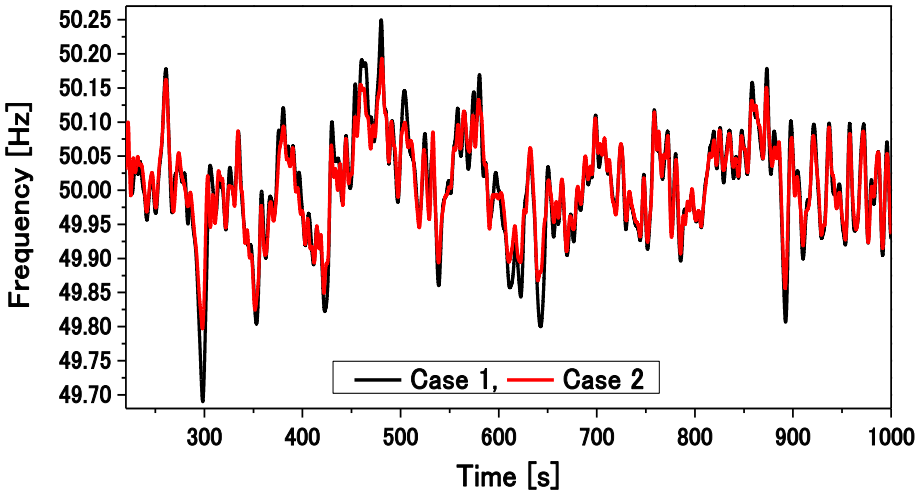

Fig.4.33: Frequency response of the hybrid power system.

Table 4.3: Comparison between two cases based on frequency response curve.

	Case 1	Case 2
Maximum Frequency Deviation (+Δf) [Hz]	0.2496	0.1934
Minimum Frequency Deviation (-Δf) [Hz]	-0.3097	-0.2031
Standard Deviation (σ) [Hz]	0.0795	0.0652

Fig. 4.32 illustrates the active power profile of conventional SGs. The SGs are injecting slightly higher amount of active power in Case 2 than Case 1, because they are adjusting their output based on the VSWT-PMSG output.

Finally, the hybrid power system frequency response is shown in Fig. 4.33. The frequency

fluctuations are smaller in Case 2 than Case 1. This is because in Case 2 the PMSG-based OWF is reserving some amount of active power and using it in the droop controller.

From Table 4.3, the $+\Delta f$, $-\Delta f$ and σ based on the frequency response curve are smaller in Case 2 than in Case 1.

Therefore, the proposed centralized frequency controller can effectively decrease the frequency fluctuations.

4.4 Chapter Conclusion

In this chapter, two fixed deloaded method with centralized droop controller are proposed for VSWT-PMSGs based OWF to reduce the frequency oscillations of the connected onshore grid system.

In Section 4.2, a centralized frequency controller is proposed for VSWT-PMSGs based OWF, which incorporates both droop controller with dead band and rotor speed control based fixed deloaded operation to contribute to the power system frequency regulation. Through simulation analysis, it is shown that the proposed centralized frequency controller can suppress the frequency fluctuations of the power system effectively.

In Section 4.3, another novel centralized frequency control technique which is suitable for VSWT-PMSGs is proposed to reduce the frequency oscillations of hybrid power system. The centralized frequency control system integrates both fixed deloaded operation based on the modified MPPT equation and droop controller with dead band. The deloaded power is used by the droop controller for better frequency regulation. The simulations results confirmed that the frequency oscillations can be reduced effectively by the proposed frequency controller.

Therefore, the proposed control strategies have promising potential value to reduce the frequency fluctuations.

Chapter 5

Frequency Regulation of Hybrid Power System by Variable Deloaded Operation of PMSG-based Offshore Wind Farm using Centralized Droop Controller

In this chapter, a novel variable deloaded operation is proposed for variable speed wind turbines with permanent magnet synchronous generators (VSWT-PMSGs) based offshore wind farm (OWF) to maintain primary reserve, which is connected to onshore grid through voltage source converter based high voltage DC (VSC-HVDC) transmission system. A centralized droop controller with dead band is designed for VSWT-PMSGs to utilize this reserve power to suppress the frequency fluctuations of the onshore grid due to the installations of large-scale fixed speed wind turbines with squirrel cage induction generators (FSWT-SCIGs) based wind farm (WF) and photovoltaic (PV) power station. The combination of variable deloaded operation and centralized droop controller can give better frequency regulation and decrease energy loss due to the deloaded operation. The effectiveness of the proposed variable deloaded operation and centralized droop controller is verified through simulation analyses on a modified IEEE nine-bus test system. The simulation results reveal that the variable deloaded operation can decrease the energy loss compared to the fixed deloaded operation as well as suppress the frequency fluctuations in the same level as the fixed deloaded operation.

5.1 Introduction

Due to the drawback of the conventional power plants based on fossil fuels and their negative impacts on the environment, recently the attention on renewable energy sources (RESs) has been increasing all over the world. Solar PV is a popular type of RES which will occupy an important place and supply nearly 28% of all the overall energy demand [21] until 2040. Also, penetration of grid connected OWF has been increasing since the last decade because of the stronger and steadier wind resources in offshore areas compared to onshore sites. Around 4,334 MW of new offshore wind power (OWP) was installed across the world in 2017 [16]. This is equivalent to 195% of that in 2016. According to the global wind energy council (GWEC), currently, 18,814 MW of OWP is installed globally [16]. This increasing penetration of OWF and PV stations into

the grid system certainly leads to the retirements of conventional synchronous generators (SGs) [62]. Thus, the frequency fluctuations due to varying output of WFs and PV stations have become a major concern [62].

Normally, the frequency fluctuation is damped by the conventional units, which are equipped with automatic generation control (AGC) or load frequency control (LFC) system [63]. Therefore, to maintain the frequency stability of the power system with large penetration ratio of RESs, RESs are required to operate like conventional units. They need to not only supply power to the grid, but also need to damp frequency fluctuations [62, 64]. One possible solution is a frequency control by OWF.

Generally, VSWT-PMSG is preferable for OWF due to its gear-less feature, brushless operation, and 35% lower losses compared to doubly fed induction generator (DFIG) [41]. To integrate large-scale OWF into the onshore grid, VSC-HVDC transmission system is attractive and more preferable than high voltage AC (HVAC) transmission system from an economic and technical point of view [29], especially in the case of very long transmission system. VSC-HVDC system has some advantages, i.e. lower cable losses, independent and fast control of active and reactive power, and stabilization potential of connected AC networks [29, 31, 41].

For the frequency regulation of the onshore grid system, the VSWT-PMSG-based OWF connected to the onshore grid through VSC-HVDC transmission system should have sufficient power reserve. In this case, power reserve is possible by operating the VSWT-PMSGs at a reduced output power level instead of maximum power point tracking (MPPT) mode which is called deloaded operation [65].

Many researchers have focused on the primary reserve implementation by the fixed level of deloaded operation of VSWT with some auxiliary control loop [66-101]. For example, the deloaded operation is performed by the modified pitch angle control of VSWT-PMSG in [66-67,79, 85, 94]; the rotor speed controller is used for the deloaded operation in [68, 78, 87, 89]; and the over-speeding and pitching techniques are used for the deloaded operation of wind turbines in [69-75, 101]. However, in the above mentioned schemes for the deloaded operation, output power injected to the grid system from OWF is reduced by a fixed ratio at all times, and hence, the energy loss becomes large.

Therefore, this Chapter proposes a centralized frequency control scheme with a novel variable deloaded operation for VSWT-PMSGs based OWF connected to the onshore grid through

VSC-HVDC transmission system to damp frequency fluctuations of the onshore grid, in which a large-scale WF composed of FSWT-SCIGs and solar PV station are installed. In the frequency control method, the variable deloaded operation is proposed in order to decrease the energy loss, in which deloading level is variable (from 0% to 10%). The variable deloading level is achieved by designing a variable gain based on the standard deviation of the frequency fluctuations of the onshore grid. A centralized droop controller with dead band is designed for VSWT-PMSGs to utilize this reserve power to suppress the frequency fluctuations of the onshore grid.

The effectiveness of the proposed centralized frequency controller equipped with the variable deloaded function is verified through simulation analysis using PSCAD/EMTDC software on a modified IEEE nine-bus system composed of VSWT-PMSGs-based OWF connected to the onshore system through VSC-HVDC transmission line, FSWT-SCIGs based onshore WF, PV power station, and conventional SGs. Real wind speed data and solar irradiance data measured in Hokkaido Island, Japan, are used in the simulation analyses to obtain the realistic responses.

5.2 Hybrid Power System Model

Fig. 5.1 illustrates the hybrid power system model used in this study, which is composed of IEEE nine-bus main system, two WFs, and one PV power station. The nine-bus main system is composed of three conventional SGs. SG1 and SG2 are thermal power plants whereas SG3 is a hydro power plant. The LFC system is equipped with in SG1. SG2 and SG3 are operated under governor free (GF) control. The ratings and parameters of SG1, SG2, and SG3 are listed in Table 5.1. In this work, IEEE type AC4A exciter model is used for all conventional SGs which is already presented in Chapter 3.

The VSWT-PMSG-based OWF is connected to bus 6 through VSC-HVDC transmission system as shown in Fig. 5.2. The OWF consists of five VSWT-PMSGs and the total capacity is 100 MW (20 MW each). The symmetric monopole type with 300 km long and ±150 kV DC transmission lines are used in this study and the specifications of HVDC line are taken from Ref. [115]. Also, a SCIG-based onshore WF is connected to bus 5 of the main system through double circuit transmission line and transformers as depicted in Fig. 5.3. The total capacity of onshore WF is 100 MW which is composed of five FSWT-SCIGs (20 MW each). A PV station is also connected to bus 8. The capacity of solar PV station is 90 MW. The PV model is illustrated in Fig. 5.4 [114]. A

simple model using current sources is used in this work [114], in which P_{PV} is the kilowatts data. The PV current (I_{PV}) is calculated from P_{PV} [kW] and V_{PV} [kV]. The power flow conditions of onshore WF, OWF and PV station at t=0 s are: 0.55 pu, 0.38 pu, and 0.60 pu, respectively. The aerodynamic model of wind turbine are already discussed in Chapter 2.

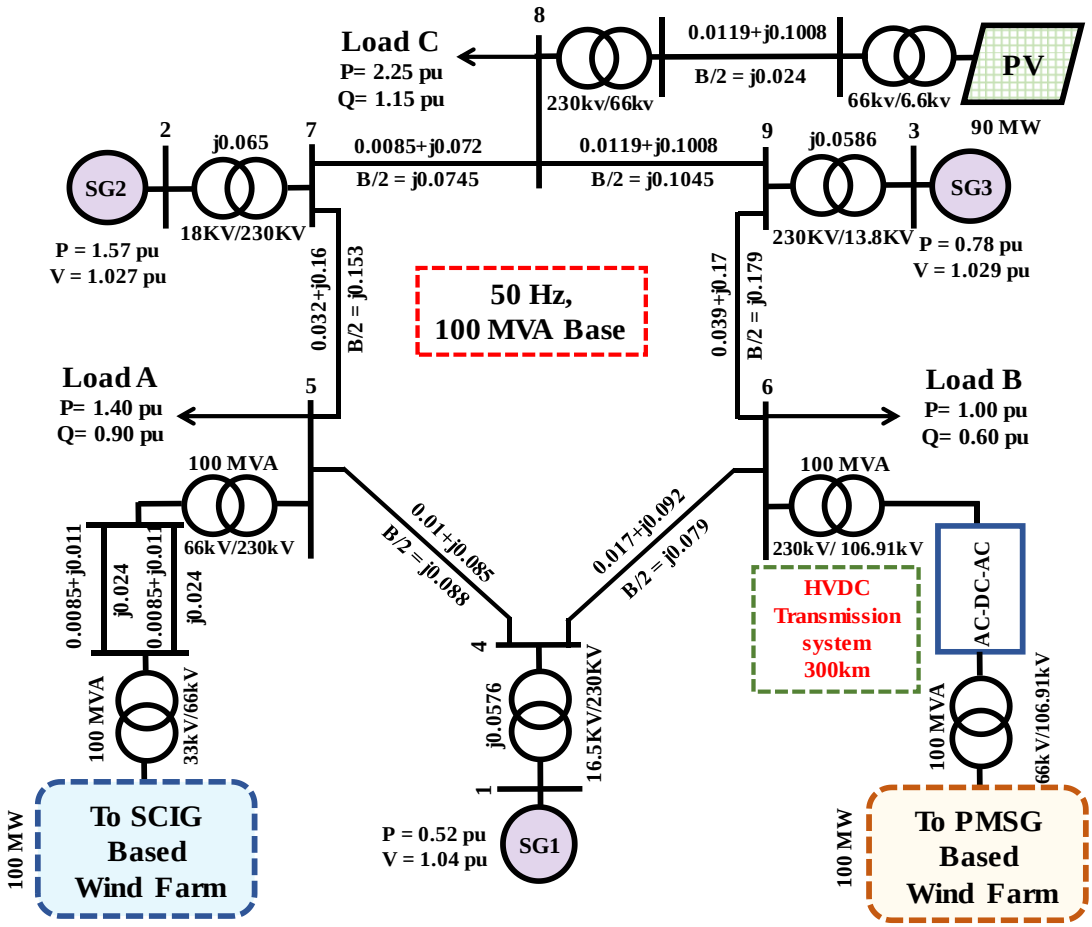

Fig. 5.1. Hybrid power system model.

The standard thermal and hydro governor models for SGs are depicted in Figs. 5.5 and 5.6 [110]. The values of 65M and 77M are presented in Table 5.2. In Figs. 5.5 and 5.6, $\triangle \omega sg$: the revolution speed deviation [pu], 65M: the initial output [pu], 77M: the load limits (65M + rated MW output $\times$ PLM [%]), PLM: the spare governor operation [%], and *Pm*: the turbine output [pu]. Fig. 5.7 represents the LFC model used in this study. The LFC sends the output signal to the power plant (SG1) according to frequency deviations. Then, governor output value (65M) of power plant is changed by LFC signal, and finally the power plant output is changed. The parameters of PMSGs and SCIGs are presented in Table 5.3.

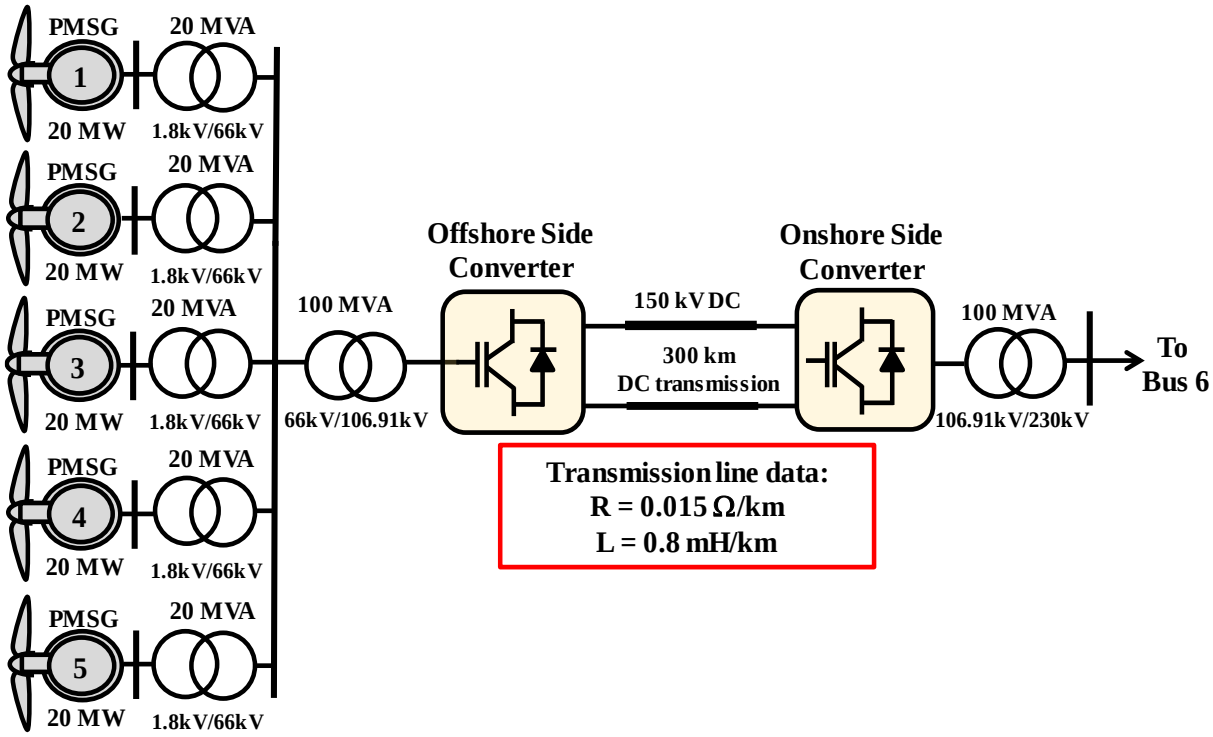

Fig. 5.2. Configuration of VSWT-PMSG based OWF connected through VSC-HVDC transmission system.

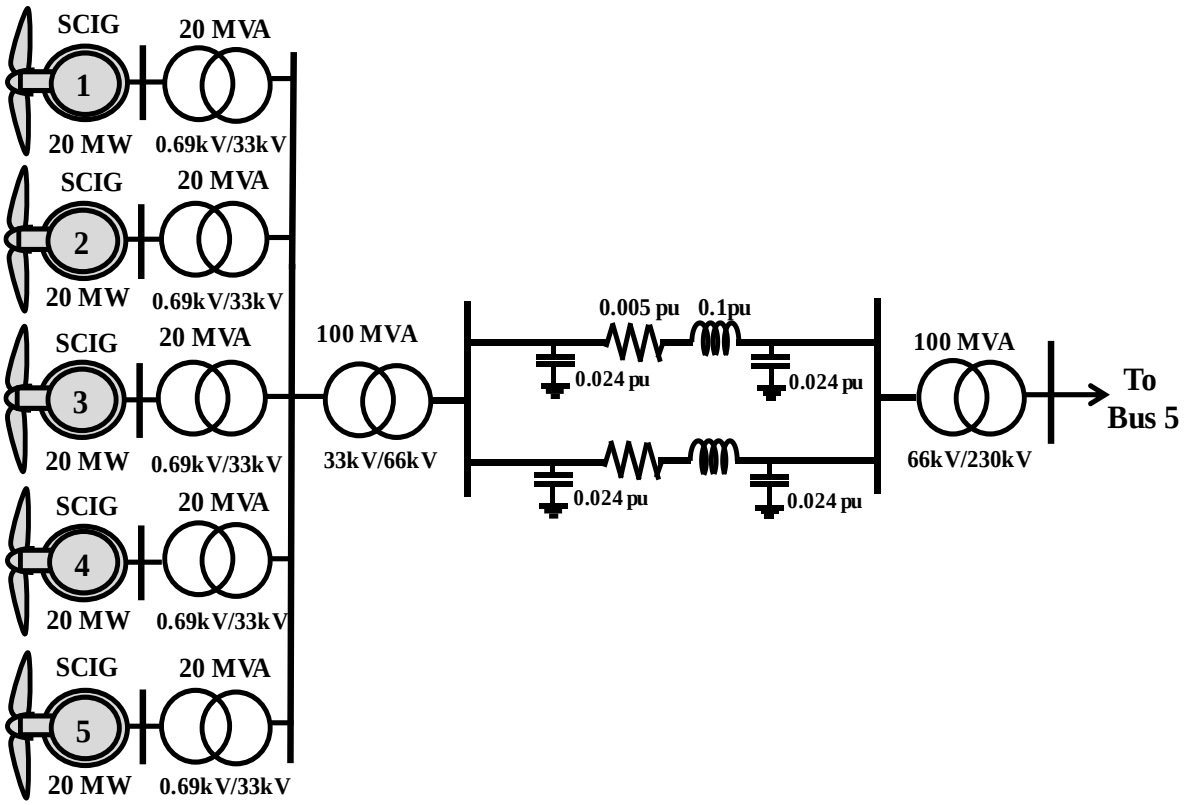

Fig. 5.3. Configuration of FSWT-SCIGs based onshore wind farm.

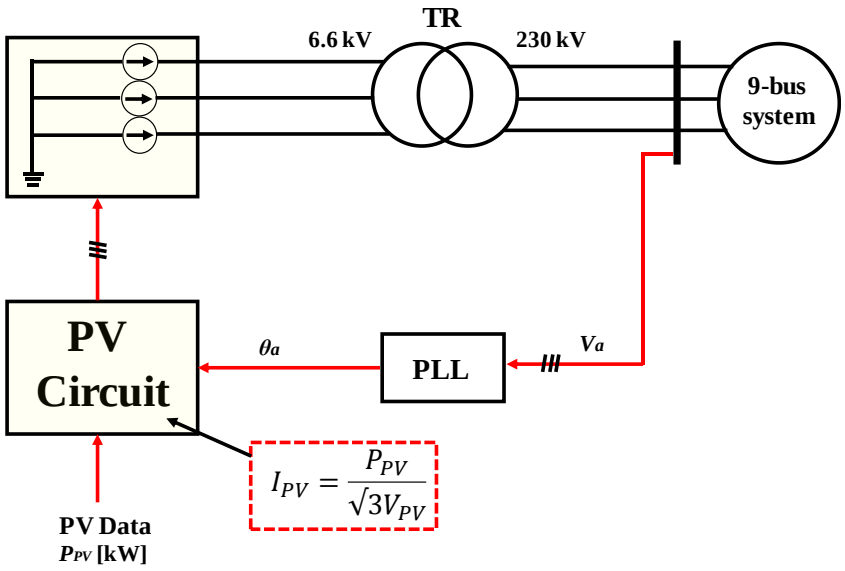

Fig. 5.4. Simple PV power system model.

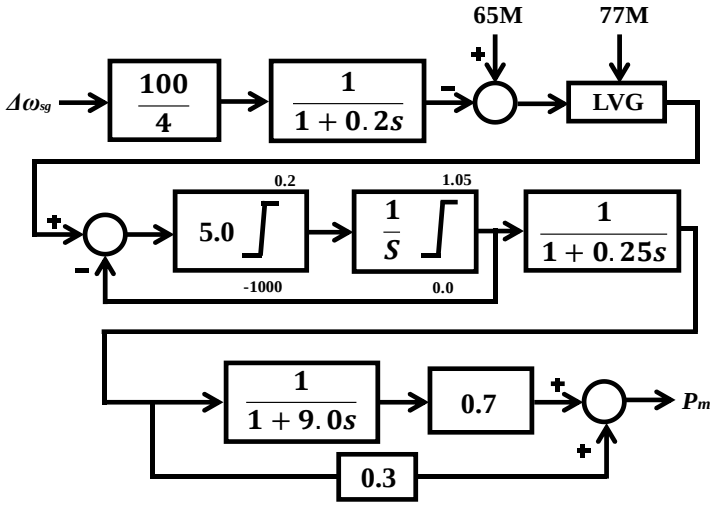

Fig. 5.5. Thermal turbine governor model.

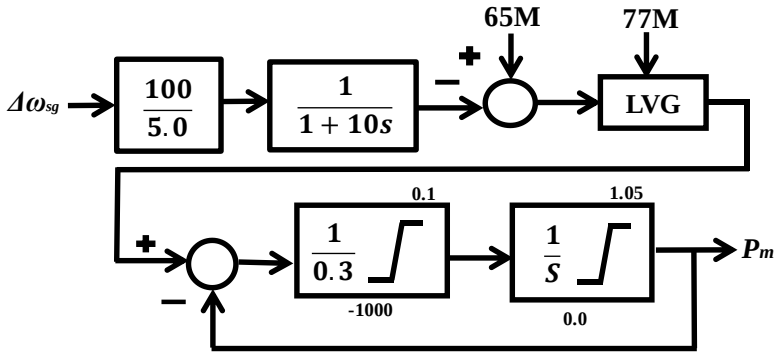

Fig. 5.6. Hydro turbine governor model.

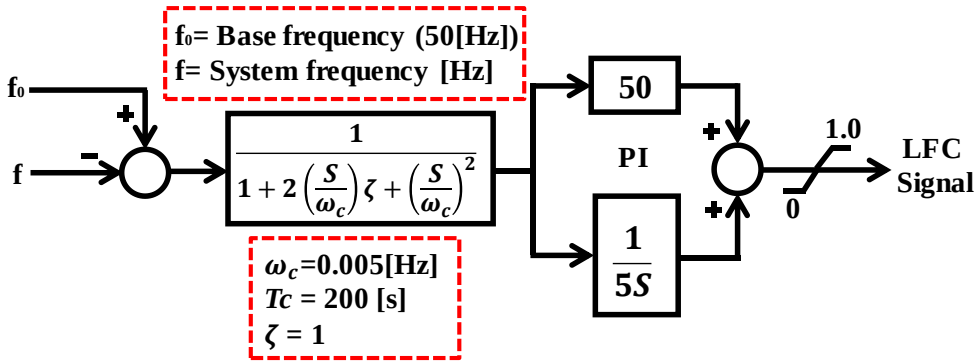

Fig. 5.7. LFC model.

Table 5.1. Parameters of synchronous generators.

Parameter	SG1	SG2	SG3
Rated Power	300 MVA	200 MVA	100 MVA
Voltage	16.5 kV	18 kV	13.8 kV
R_a	0.003 pu	0.003 pu	0.003 pu
X_l	0.1 pu	0.1 pu	0.1 pu
X_d	2.11 pu	2.11 pu	1.20 pu
X_q	2.05 pu	2.05 pu	0.700 pu
$X`_d$	0.25 pu	0.25 pu	0.24 pu
$X``_d$	0.21 pu	0.21 pu	0.20 pu
$X``_q$	0.21 pu	0.21 pu	0.20 pu
$T`_{do}$	6.8 s	7.4 s	7.2 s
$T``_{do}$	0.033 s	0.033 s	0.031 s
$T``_{qo}$	0.030 s	0.030 s	0.030 s
H	4.0 s	4.5 s	4.3 s

Table 5.2. 65M and 77M for each synchronous generator.

SG1 (Thermal)	**Frequency control**	**65M**	**77M**
	LFC	LFC signal	1
SG2 (Thermal)	**Frequency control**	**65M**	**77M**
	GF	0.80	0.84
SG3 (Hydro)	**Frequency control**	**65M**	**77M**
	GF	0.80	0.84

Table 5.3. Parameters of wind generators.

PMSG		SCIG	
MVA	20 (each)	MVA	20 (each)
R_{st}	0.02 pu	R_1	0.01 pu
L_{dst}	0.96 pu	X_1	0.1 pu
L_{qst}	0.76 pu	X_m	3.5 pu
ψ_m	1.4 pu	R_{21}	0.035 pu
H	3.0 s	R_{22}	0.014 pu
		X_{21}	0.03 pu
		X_{22}	0.089 pu
		H	1.5 s

5.3 VSC-HVDC Transmission System Model

In this study, a simplified model of VSC-HVDC system is used instead of detailed model to diminish the complexity and reduce the large computing time [112]. Fig. 5.8 illustrates the system configuration of the simplified model of VSC-HVDC system with its control system. The system is consisting of the two main part, one is a converter on the offshore side and the other is an inverter on the onshore side, which are modelled using voltage sources instead of detailed switching circuit with insulated gate bipolar transistors (IGBTs) [105].

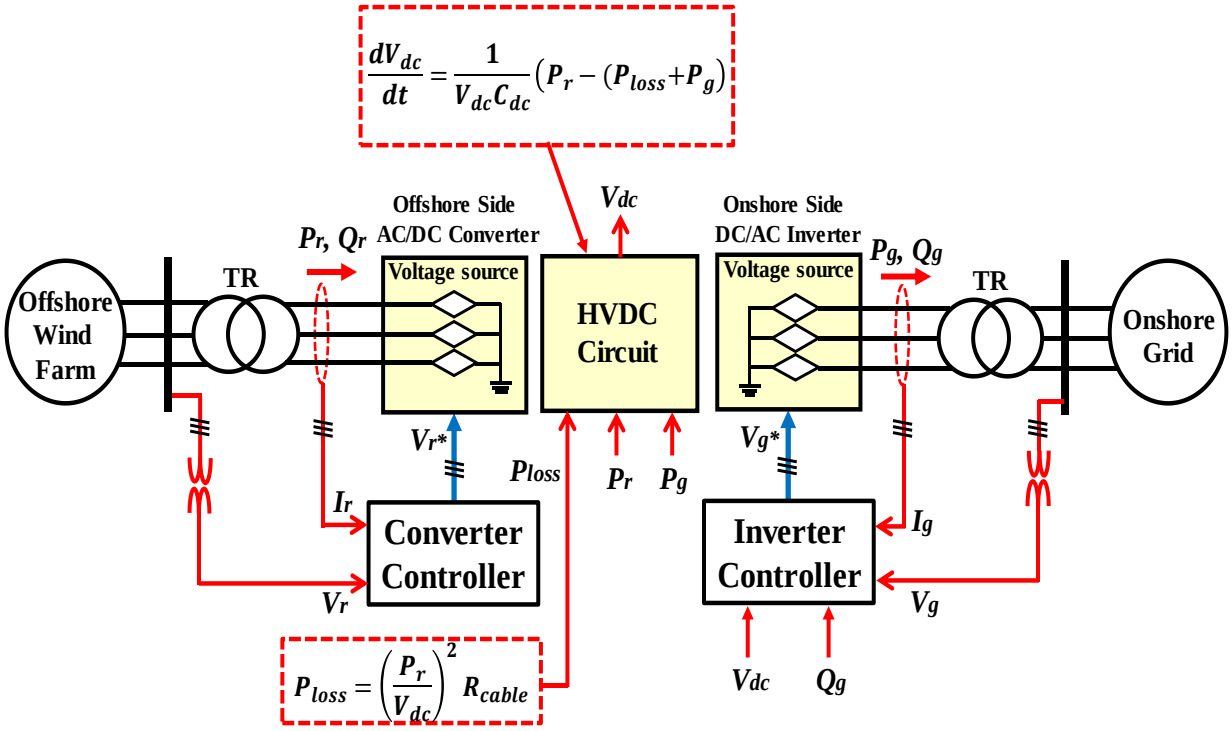

Fig. 5.8. Schematic diagram of VSC-HVDC system.

Three phase AC voltage generated by OWF is rectified to DC voltage through the converter. Three phase current (I_r), voltage (V_r), active power (P_r), and reactive power (Q_r) are detected on the offshore side AC system. The rectified DC voltage is transmitted to the onshore side. The transmitted DC voltage is converted again into AC voltage through the onshore side inverter. The converter is controlled by the converter controller (CC) and the inverter is controlled by the inverter controller (IC). Comparative analyses between the VSC-HVDC simplified model and the detailed model using IGBT based switching circuits are presented in [112] and it is concluded the simple model is very accurate.

5.3.1 Converter Controller (CC)

The block diagram of CC is depicted in Fig. 5.9. The main objective of the CC is to ensure the normal operation of VSC-HVDC connection based OWF. The converter station must establish an AC voltage of stable amplitude and frequency for the local grid of OWF. The voltage magnitude and phase of OWF are controlled by q-axis current (*Irq*) and d-axis current (*Ird*) of VSC-HVDC rectifier system. The voltage magnitude reference (*Magnitude**) is chosen as 1.0 pu and voltage phase reference (*Phase**) is set to 0.0 degree.

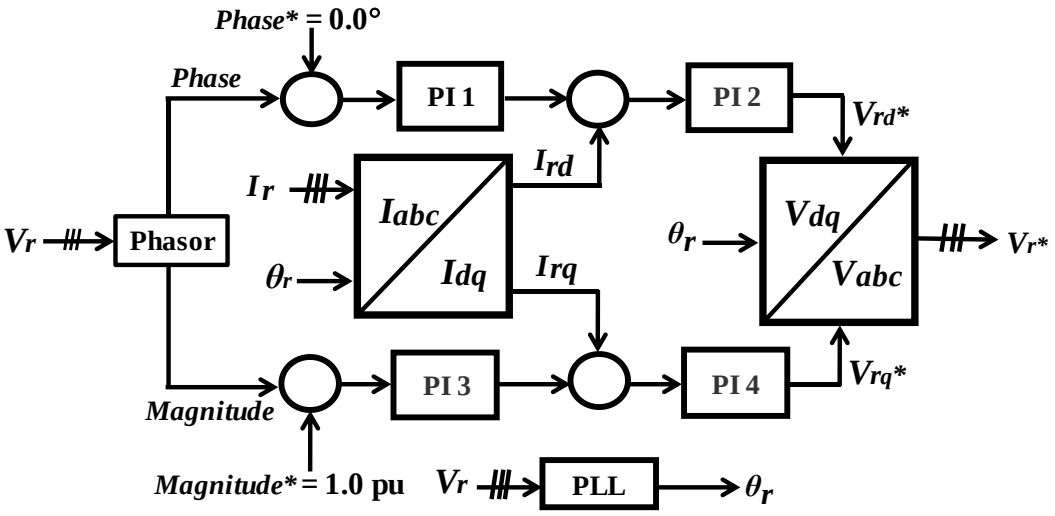

Fig. 5.9. Block diagram of CC.

5.3.2 Inverter Controller (IC)

The block diagram of IC is illustrated in Fig. 5.10. The aim of the IC is to control the reactive power (*Qg*) delivered to the onshore grid and keep the DC-Link voltage (*Vdc*) constant by using

d-axis (*Igd*) and q-axis (*Igq*) currents of VSC-HVDC inverter system, respectively. The reactive power reference (Q_g^*) is set to 0.0 pu for unity power factor operation and DC-Link voltage reference (V_{dc}^*) is set to 1.0 pu.

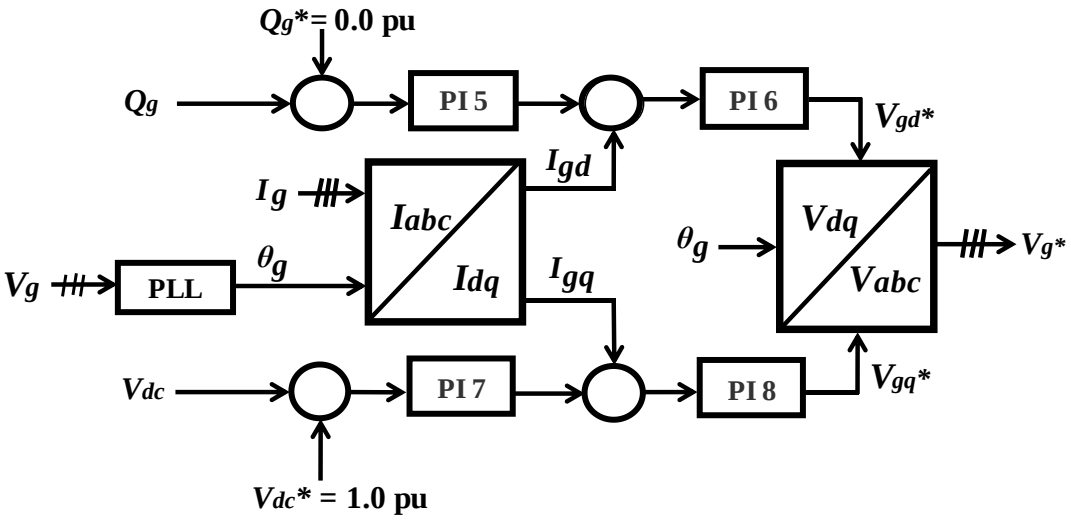

Fig. 5.10. Conventional rotor side controller.

5.3.3 DC-Link Model

The portion of the HVDC circuit is expressed based on the power balance [112], which means that the power supplied from the OWF must be equal to the sum of the power received by the grid and transmission line loss. In Fig. 5.8, *Vdc* is the DC-Link circuit voltage, *Cdc* is the DC-Link capacitor, *Pr* is the supplied power from the OWF, *Pg* is the grid side power, and *Ploss* is the power loss.

5.4 PMSG Model and Control Strategy

The overall block diagram of VSWT-PMSG model is shown in Fig. 5.11. In this study, the simplified model is used to decrease the simulation time [105]. The model consists of mechanical part, electrical part, and control system part. The mechanical part includes wind turbine and drive train models; the electrical part includes PMSG, DC-Link circuit, and LCL filter models; and the controller system part includes pitch controller, DC-Link circuit protection controller, stator side controller (SSC), grid side controller (GSC), and the interface with grid system. The interface inputs the terminal grid voltage to the simplified model and injects the output current from the simplified model to the grid system through a three phase current source [105].

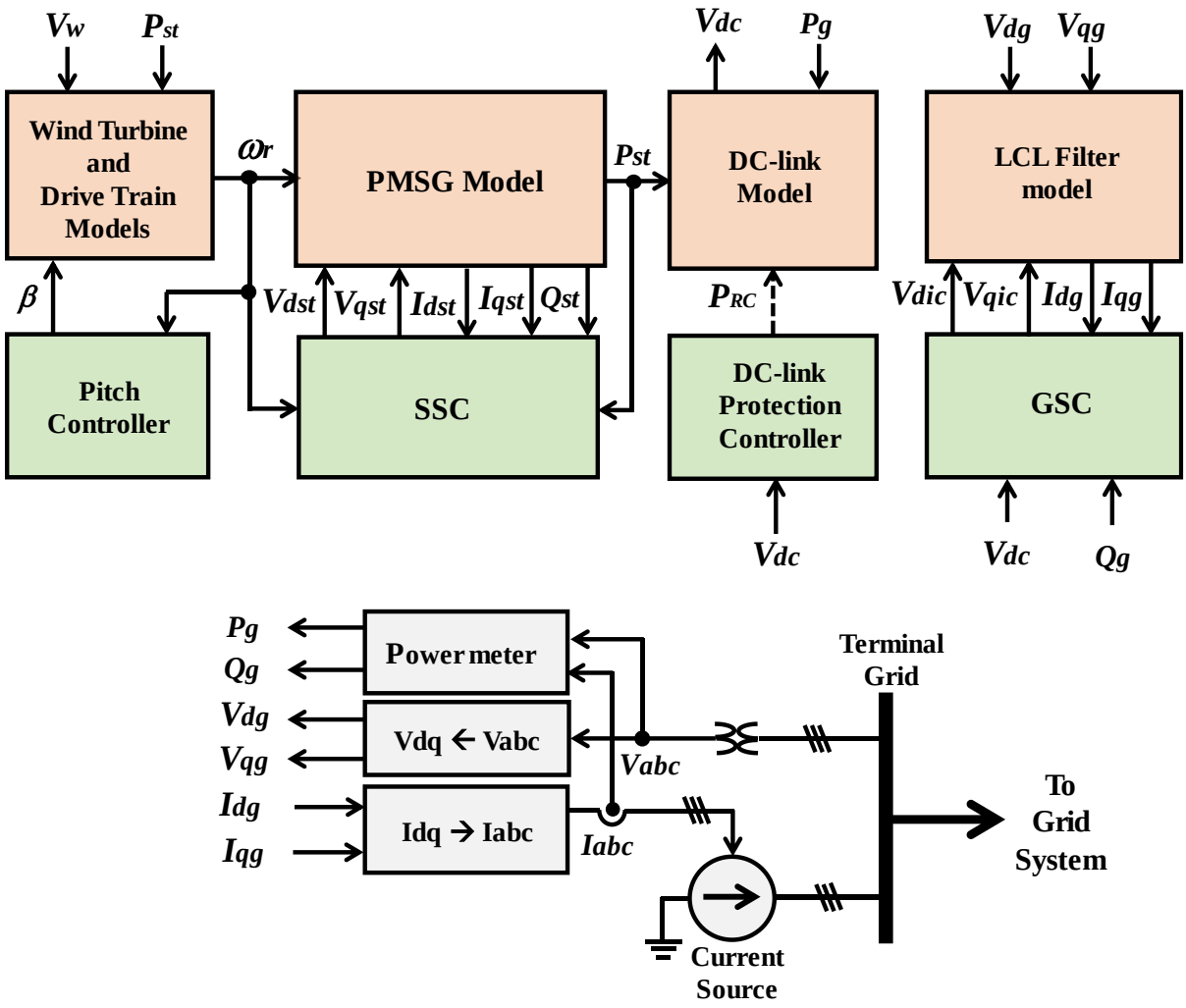

Fig. 5.11. Simplified model of VSWT-PMSG.

5.4.1 Stator Side Controller (SSC)

The block diagram of SSC is depicted in Fig. 5.12, which controls the active and reactive power of PMSG by controlling the q-axis stator current (I_{qst}) and the d-axis stator current (I_{dst}), respectively. SSC consists of four conventional PI controllers to compensate different error signals. The reactive power reference (Q_{st}*) is set to zero for unity power factor operation. The calculation method of active power reference (P_{ref}) will be discussed in the later section.

5.4.2 Grid Side Controller (GSC)

The block diagram of GSC is shown in Fig. 5.13, which controls the DC-Link voltage (*Vdc*) and the reactive power delivered to the grid system (*Qg*) by controlling the q-axis current (*Iqg*)

and the d-axis current (*Idg*) of LCL filter output current, respectively. The four PI controllers are used to track the different error signals.

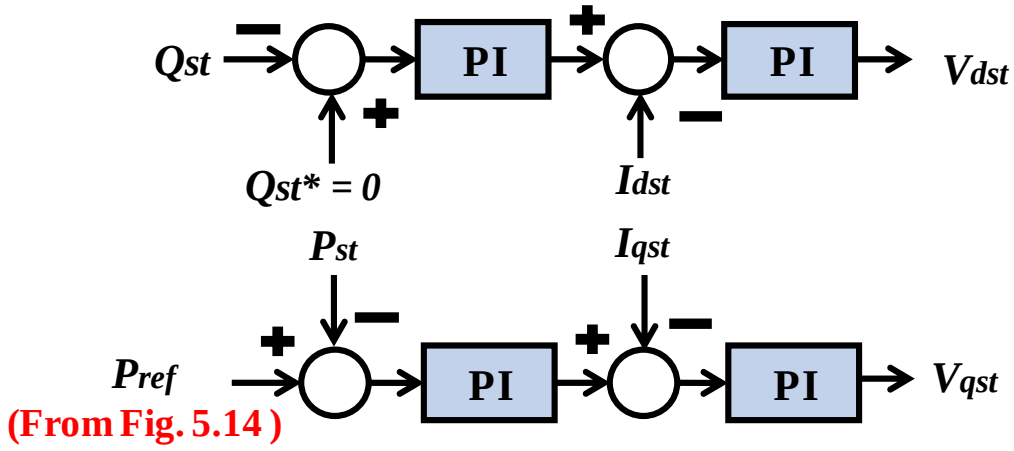

Fig. 5.12. Conventional stator side controller.

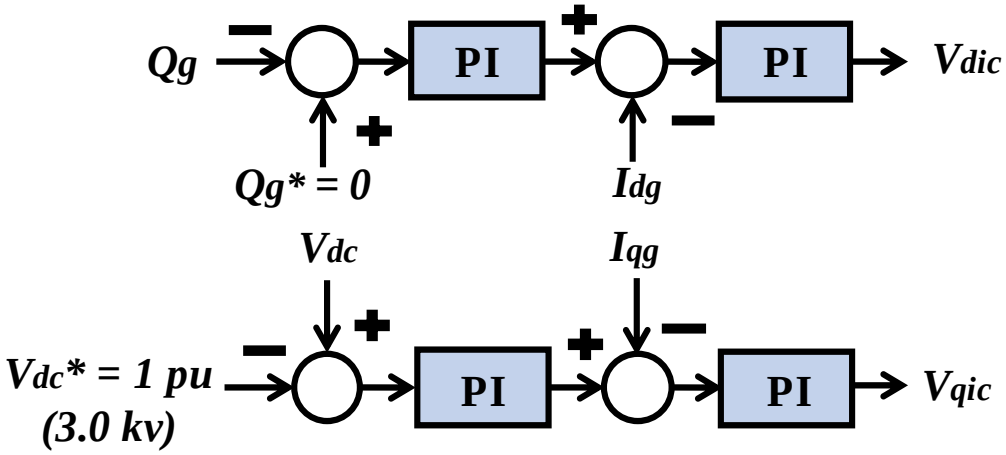

Fig. 5.13. Conventional grid side controller.

5.5 Proposed Coordinated Frequency Control Scheme of PMSG

5.5.1 Proposed Variable Deloaded Operation

When a VSWT-PMSG is operating under MPPT algorithm, it cannot provide primary frequency reserve like as conventional units. However, with some additional control loop, the VSWT-PMSG can provide reserve power. When the VSWT-PMSG generates less amount of active power than its available MPPT power, it can hold the difference between the available

MPPT power and generated actual active power as the primary frequency reserve. This operation with reduced output is called deloaded operation.

Though the fixed reserve margin is considered for the deloaded operation of VSWTs [66-110] conventionally, the power losses can increase in this case. Thus, in this study the variable reserve margin algorithm is designed to decrease the energy loss. The proposed method is depicted in Fig. 5.14. In this figure, the MPPT power (P_{mppt}) is multiplied by the gain ($G=1-K_{DL}$) to obtain the variable reserve power. The MPPT operation shown in Equation (2.6) is already discussed in Chapter 2. The variable deloading gain K_{DL} is decided based on the standard deviation (σ) of the onshore grid frequency over the past 60 s and it is computed at every 1 s in this study. The duration of 60 s has been determined by trial and error method. When σ is larger, the system needs more reserve power and vice versa. Depending upon the σ, the deloading coefficient (from 0% to 10%) is determined by the variable gain (K_{DL}) as shown in Fig. 5.15.

The characteristic of the variable gain shown in Fig. 5.15 has been determined by trial and error basis to achieve low energy loss as well as high onshore grid frequency control capability based on the considerations below:

1. If "a" becomes larger, the range of 0% deloaded operation (MPPT operation) also becomes large and thus the energy loss may become less.
2. If "c" becomes less, the range of 10% deloaded operation becomes large and then output increase from OWF can be done more easily. As system frequency becomes below 50 Hz when active power in the main grid is not sufficient, output increase from OWF can contribute to eliminate the system frequency decrease.

According to Fig. 5.15, deloaded output from each wind generator, *Pdel,* in Fig. 5.14 is determined as follows:

a) When σ is smaller than or equal to "a" (=0.035), K_{DL} = 0. Thus, the deloading rate is 0%, which means that *Pdel* = *Pmppt*.
b) When σ > a (=0.035), K_{DL} increases on the linear relationship until σ = c (=0.08) as shown in Fig. 16, and the deloading rate also increases. Therefore *Pdel* = $(1-K_{DL})$**Pmppt.*
c) When σ > c (=0.08), *KDL* = 0.1. Thus, the deloading rate is 10%, which means that *Pdel* = 0.9**Pmppt*.

In Fig. 5.14, a delay of 2 s is considered after grid frequency signal because of the communication delay in the data transmission from the onshore grid to OWF. The frequency signal

is detected on the onshore power system and it is transmitted to the OWF by using, for example, optical fiber or microwave link, but there must be a delay in this process. This delay includes sensing of onshore grid frequency, transmitting using communication channel, receiving and processing of the data for entering it to the OWF control system. The delay of 2 s has been determined by reference to [116].

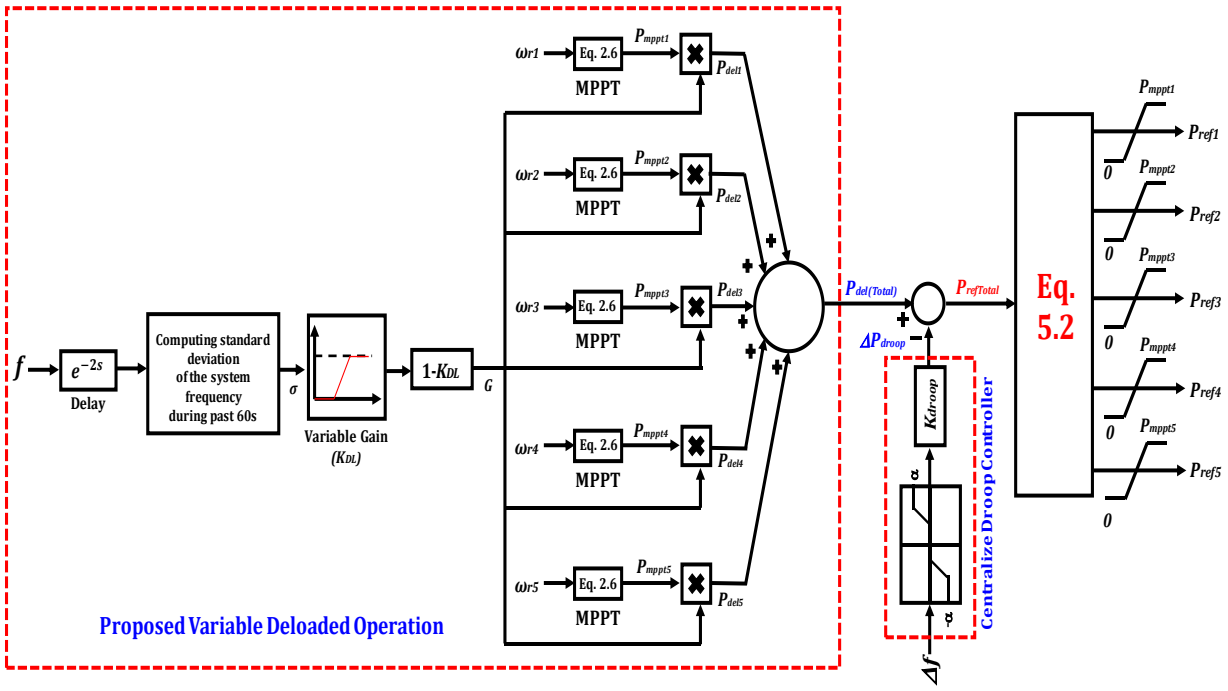

Fig. 5.14. Proposed centralized droop controller with variable deloaded operation.

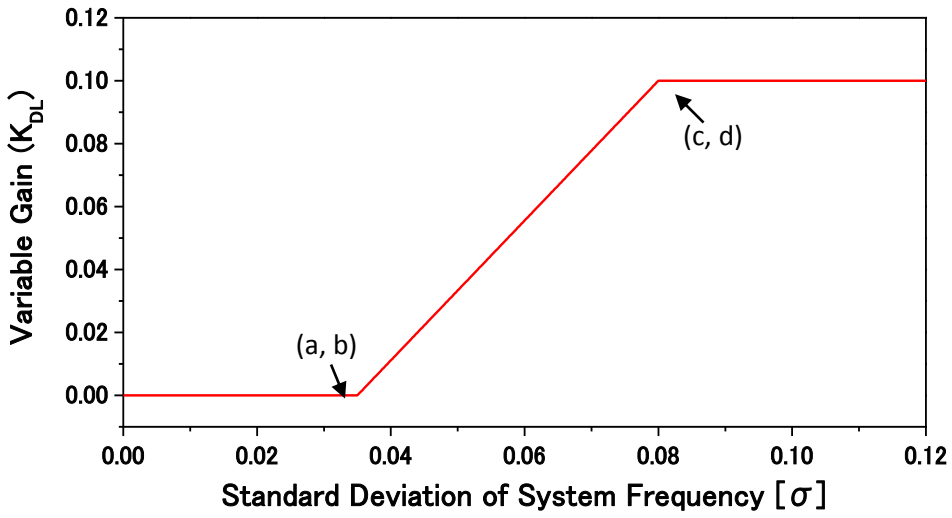

Fig. 5.15. Variable Gain (*KDL*).

5.5.2 Centralized Droop Control

Fig. 5.14 depicts also the schematic diagram of droop control system. In the droop control portion, a dead band is installed. The deviation of the onshore grid frequency ($\Delta f = f_{sys} - f_{set}$) is taken as input to this controller, where f_{sys}=measured onshore grid frequency and f_{set} is the rated frequency (=50 Hz). The droop controller of VSWT-PMSGs is only activated when the frequency variation is outside the predefined threshold limit ($|\alpha| = 0.05$). The threshold value and droop gain (K_{droop} =15) have been chosen by trial and error method to obtain the optimum performance from the centralized droop controller.

The reserved power obtained by the proposed variable deloaded operation is used by the centralized droop controller to control the onshore grid frequency fluctuations as shown Fig. 5.14, where the compensating power ΔP_{droop} is expressed as follows:

$$\Delta P_{droop} = K_{droop} \Delta f \tag{5.1}$$

The active power reference (P_{ref}) for each wind generator is determined according to Equation (5.2) as shown in the last stage of Fig. 5.14.

$$P_{refn}(n = 1,2,..,5) = P_{refTotal} \times \frac{P_{deln}(n=1,2..,5)}{P_{del(Total)}} \tag{5.2}$$

The limiter is used in the last stage so that the output reference of each VSWT-PMSG will not be greater than the MPPT output.

5.6 Simulation Results and Discussions

In this work, simulation study has been performed on the hybrid power system model shown in Fig. 5.1 by using PSCAD/EMTDC software. The rated frequency is 50 Hz. The relatively large solution time step of 100 μs is used in this simulation work because the simplified models are used for both PMSG and HVDC transmission system. Three cases are considered in this study in order to validate the proposed variable deloaded operation with centralized droop controller. They are:

Case 1: Without any frequency controller in the OWF. Each wind generator operates under the conventional MPPT mode.

Case 2: With the centralized frequency controller shown in Fig. 5.14 with fixed deloaded (10%, K_{DL} is 0.1 constant) operation.

Case 3: With the centralized frequency controller shown in Fig. 5.14 with variable deloading gain shown in Fig. 5.15.

The actual wind speed data measured at every 3 s in Hokkaido Island, Japan, shown in Figs. 5.16 and 5.17, are used for VSWT-PMSG based OWF and FSWT-SCIG based WF, respectively.

Fig. 5.18 shows the total active power profiles of OWF (VSWT-PMSGs). It is seen that the active power output in Cases 2 and 3 are often smaller than that in Case 1. This is because the deloaded operation is activated in Cases 2 and 3. In addition, the active power in Case 2 is often smaller than that in Case 3, because the fixed deloaded operation (10%) is used in Case 2 while the proposed variable delaoded operation shown in Fig. 5.15 is implemented in Case 3.

Fig. 5.19 illustrates the DC-Link voltage of HVDC transmission system. The DC-Link voltage is approximately constant for all cases. The total active power profiles of FSWT-SCIGs WF and PV power station are depicted in Figs. 5.20 and 5.21, respectively. As can be seen from Figs. 5.20 and 5.21, there is almost no difference in active power among three cases.

Fig. 5.22 depicts the active power profiles of conventional SGs. The SGs are generating slightly higher amount of active power in Cases 2 and 3 than in Case 1, because they are compensating the decrease in the output from OWF due to the deloaded operation.

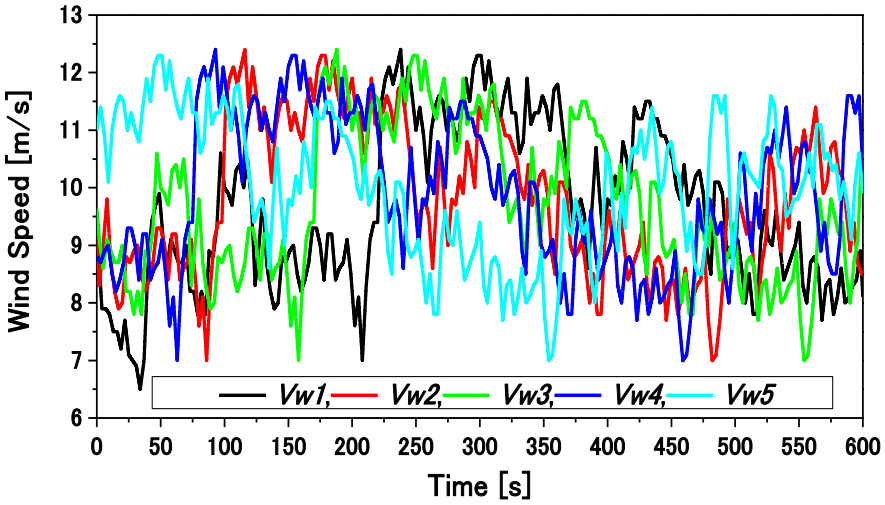

Fig. 5.16. Wind speed profiles (VSWT-PMSGs).

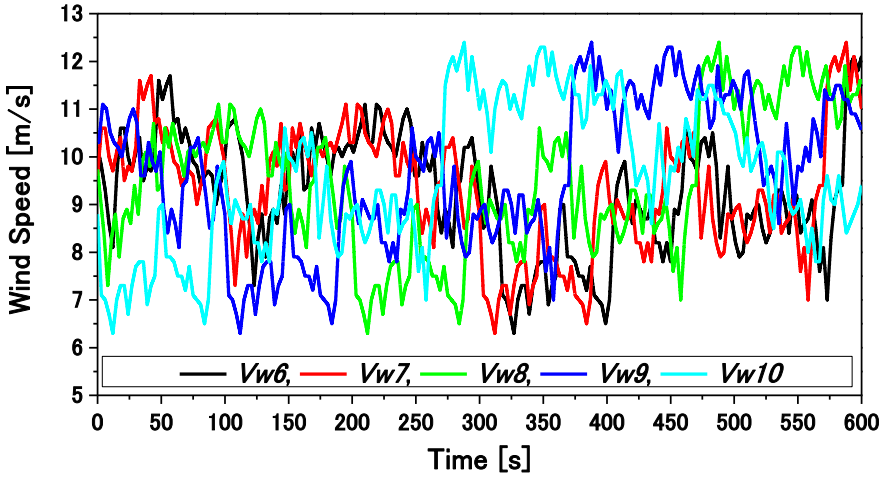

Fig. 5.17. Wind speed profiles (FSWT-SCIGs).

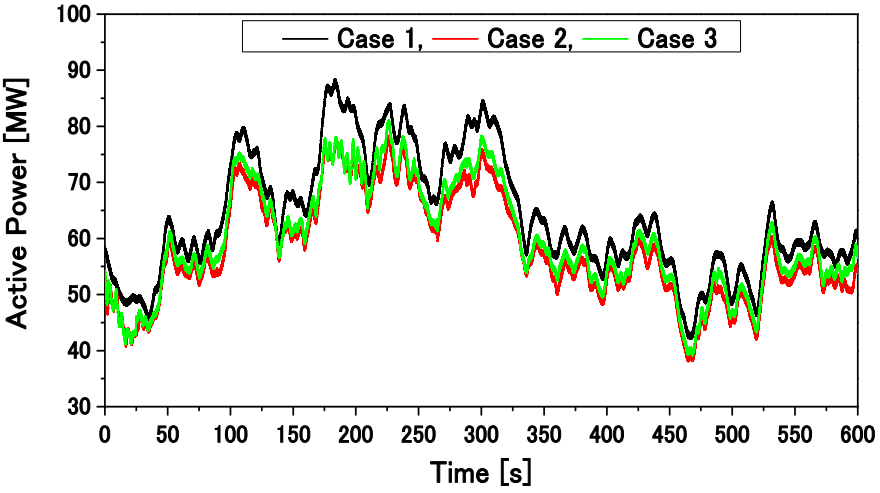

Fig. 5.18. Active power profiles of VSWT-PMSGs.

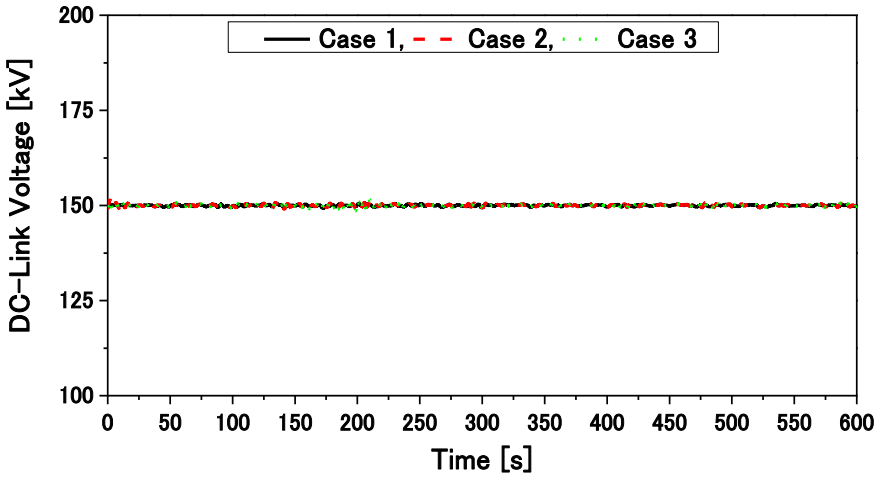

Fig. 5.19. DC-Link Voltage responses of VSC-HVDC transmission system.

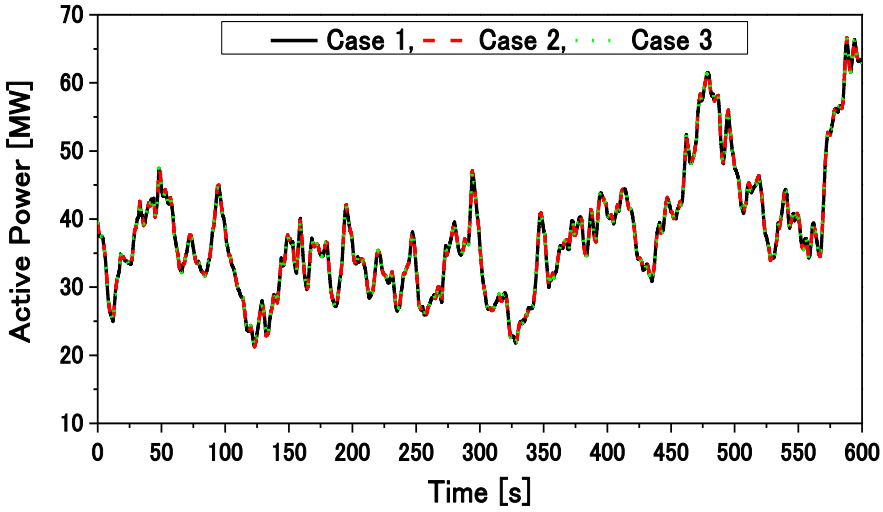

Fig. 5.20. Active Power profiles of FSWT-SCIGs.

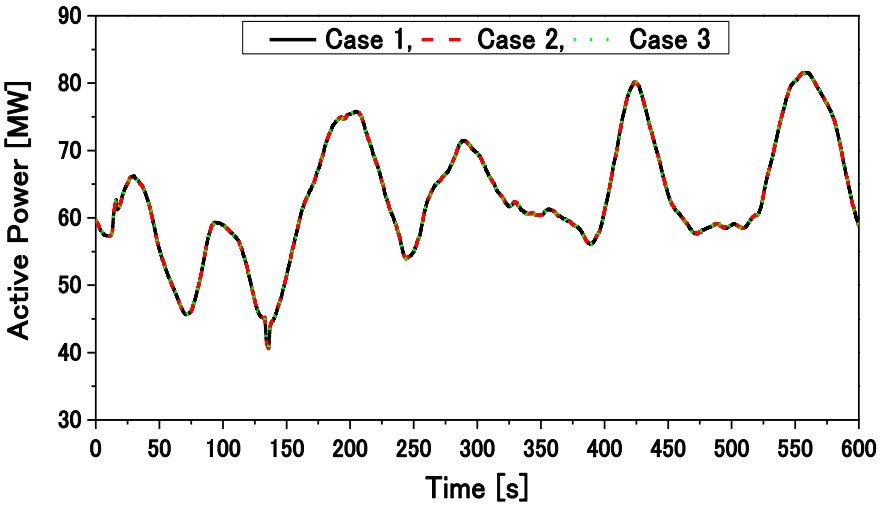

Fig. 5.21. Active Power profiles of PV power station.

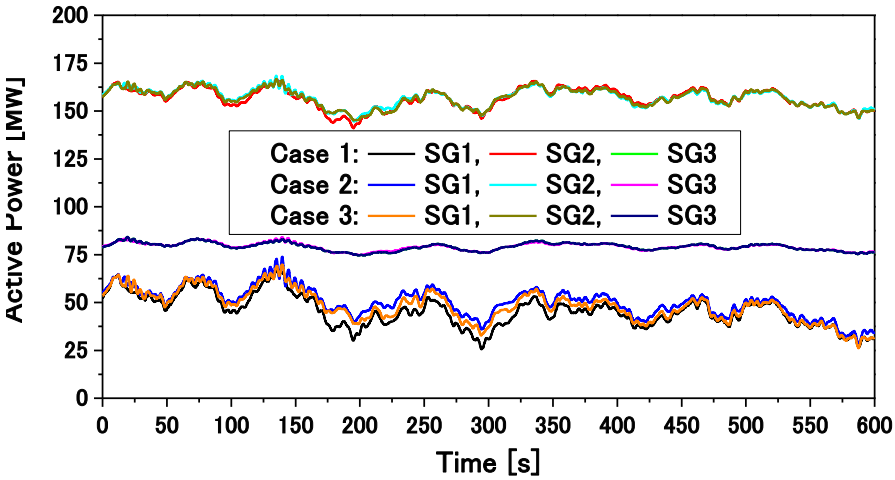

Fig. 5.22. Active power profiles of conventional SGs.

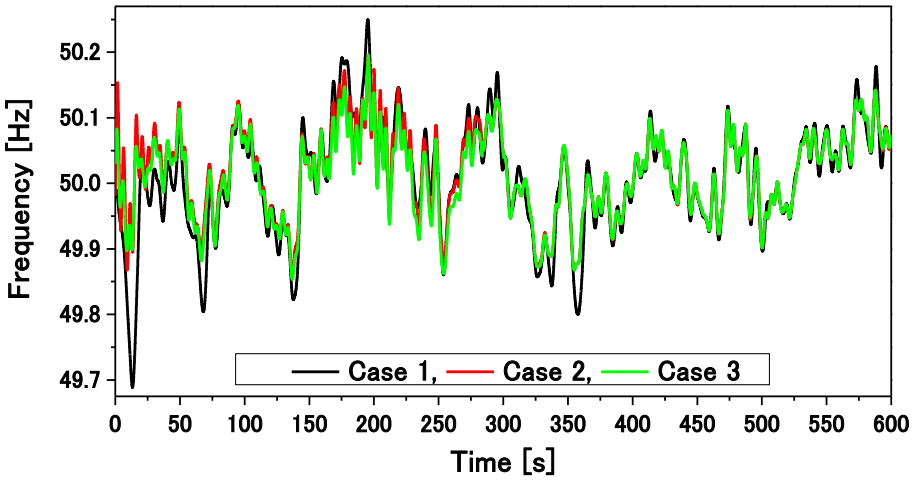

Fig. 5.23. Frequency responses of the onshore power system.

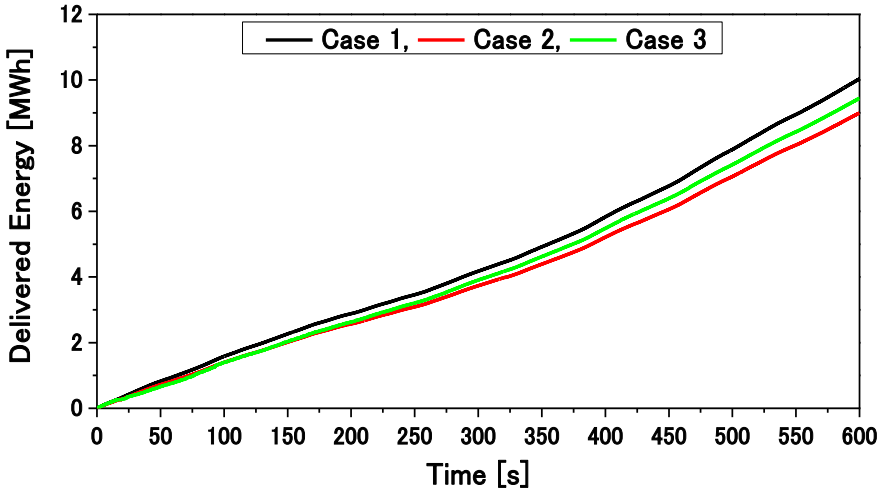

Fig. 5.24. Delivered energy of OWF (VSWT-PMSGs).

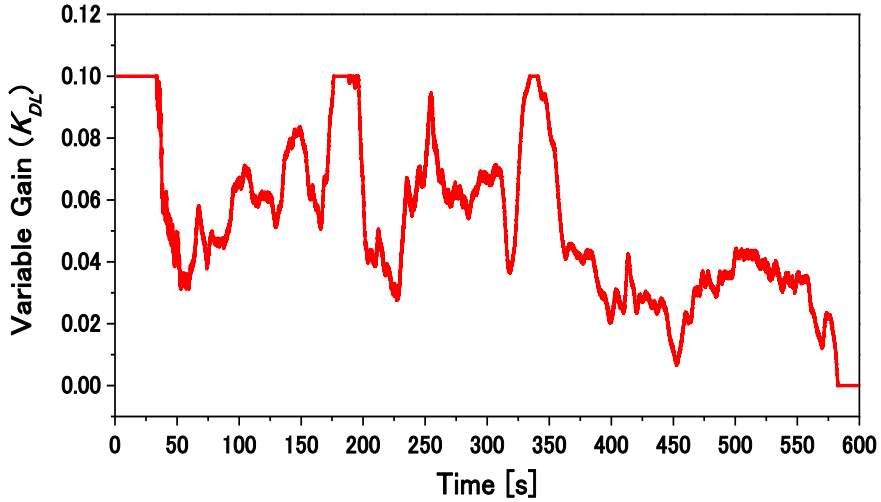

Fig. 5.25. Variable gain (KDL).

Finally, the onshore grid system frequency response is shown in Fig. 5.23, from which it is seen that the frequency fluctuations are smaller in Cases 2 and 3 than in Case 1, and thus the frequency fluctuations are effectively decreased in Cases 2 and 3. This is because the PMSG-based OWF is controlling the onshore grid system frequency through the droop controller using the reserved active power in Cases 2 and 3.

The energy (MWh) delivered from OWF in Cases 1, 2, and 3 are shown in Fig. 5.24. It can be seen that the decrease of MWh output in Case 3 is smaller than that in Case 2. This is because the reserve power is variable (from 0% to 10%) in Case 3 while the fixed amount of power (10%) is reserved in Case 2. In other words, the energy loss is smaller in Case 3 compared to Case 2.

Fig. 5.25 shows response of the variable gain (K_{DL}). It is seen that the gain is varying between 0.0 and 0.1 as described in section 5.5.

Table 5.4: Characteristics of system frequency in three cases.

	Case 1	**Case 2**	**Case 3**
$+\Delta f$ [Hz]	0.2496	0.1884	0.1943
$-\Delta f$ [Hz]	-0.3116	-0.1381	-0.1408
σ_f [Hz]	0.0792	0.0650	0.0656
MWh Loss (%)	0	7.13	3.54

Finally, Table 5.4 shows characteristics of the onshore grid system frequency in the three cases, where $+\Delta f$ denotes the maximum frequency deviation in the positive direction, $-\Delta f$ denotes that in the negative direction, and σ_f denotes the standard deviation of the frequency fluctuations. It is seen from the table that all of $+\Delta f$, $-\Delta f$, and σ_f are smaller in Cases 2 and 3 than in Case 1. In Cases 2 and 3, the maximum frequency deviations can be well controlled within ±0.2 Hz, the standard permissible range of power system frequency deviation in Japan, and the standard deviation can also be controlled by about 20% compared to that in Case 1. In addition, though the capability to control the system frequency fluctuations in Case 3 is almost in the same level as that in Case 2, the energy loss is smaller in Case 3 by almost 50% than that in Case 2.

Therefore, it is concluded that the proposed variable deloaded operation with centralized droop controller can effectively decrease the onshore grid frequency fluctuations with lower energy loss.

5.7 Chapter Conclusion

In this chapter, a novel variable deloaded operation method with centralized droop controller is proposed for VSWT-PMSGs based OWF to reduce the frequency oscillations of the connected onshore grid system. The variable deloaded operation is performed according to the standard deviation of the onshore system frequency fluctuations to maintain sufficient primary reserve and reduce the energy loss. A dead band is also used in the centralized frequency control scheme. The reserve power owing to the variable deloaded operation is used by the droop controller in the centralized frequency control system for better frequency regulation.

Comparative analysis has been performed among three cases, i.e., no control, the fixed deloaded operation, and the variable deloaded operation. The simulation results show that the frequency oscillations and energy loss can be reduced effectively by the proposed scheme. Therefore, the proposed control strategy has a promising potential value to reduce the frequency fluctuations with low amount of energy loss. It is needless to say that, the proposed variable deloaded operation method can be applied to onshore WFs composed of variable speed wind turbine generators in order to control the grid frequency fluctuations, though it is applied to an OWF in this chapter.

Chapter 6

Conclusions

Penetration of renewable energy sources (RESs) like offshore wind farm (OWF) and solar photovoltaic (PV) station into the power system has been increasing significantly since the last decade. This large integration of RESs has introduced some vulnerabilities to the power system. Frequency stability is one of the main concern that should be taken into account. Normally, the frequency fluctuation is damped by the conventional power plants. Therefore, to maintain the frequency stability of the power system with large penetration ratio of RESs, RESs are required to operate like conventional units. They need to not only supply power to the grid, but also need to damp frequency fluctuations. One possible solution is a frequency control by OWF.

Normally, variable speed wind turbine with permanent magnet synchronous generator (VSWT-PMSG) is preferable for OWF. To integrate large-scale OWF into the onshore grid, voltage source converter based high voltage DC (VSC-HVDC) transmission system is attractive and more preferable than high voltage AC (HVAC) transmission system from an economic and technical point of view, especially in the case of very long transmission system.

For the frequency regulation of the onshore grid system, the VSWT-PMSG-based OWF connected to the onshore grid through VSC-HVDC transmission system should have sufficient power reserve. In this case, power reserve is possible by operating the VSWT-PMSGs at a reduced power level instead of maximum power point tracking (MPPT) mode which is called deloaded operation. Normally, the primary reserve is implement by the fixed level of deloaded operation of VSWT with some auxiliary control loop. However, in the fixed deloaded operation, output power injected to the grid system from OWF is reduced by a fixed ratio at all times, and hence, the energy loss becomes large.

This thesis proposes some centralized frequency control schemes with a deloaded operation of VSWT-PMSGs based OWF connected to the onshore grid through VSC-HVDC transmission system to damp frequency fluctuations of the onshore grid, in which a large-scale WF composed of fixed speed wind turbines with squirrel cage induction generators (FSWT-SCIGs) and solar PV station are installed. This chapter concludes and summarizes the results of previous chapters.

In Chapter 2, a basic overview of the wind turbine system is presented. Then the mechanical power extraction of a practical wind turbine system is explained. After that the pitch angle

controller models are described. Finally, the different types of wind turbine technologies (e.g. FSWT-SCIG and VSWT-PMSG) are briefly discussed.

Chapter 3 presents a new simplified model of HVDC transmission system connecting OWF to onshore grid. Comparative analyses of dynamic characteristics between the simplified and detailed models have been performed in order to confirm the validity of the proposed simplified model of VSC-HVDC system. The simplified model of VSC-HVDC system has sufficient accuracy because there is almost no difference among the simulation results for the both simplified and detailed models. Moreover, the simulation time can be reduced significantly by using the proposed simplified model of VSC-HVDC system. Therefore, the proposed simplified model can be used effectively to analyze the power system with VSC-HVDC based OWF.

Chapter 4 proposes two fixed deloaded methods with centralized droop controller for VSWT-PMSGs based OWF to reduce the frequency oscillations of the connected onshore grid system. The first centralized frequency controller is proposed for VSWT-PMSGs based OWF, which incorporates both droop controller with dead band and rotor speed control based fixed deloaded operation to contribute to the power system frequency regulation. Through simulation analysis, it is shown that the proposed centralized frequency controller can suppress the frequency fluctuations of the power system effectively. Another novel centralized frequency control technique which is suitable for VSWT-PMSGs is proposed to reduce the frequency oscillations of hybrid power system. The centralized frequency control system integrates both fixed deloaded operation based on the modified MPPT equation and droop controller with dead band. The deloaded power is used by the droop controller for better frequency regulation. The simulations results confirmed that the frequency oscillations can be reduced effectively by the proposed frequency controller. Therefore, the proposed control strategies have promising potential value to reduce the frequency fluctuations.

In Chapter 5, a novel variable deloaded operation method with centralized droop controller is proposed for VSWT-PMSGs based OWF to reduce the frequency oscillations of the connected onshore grid system. The variable deloaded operation is performed according to the standard deviation of the onshore system frequency fluctuations to maintain sufficient primary reserve and reduce the energy loss. A dead band is also used in the centralized frequency control scheme. The reserve power resulting from the variable deloaded operation is used by the droop controller in the centralized frequency control system for better frequency regulation. Comparative analysis has

been performed among three cases, i.e., no control, the fixed deloaded operation, and the variable deloaded operation. The simulation results reveal that the variable deloaded operation can decrease the energy loss compared to the fixed deloaded operation as well as suppress the frequency fluctuations in the same level as the fixed deloaded operation.

In this thesis, some deloaded operation methods are presented for VSWT-PMSGs based OWF which is connected to onshore grid through VSC-HVDC transmission system, to maintain primary reserve and to suppress the frequency fluctuations of the onshore grid due to the installations of large-scale FSWT-SCIGs based onshore WF and PV power station. Considering all the chapters, it can be concluded that the proposed control strategies of OWF has promising potential value to damp the frequency fluctuations of the connected onshore grid.

Acknowledgements

This thesis has been submitted to the Department of Electrical and Electronic Engineering of Kitami Institute of Technology, Japan for the fulfillment of the requirement for the Ph.D. degree. This thesis deals with coordinated frequency control of hybrid onshore power system by PMSG-based offshore wind farm.

It is my great pleasure to acknowledge the generous contributions of many individuals, experts and institutions which have assisted me during my Ph.D. study.

Firstly, I would like to express my sincere gratitude to my supervising professor, Prof. Dr. Junji Tamura for the continuous support of my Ph.D. study and related research, for his patience, motivation, and immense knowledge. His guidance helped me in all the time of research and writing of this thesis. I could not imagine having a better advisor and mentor for my Ph.D study.

I am deeply grateful to co-supervisors, Associate Prof. Dr. Rion Takahashi and Assistant Prof. Dr. Atsushi Umemura of Electrical and Electronic Engineering Department, Kitami Institute of Technology, Japan, for their support and kindness I have been provided with.

I am also grateful to Prof. Dr. Shinya Obara, Prof. Dr. Kenji Kurokawa and Associate Prof. Dr. Takeshi Kawamura of Electrical and Electronic Engineering Department, Kitami Institute of Technology, Japan, for their kind review of this thesis.

I am indebted to Prof. Dr. Mohammad Abdul Mannan, Head (Undergraduate Program), Department of Electrical and Electronic Engineering, American International University-Bangladesh (AIUB), Dhaka, Bangladesh, Associate Prof. Dr. S. M. Muyeen, Department of Electrical and Computer Engineering, Curtin University, Australia and Dr. Marwan Rosyadi, Planning Engineer, Hitachi Power Solutions Company Ltd., Japan for their help and inspiration during my Ph.D. study.

I wish to express my gratefulness to Kitami Institute of Technology, Japan, which has given me a unique opportunity to augment my engineering knowledge as well as has given me financial support during my study and attendance in various national and international conferences.

Also, Hitachi Research Laboratory (Energy Department), Hitachi Co. Ltd., Japan is highly appreciated for their support and collaboration during internship program in Ibaraki, Japan, which gave me the opportunity to learn new ideas in my research work.

I am also grateful to all the members of our Laboratory and Bangladeshi community for their patience and support in overcoming numerous obstacles I have been facing through my research.

I must express my very profound gratitude to my parents and to my sisters, Mr. Javed Ali, Mrs. Rabeya Akter, my elder sister Mrs. Zeenat Afroze and my younger sister Ms. Rifat Jahan. It is because of their endless pray and love; finally, I have accomplished this work.

My most heartfelt acknowledgement must go to my husband, Dr. Md. Rifat Hazari for providing me with unfailing support and continuous encouragement throughout my years of study and through the process of researching and writing this thesis. This accomplishment would not have been possible without him.

At last, my Almighty, thank you very much for everything.

Effat Jahan

September 2019, Kitami, Japan

References

[1] BP Statistical Review of World Energy, June 2013 Available online: https://www.bp.com/en/global/corporate/energy-economics/statistical-review-of-world-energy.html [Accessed on 13 August 2013]

[2] N. Gao, "Energy-saving target prediction from the perspective of carbon dioxide emissions reduction", *Electronics, communications and control (ICECC), 2011 international conference*; p. 3723-25, 2011.

[3] J. Dong, G. Xue, M. Dong, X. Xu, "Energy-saving power generation dispatching in China: Regulations, pilot projects and policy recommendations—a review," *Renewable and Sustainable Energy Reviews,* vol. 43, pp. 1285-1300, 2015.

[4] The United Nations Framework Convention on Climate Change: 'The Kyoto Protocol', Available online : http:// unfccc.int/resource/docs/convkp/kpeng.pdf, 1997

[5] J. Yuan, J. Kang, C. Yu, Z. Hu, "Energy conservation and emissions reduction in China—progress and prospective", *Renewable Sustainable Energy Rev*, vol. 15, pp. 4334-4347, 2011.

[6] R. Saidur, N. A. Rahim, M. R. Islam, K. H. Solangi, "Environmental impact of wind energy," *Renewable and Sustainable Energy Reviews*, vol. 15, no. 5, pp. 2423-2430, 2011.

[7] O. Ellabban, H. A. Rub, F. Blaabjerg, "Renewable energy resources: Current status, future prospects and their enabling technology," *Renewable and Sustainable Energy Reviews*, vol. 39, pp. 748-764, 2014.

[8] V. Diakov, G. Brinkman, P. Denholm, T. Jenkin, R. Margolis, "Renewable generation effect on net regional energy interchange", *Power & Energy Society General Meeting 2015 IEEE*, pp. 1-4, 2015.

[9] Armando L. Figueroa-Acevedo, Agustín A. Irizarry-Rivera, "Variability assessment of solar and wind resources in Puerto Rico", *Probabilistic Methods Applied to Power Systems (PMAPS) 2014 International Conference on*, pp. 1-6, 2014.

[10] "IPCC" in Special Report on Renewable Energy Sources and Climate Change Mitigation: Final Release, U.K., Cambridge:Cambridge Univ. Press, 2011.

[11] A. Brown, S. Müller, Z. Dobrotková, "Renewable energy: markets and prospects by technology" *International Energy Agency Information Paper*, 2011.

[12] S. R. Bull, "Renewable energy today and tomorrow," *Proceedings of the IEEE*, vol. 89, no. 8, pp. 1216-1226, Aug. 2001.

[13] REN21, Renewables 2018: Global Status Report, A comprehensive annual overview of the state of the renewable energy. [Accessed on 23 October 2018]

[14] The Global Wind Energy Council (GWEC) (2017). [Online]. Available: http://gwec.net/cost-competitiveness-puts-wind-in-front/. [Accessed on 23 October 2018]

[15] Offshore Wind Power 2010Archived June 30, 2011, at the Wayback Machine *BTM Consult*, 22 November 2010. Retrieved: 22 November 2010

[16] The Global Wind Energy Council (GWEC) (2017). gwec.net. GWEC. Retrieved 3 May 2018.

[17] Tillessen, Teena, "High demand for wind farm installation vessels". *Hansa International Maritime Journal*. vol. 147 no. 8. pp. 170–171, 2010.

[18] Environmental and Energy Study Institute, October 2010.

[19] Madsen & Krogsgaard. Offshore Wind Power 2010 Archived June 30, 2011, at the Wayback Machine BTM Consult, 22 November 2010. Retrieved: 22 November 2010.

[20] The Ocean Economy in 2030, pp.205-212. OECD iLibrary, 27 April 2016. ISBN 9264251723 .

[21] M. A. G. de Brito, L. P. Sampaio, G. Luigi, G. A. e Melo and C. A. Canesin, "Comparative analysis of MPPT techniques for PV applications", *Proc. Int. Conf. Clean Elect. Power* (ICCEP), pp. 99–104, 2011.

[22] Cha, H.; Lee, S. "Design and Implementation of Photovoltaic Power Conditioning System using a Current based Maximum Power Point Tracking", *Proc. of 43rd IEEE IAS*, pp. 1-5, 2008.

[23] Kwon, J.; Nam, K. H.; Kwon, B. H. "Photovoltaic Power Conditioning System With Line Connection. *IEEE Transactions on Industrial Electronics"*, v. 53, n. 5, pp. 1048-1054, 2006

[24] European Renewable Energy Council, EREC-2005. Available online: http://www.erec.org/renewableenergy/photo-voltaics.html.

[25] Hsieh, G. C.; Chen, H. L.; Chen, Y.; Tsai, C. M; Shyu, S. S. " Variable Frequency Controlled Incremental Conductance Derived MPPT Photovoltaic Stand-Along DC Bus System", *Proc. of 23rd IEEE APEC*, 2008, pp. 1849-1854.

[26] Global Wind Energy Council (GWEC). Global Wind Energy Outlook 2016: Wind Power to Dominate Power Sector Growth. 2016. Available online: http://www.gwec.net/ (Accessed on 30 October 2018).

[27] "OFFSHORE WIND | GWEC". www.gwec.net. Retrieved 5 August 2017

[28] Global Wind Energy Council (GWEC). 10 February 2016. Retrieved 14 April 2017. Online: https://www.gwec.net/wp-content/uploads/vip/GWEC-PRstats-2015_LR.pdf

[29] J. Jallad, S. Mekhilef, and H. Mokhlis, "Frequency Regulation Strategies in Grid Integrated Offshore Wind Turbines via VSC-HVDC Technology: A Review", *Energies*, vol. 10, No. 9, 2017

[30] E. Jahan, M. R. Hazari, M. Rosyadi, A. Umemura, R. Takahashi and J. Tamura, "Simplified model of HVDC transmission system connecting offshore wind farm to onshore grid", *2017 IEEE Manchester PowerTech*, United Kingdom, pp. 1-6 (2017)

[31] S. M. Muyeen, R. Takahashi, T. Murata and J. Tamura, "Operation and control of HVDC connected Offshore Wind Farm", *IEEE Trans. on Sustainable Energy*, vol. 1, No. 1, pp. 30-37, 2010

[32] B. Van Eeckhout, D. Van Hertem, M. Reza, K. Srivastava, and R. Belmans, "Economic comparison of VSC HVDC and HVAC as transmission system for a 300 MW offshore wind farm," *Eur. Trans. Electr. Power*, pp. 661–671, Jun. 2009.

[33] A. Arapogianni, J. Moccia, J. Wilkes, J. Guillet, P. Wilczek, J. Scola, and S. Azau, "The European Offshore Wind Industry - Key Treds and Statistics 2012*." European Wind Energy Association*, Jan-2013.

[34] "Offshore Wind: Nordzee Ost," Oct-2013. [Online]. Available: http://ec.europa.eu/energy/eepr/projects/files/offshorewind-energy/nordsee-ost_en.pdf. [Accessed: 18-Feb2014].

[35] P. Giller, "Multi-Contracting for the first project financing in the German Offshore Wind Market: Projekt Offshore Wind Farm Meerwind Sud/Ost [288 MW Offshore Wind Farm]," 03-Jan-2012

[36] AK. Skytt, P. Holmberg, KE. Juhlin, "HVDC light for connection of wind farms," *2nd International Workshop on Transmission Networks for Offshore Wind Farms*, 2001.

[37] KH. Sobrink, PL. Sorensen, P. Christensen, N. Sandersen, K. Eriksson, P. Holmberg, "DC feeder for connection of a wind farm," *CIGRE Symposium*, 1999.

[38] W. Lu, BT. Ooi, "Optimal acquisition and aggregation of offshore wind power by multi terminal voltage-source HVDC," *IEEE Trans. on Power Delivery*, vol.18, No.1, pp.201–206, 2003.

[39] L. Xu, and B. R. Andersen, "Grid connection of large offshore wind farms using HVDC," *Wind Energy*, Vol.9, No.4, pp.371-382, 2006.

[40] S. M. Muyeen, J. Tamura and T. Murata, "Stability augmentation of a grid connected wind firm", London, Springer-Verlag, 2009.

[41] G. Lalor, J. Ritchie, S. Rourke, D. Flynn, and M. J. O'Malley, "Dynamic frequency control with increasing wind generation", *IEEE Power Eng. Soc. Gen. Meet*, vol. 2, pp. 1715–1720, (2004)

[42] H. Polinder, S. W. H. de Haan, M.R. Dubois, J. Slootweg, "Basic operation principles and electrical conversion systems of wind turbines," *Proc. of Nordic Workshop on Power and Industrial Electronics, Trondheim,* Norway, 14–16 June 2004.

[43] G. Michalke, A. D. Hansen, T. Hartkopf, "Control strategy of a variable speed wind turbine with multipole permanent magnet synchronous generator," *Proc. of European Wind Energy Conference and Exhibition*, Milan, Italy, 7–10 May 2007.

[44] T. J. E. Miller, "Brushless permanent-magnet and reluctance motor drive", New York: Oxford Univ. Press (1989)

[45] Shuhui Li, Timothi A. Haskew, Ling Xu, "Conventional and novel control design for direct driven PMSG wind turbines," *Journal of Electric Power System Research*, vol. 80, pp. 328-338, March. 2010.

[46] L. M. Fernandes, C. A. Garcia, F. Jurado, "Operating capability as a PQ/PV node of a direct-drive wind turbine based on a permanent magnet synchronous generator", *Renewable Energy*, vol. 35, pp. 1308-1318, 2010.

[47] S. M. Muyeen, R. Takahashi, T. Murata, J. Tamura, "Multi-converter operation of variable speed wind turbine driving permanent magnet synchronous generator during network fault," *12th International Conference on Electrical Machines and Systems*, LS1C-4, Nov. 2009.

[48] M. F. M. Arani and Y. A. I. Mohamed, "Assessment and enhancement of a full-scale PMSG-based wind power generator performance under faults," *IEEE Trans. on Energy Conversion*, vol. 31, no. 2, pp. 728-739, June 2016.

[49] K. Kim, Y. Jeung, D. Lee and H. Kim, “LVRT scheme of PMSG wind power systems based on feedback linearization,” *IEEE Trans. on Power Electronics*, vol. 27, no. 5, pp. 2376-2384, May 2012.

[50] D. Xiang, J. C. Turu, S. M. Muratel and T. Wang, “On-site LVRT testing method for full-power converter wind turbines,” *IEEE Trans. on Sustainable Energy*, vol. 8, no. 1, pp. 395-403, Jan. 2017.

[51] P. Xing, L. Fu, G. Wang, Y. Wang and Y. Zhang, “A compositive control method of low-voltage ride through for PMSG-based wind turbine generator system,” *IET Generation, Transmission & Distribution*, vol. 12, no. 1, pp. 117-125, 2 1 2018.

[52] S. M. Muyeen, A. Al-Durra, J. Tamura, “Variable speed wind turbine generator system with current controlled voltage source inverter”, *Electric Power Systems Research*, vol. 80, pp. 328–338, 2010.

[53] E.ON Netz, "Grid Code – high and extra high voltage", April 2006.

[54] E.ON Netz, "Requirements for Offshore Grid Connections in the E.ON Netz Network", 1. April 2008.

[55] "Oceans of opportunity – Harnessing Europe’s largest domestic energy resource", *A report by the European Wind Energy Association*, September 2009.

[56] "Planning of the Grid Integration of Wind Energy in Germany Onshore and Offshore up to the Year 2020", Consortium DEWI/E.ON Netz/EWI/ REW Transport Grid, Electricity /VE Transmission, Summary, 2005.

[57] Information found at www.offshore-wind.de/page/index.php?id=4761 &L=1 (visit May 2010).

[58] REN21, Renewables 2011 Global Status Report, Version 1.1, July 2011. Online: http://www.ren21.net.

[59] The Global Wind Energy Council (GWEC), Global wind report 2010, April 2011. [Online]. Available: http://www.gwec.net.

[60] R. Doherty, E. Denny, M. O’Malley, “System operation with a significant wind power penetration”, *IEEE Power Engineering, Summer Meeting*, vol. 1, pp. 1002–1007, Jun. 2004.

[61] K. S. Salman, A.L.J. Teo, “Windmill modeling consideration and factors influencing the stability of a grid-connected wind power-based embedded generator”, *IEEE Trans. Power System*, vol. 18. no. 2, pp. 793–802, May 2003.

[62] H. Bevrani, A. Ghosh and G. Ledwich, "Renewable energy sources and frequency regulation: survey and new perspectives", *IET Ren. Power Gen*, vol. 4, No. 5, pp. 438-457, 2010.

[63] M. Liserre, R. Cardenas, M. Molinas and J. Rodriguez, "Overview of Multi-MW Wind Turbines and Wind Parks", *IEEE Trans. on Industrial Electronics*, Vol. 58, No. 4, pp. 1081-1095 (2011).

[64] H. Bevrani, Robust power system frequency control, Springer Ltd.

[65] Y. Sun, Z. Zhang, G. Li, and J. Lin, "Review on frequency control of power systems with wind power penetration", *Proceedings of the Power System Technol. Conference*, Hangzhou, China, pp. 1–8, 2010.

[66] H. Liu and Z. Chen, "Contribution of VSC-HVDC to frequency regulation of power systems with offshore wind generation," *IEEE Transactions on Energy Conversion*, vol. 30, no. 3, pp. 918-926, 2015.

[67] V. Gholamrezaie, M. G. Dozein, H. Monsef, "An Optimal Frequency Control Method Through a Dynamic Load Frequency Control (LFC) Model Incorporating Wind Farm", *IEEE Systems Journal*, 2016.

[68] E. Jahan, M. R. Hazari, S. M. Muyeen, A. Umemura, R. Takahashi and J. Tamura, "Coordinated power system frequency regulation by PMSG-based offshore wind farm", *Australasian Universities Power Engineering Conference (AUPEC)*, Melbourne, VIC, 2017, pp. 1-6,2017.

[69] F. D. González, M. Hau, A. Sumper, O. G. Bellmunt, "Participation of wind power plants in system frequency control: Review of grid code requirements and control methods", *Renewable and Sustainable Energy*, Vol. 34, 2014.

[70] Y. Sun, Z. Zhang, G. Li and J. Lin, "Review on Frequency Control of Power Systems with Wind Power Penetration", *International Conference on Power System Technology*, 2010.

[71] H. T. Ma and B. H. Chowdhury, "Working towards frequency regulation with wind plants: Combined control approaches", *IET Renewable Power Generation*, vol. 4, no. 4, pp. 308-316, 2010.

[72] J. Zhao, X. Lyu, Y. Fu, X. Hu, and F. Li, "Coordinated Microgrid Frequency Regulation Based on DFIG Variable Coefficient Using Virtual Inertia and Primary Frequency Control", *IEEE Trans. on Energy Conversion*, Vol. 31, No. 3, 2016.

[73] A. Aziz, Al.Stojcevski, “Frequency regulation capabilities in wind power plant”, *Sustainable Energy Technologies and Assessments*, Vol. 26, pp. 47-76, 2017.

[74] Z. WU, W. GAO, T. GAO, W. YAN, H. ZHANG, S. YAN, X. WANG, “State-of-the-art review on frequency response of wind power plants in power systems”, J. Mod. *Power Syst. Clean Energy*. vol. 6, No. 4, pp.-1-16, 2018.

[75] A. S. Fini, and M. Sheikhipoor, “Combined inertia and de-loading frequency response control by variable speed wind turbines”, *Global Journal of Scientific Researches*, vol. 4, No. 4, pp. 54-62, 2016.

[76] R. N. Andriamalala, Y. Wang, F. Colas, B. Francois, X. Guillaud, E. Semail, "Experimental assessment of the wind turbine contribution to the primary frequency control in an isolated power system", *PowerTech (POWERTECH) 2013 IEEE Grenoble*, pp. 1-6, 2013.

[77] R.N. Andriamalala, Y. Wang, F. Colas, B. Francois, X. Guillaud, E. Semail, "Power hardware in the loop simulation of wind farm contribution to grid frequency control", *Power Electronics and Applications (EPE) 2013 15th European Conference on*, pp. 1-8, 2013.

[78] A. Zertek, G. Verbic, M. Pantos, "A Novel Strategy for Variable-Speed Wind Turbines' Participation in Primary Frequency Control", *Sustainable Energy IEEE Transactions on*, vol. 3, no. 4, pp. 791-799, 2012.

[79] P. Venne ; X. Guillaud, “Impact of wind turbine controller strategy on deloaded operation”, *2009 CIGRE/IEEE PES Joint Symposium Integration of Wide-Scale Renewable Resources Into the Power Delivery System*, 29-31 July 2009.

[80] G. S. Feng, Z. J. Tan, A. Philip, H. L. Li, J. Jing, “A Review of Wind Turbine Deloaded Operation Techniques for Primary Frequency Control in Power System”, *2018 China International Conference on Electricity Distribution (CICED)*, 17-19 Sept. 2018.

[81] N. R. Ullah, T. Thiringer, D. Karlsson, "Temporary primary frequency control support by variable speed wind turbines potential and applications", *IEEE Trans. Power Systems*, vol. 23, no. 2, pp. 601-612, 2008.

[82] M. Kayikci, J. V. Milanović, "Dynamic contribution of dfig-based wind plants to system frequency disturbances", *IEEE Trans. Power Systems*, vol. 24, no. 2, pp. 859-867, 2009.

[83] K. Vidyanandan, N. Senroy, "Primary frequency regulation by deloaded wind turbines using variable droop", *IEEE Trans. Power Systems*, vol. 28, no. 2, pp. 837-846, 2013.

[84] Y. Gui, C.Kim, C. C. Chung, “Temporary primary frequency control support by deloaded wind power plant using input-output linearization”, *2016 16th International Conference on Control, Automation and Systems (ICCAS),* 16-19 Oct. 2016.

[85] Zarina P.P, S. Mishra, “Power oscillation reduction contribution by PV in deloaded mode”, *2016 IEEE 6th International Conference on Power Systems (ICPS),* March 2016.

[86] A. Kumar, G. Shankar, “Optimal load frequency control in deloaded tidal power generation plant-based interconnected hybrid power system”, *IET Renewable Power Generation,* vol. 12, Issue: 16 , Oct 2018.

[87] A. Zertek, G. Verbic, M. Pantos, "Optimised control approach of frequency control contribution of variable speed wind turbines", *IET Renew. Power Gener*, vol. 6, no. 1, pp. 17-23, 2012.

[88] L. Miao, J. Wen, H. Xie, W. Lee, "Coordinate control strategy of wind turbine generator and energy storage equipment for frequency support*", IEEE Trans. Ind. Appl*, vol. 51, no. 4, pp. 2732-2742, 2015.

[89] G. Xu, D. Ge, T. Cao, “Combined deload and kinetic energy control of variable speed wind turbines for frequency support”, *2016 IEEE PES Asia-Pacific Power and Energy Engineering Conference (APPEEC),* Oct. 2016

[90] H. Camblong, M. Rodriguez, J. R. Puiggali, A. Abad, "Comparison of different control strategies to study power quality in a variable-speed wind turbine", *1st world wind energy conference proceeding*, Berlin, 2002

[91] N. Khezami, X. Guillaud, N. B. Braiek, “Multimodel LQ controller design for variable-speed and variable pitch wind turbines at high wind speeds”, *2009 6th International Multi-Conference on Systems, Signals and Devices*, March 2009.

[92] K. V. Vidyanandan, N. Senroy, “Primary frequency regulation by deloaded wind turbines using variable droop”, *IEEE Transactions on Power Systems*, vol. 28, Issue: 2 , May 2013

[93] G. Ramtharan, J. B. Ekanayake, N. Jenkins, "Frequency support from doubly fed induction generator wind turbines", *IET Renew. Power Gen.*, pp. 3-9, Mar. 2007.

[94] R. G. de Almeida, J. Lopes, "Participation of doubly fed induction wind generators in system frequency regulation", *IEEE Trans. Power Syst.,* vol. 22, no. 3, pp. 944-950, Aug. 2007.

[95] M. E. Mokadem, V. Courtecuisse, C. Saudemont, B. Robyns, J. Deuse, "Experimental study of variable speed wind generator contribution to primary frequency control", *Renew. Energy*, vol. 34, pp. 833-844, 2009.

[96] L.-R. Chang-Chien, W.-T. Lin, Y.-C. Yin, "Enhancing frequency response control by DFIGs in the high wind penetrated power systems", *IEEE Trans. Power Syst.*, vol. 26, no. 2, pp. 710-718, May 2011.

[97] James F. Conroy, Rick Watson, "Frequency response capability of full converter wind turbine generators in comparison to conventional generation," *IEEE Trans. Power Systems*, vol.23, no.2, pp.649-656, May.2008.

[98] H.T. Ma and B.H.Chowdhurry, "Working towards frequency regulation with wind plants: combined control approaches," *IET Renew. Power Gen.*, vol.4, no.4, pp.308-316, 2009.

[99] Le-Ren Chang-Chien, Wei-Ting Lin and Yao-Ching Yin, "Enhancing Frequency Response Control by DFIGs in the High Wind Penetrated Power Systems," *IEEE Trans.Power Gen.*, vol.26, no.2, pp.710-71, May. 2011.

[100] A. Kumar, G. Shankar, "Optimal load frequency control in deloaded tidal power generation plant-based interconnected hybrid power system", *IET Renewable Power Generation*, Volume: 12 , Issue: 16 , 12 10 2018.

[101] Z. Wu, W. Gao, J. Wang, S. Gu, "A coordinated primary frequency regulation from Permanent Magnet Synchronous Wind Turbine Generation", *2012 IEEE Power Electronics and Machines in Wind Applications*, July 2012

[102] Brendan Fox et all, "Wind Power Integration Connection and System Operational Aspects," *The Institution of Engineeing and Technology*, London, United Kingdom, IET Pres, 2nd Edition, 2014.

[103] Wind power in Brazil and the US, [Available online]: https://sites.google.com /site/comparingwindpower/ (Accessed on 31 October 2018).

[104] Wind Energy Basics theory. [Online]: http://windeis.anl.gov/guide/basics/index.cfm, (Accessed on 2 November 2012).

[105] M. Rosyadi, A. Umemura, R. Takahashi, J. Tamura, N. Uchiyama and K. Ide, "Simplified model of variable speed wind turbine generator for dynamic simulation analysis," IEEJ Trans. on Power and Energy, vol. 135, no. 9, pp. 538-549, 2015.

[106] Matlab Documentation Center. Available online: http://www.mathworks.co.jp/jp/help/ (accessed on 20 December 2016).

[107] S. Achilles, N. Poller, "Direct drive synchronous machine models for stability assessment of wind farms," 2011.

[108] N. W. Miller, W. W. Pric and J. J. Samches-Gasca, "Dynamic modeling of GE 1.5 and 3.6 wind turbines-generators," *GE-Power System Energy Consulting*, 2003.

[109] P. Kundur, "Power System Stability & Control," McGraw-Hill Inc.

[110] IEE of Japan, Technical Reports Vol. 754: *Standard Model of Electrical Power System*, pp. 40-43.

[111] M. Rosyadi, S. M. Muyeen, R. Takahashi and J. Tamura, "Transient stability enhancement of variable speed permanent magnet wind generator using adaptive PI-Fuzzy controller," *2011 IEEE Trondheim PowerTech*, Trondheim, pp. 1-6, 2011.

[112] T. Sato, A. Umemura, R. Takahashi, J. Tamura, "Frequency Control of Power System with Large Scale Wind Farm Installed by Using HVDC Transmission System", *IEEE PES PowerTech Manchester 2017*, No.108, 2017.

[113] X. Yingcheng, T. Nengling, "Review of contribution to frequency control through variable speed wind turbine," Renewable Energy, vol. 36, no. 6, pp. 1671-1677, 2011.

[114]] K. Tada, A. Umemura, R. Takahashi, J. Tamura, Y. Matsumura, D. Yamaguchi, H. Kudo, M. Niiyama, Y. Taki, "Frequency control of power system with solar and wind power stations installed by flow control of HVDC interconnection line," *The 20th International Conference on Electrical Machines and Systems (ICEMS 2017)*, ID: 621, 2017/08, pp. 1-6.

[115] ABB HVDC Light: Projects worldwide (2018). Available: https://library.e.abb.com/public/80b8069429b147d984f16c8118027ef4/POW0027_REV25.pdf.

[116] Y. Yoshida, A. Umemura, R. Takahashi and J. Tamura, "Control of power system frequency fluctuations by on-line output frequency band control of variable speed wind power generators", IEEJ Trans. on Power and Energy, Vol. 137, No. 4, pp. 274-284, 2017.

List of Publications

Transactions/Journal Papers:

[1] **Effat Jahan,** Md. Rifat Hazari, Mohammad Abdul Mannan, Atsushi Umemura, Rion Takahashi, Junji Tamura "Damping of Frequency Fluctuations of Hybrid Power System by Variable Deloaded Operation of PMSG Based Offshore Wind Farm," IEEJ Transactions on Power and Energy, Vol. 139, No. 4, pp. 259-268, April 2019.

[2] **Effat Jahan,** Md. Rifat Hazari, S. M. Muyeen, Atsushi Umemura, Rion Takahashi and Junji Tamura, ''Primary Frequency Regulation of Hybrid Power System by Deloaded PMSG-based Offshore Wind Farm using Centralized Droop Controller,'' The Journal of Engineering (IET) (5 pages) (Open Access, DOI:10.1049/ joe.2018.9326), 2019.

International Conference Papers:

[3] **Effat Jahan,** Md. Rifat Hazari, Marwan Rosyadi, Atsushi Umemura, Rion Takahashi and Junji Tamura, "Simplified Model of HVDC Transmission System Connecting Offshore Wind Farm to Onshore Grid," Proceedings on 12th IEEE PowerTech Conference, University of Manchester, UK, paper-id: 51 (6 Pages), June 2017.

[4] **Effat Jahan,** Md. Rifat Hazari, S. M. Muyeen, Atsushi Umemura, Rion Takahashi and Junji Tamura, ''Coordinated Power System Frequency Regulation by PMSG-based Offshore Wind Farm'' Proceedings on 2017 Australasian Universities Power Engineering Conference (AUPEC 2017), Victoria University, Melbourne, Australia, pp. 1-6, paper-id: 83, November 2017.

[5] **Effat Jahan,** Md. Rifat Hazari, S. M. Muyeen, Atsushi Umemura, Rion Takahashi and Junji Tamura, ''Primary Frequency Regulation of Hybrid Power System by Deloaded PMSG-based Offshore Wind Farm using Centralized Droop Controller,'' Proceedings on 7th IET International Conference on Renewable Power Generation 2018 (RPG 2018), Technical University of Denmark, Lyngby, Copenhagen, Denmark, pp. 1-6, paper-id: 97, September 2018.

National Conference Papers:

[6] **Effat Jahan,** Md. Rifat Hazari, Marwan Rosyadi, Atsushi Umemura, Rion Takahashi and Junji Tamura, ‘‘Simplified Model of VSC-HVDC Transmission System connecting Offshore Wind Farm with Multi-Machine Power System,’’ Proceedings on 2016 Joint Conventional Record, The Hokkaido Chapters of Institute of Electrical and Information Engineer, Sapporo, Japan, No.29, September 2016.

[7] **Effat Jahan,** Md. Rifat Hazari, Atsushi Umemura, Rion Takahashi and Junji Tamura, “Frequency Regulation of Power System by Output Control of Offshore Wind Farm Connected to the Main System through VSC-HVDC Line,” Proceedings on 2017 IEEJ Technical Meeting on Power Engineering/Power System Engineering, Kitami Institute of Technology, Japan, PE-17-084/PSE-17-084, pp. 1-6, September 2017.

[8] **Effat Jahan,** Md. Rifat Hazari, Atsushi Umemura, Rion Takahashi and Junji Tamura, ‘‘A New Centralized Controller for PMSG-based Offshore Wind Farm to Damp Frequency Fluctuations of Hybrid Power System,’’ Proceedings on 2017 Joint Conventional Record, The Hokkaido Chapters of Institute of Electrical and Information Engineer, Hakodate, Japan, No.27, October 2017.

[9] **Effat Jahan,** Md. Rifat Hazari, Atsushi Umemura, Rion Takahashi and Junji Tamura, ‘‘A Novel Variable Deloaded Operation for PMSG-based Offshore Wind Farm to Damp Frequency Fluctuations of Onshore Hybrid Power System (Part 1),’’ Proceedings on 2018 Joint Conventional Record, The Hokkaido Chapters of Institute of Electrical and Information Engineer, Sapporo, Japan, No.30, October 2018.

[10] **Effat Jahan,** Md. Rifat Hazari, Atsushi Umemura, Rion Takahashi and Junji Tamura, ‘‘A Novel Variable Deloaded Operation for PMSG-based Offshore Wind Farm to Damp Frequency Fluctuations of Onshore Hybrid Power System (Part 2),’’ Proceedings on 2018 Joint Conventional Record, The Hokkaido Chapters of Institute of Electrical and Information Engineer, Sapporo, Japan, No.31, October 2018.